University of Ioannina

Department of Health Sciences

Faculty of Medicine

Biological Chemistry Laboratory

Inter-institutional Interdepartmental Program of

Postgraduate Studies

“Molecular and Cellular Biology and Biotechnology”

The role of nuclear lamina and nuclear envelope proteins in chromatin architecture

Evangelia Triantopoulou

Biologist

Master’s Degree Thesis

September 2023,

Ioannina

Prologue

This work has been conducted in the Laboratory of Biological Chemistry, Faculty of Medicine, University of Ioannina, under the supervision of Professor Politou Anastasia, between the years 2021 and 2023. I would like to express my appreciation to Dr. Politou for accepting me as a member of her team, for putting her trust in me and for all the support and guidance that she has provided during my time in her laboratory.

I would also like to thank Professor Frilingos Efstathios, Assistant Professor Liakopoulos Dimitrios, Professor Papamarkaki Thomais and Professor Georgatos Spyridon who agreed to assess and comment on my work.

I would like to especially thank Dr. Soupsana Katerina who took up my supervision in the lab and who has been guiding me through my journey to become a scientist ever since. I would also like to thank all the other members of Dr. Politou's laboratory, for being great colleagues and friends. This work would not have been completed in its current form without the contribution of Professor Mpatsidis Apostolos and his team of mathematicians, who contributed to the statistical analysis of our data and to whom I feel much obliged.

Lastly, I would like to express my deepest gratitude to my family, and especially my sisters, Fotini and Ioanna, who have always been my biggest supporters, as well as to my dear friends who kept me sane through the ups and downs of my master's journey.

Contents

Contents

ABSTRACT

The nucleus is a unique feature of eukaryotic cells inside which the genetic material is stored in the form of chromatin. During the past few decades, the development of advanced methods, such as Chromosome Conformation Capture (3C) technologies, and high-resolution microscopic techniques has revealed that the non-stochastic organization of chromatin in the nuclear interior is regulated by multiple mechanisms and factors, that act in an orchestrated manner in order to maintain nuclear integrity and chromatin architecture. The multiple levels of chromatin organization include, among others, distinct chromosome positions, called chromosome territories, loop formation followed by long-range inter- and intrachromosomal interactions (Topologically Associated Domains, TADs), as well as interactions of chromatin domains with other nuclear features, such as the Nuclear Lamina (Lamina Associated Domains, LADs) and the nucleoli (Nucleoli Associated Domains, NADs). The microenvironment of the nuclear periphery and the nuclear envelope have been extensively studied and have been found to play a key role in the establishment of the chromatin landscape and the regulation of gene expression. Conventionally, the nuclear periphery serves as a binding platform for chromatin domains of heterochromatic nature, while heterochromatin can also be found on the surface of nucleoli or in distinct foci inside the nucleoplasm. On the other hand, euchromatin is found to be dispersed in the rest of the nucleoplasm and near the openings of the nuclear pores. The inspection of cell types, such as the rod cells of the retina of nocturnal mammals, which exhibit an inversion of the conventional chromatin architecture, revealed two major tethers of the nuclear periphery that maintain heterochromatin's peripheral positioning: the A-tether, which consists of Lamin A/C and its interacting proteins, and the B-tether, which corresponds to LBR.

This work aimed to investigate the role LBR and Lamin A/C might play in the maintenance of nuclear integrity and chromatin architecture, using NIH/3T3 mouse fibroblasts that had been knocked out for these two key components of the nuclear periphery, either individually or in combination. More specifically, the nuclear envelope properties and chromatin dynamics were investigated using mostly microscopic methods. The results obtained so far indicated that the concurrent absence of these

two proteins can cause asymmetric localization of major components of the nuclear periphery and alterations in the distribution of chromatin inside the nucleus, yet, without affecting chromatin dynamics, or other cellular functions, such as cell motility. On the other hand, single (LBR or Lamin A/C) knockout cells appeared to be only mildly affected by the absence of one of these proteins. Despite these nuclear aberrations, all mutant cell populations were able to survive and proliferate. These observations implied the existence of other mechanisms that may have a compensatory effect and make up for the absence of LBR and Lamin A/C. However, there are still several questions that need to be clarified in order to gain better insight into the causal relationship between the lack of these two proteins and the phenotypes generated, as well as the principles that rule chromatin architecture in general.

ΠΕΡΙΛΗΨΗ

Ο πυρήνας αποτελεί ένα μοναδικό χαρακτηριστικό των ευκαρυωτικών κυττάρων μέσα στο οποίο αποθηκεύεται το γενετικό υλικό με τη μορφή της χρωματίνης. Τις τελευταίες δεκαετίες, η ανάπτυξη προηγμένων μεθόδων, όπως οι Chromosome Conformation Capture (3C) τεχνολογίες, και οι τεχνικές μικροσκοπίας υψηλής ανάλυσης, έχουν αποκαλύψει ότι η μη στοχαστική οργάνωση της χρωματίνης στο εσωτερικό του πυρήνα ρυθμίζεται από πολλαπλούς μηχανισμούς και παράγοντες που δρουν συγχρονισμένα για τη διατήρηση της ακεραιότητας του πυρήνα και της αρχιτεκτονικής της χρωματίνης. Τα πολλαπλά επίπεδα οργάνωσης της χρωματίνης περιλαμβάνουν, μεταξύ άλλων, την κατάληψη διακριτών θέσεων στον πυρήνα από τα χρωμοσώματα, που ονομάζονται χρωμοσωμικές επικράτειες, σχηματισμούς βρόχων που ακολουθούνται από μεγάλης εμβέλειας δια- και ενδοχρωμοσωμικές αλληλεπιδράσεις (Τοπολογικά Διασυνδεδεμένες Επικράτειες – TADs), καθώς και αλληλεπιδράσεις τμημάτων της χρωματίνης με άλλες δομές του πυρήνα, όπως η πυρηνική λάμινα (Διασυνδεδεμένες με τη Λάμινα Επικράτειες – LADs) και οι πυρηνίσκοι (Διασυνδεδεμένες με τους Πυρηνίσκους Επικράτειες – NADs). Το μικροπεριβάλλον της πυρηνικής περιφέρειας και ο πυρηνικός φάκελος έχουν μελετηθεί εκτενώς και έχει βρεθεί ότι διαδραματίζουν βασικό ρόλο στον καθορισμό του χρωματινικού τοπίου και στη ρύθμιση της γονιδιακής έκφρασης. Συμβατικά, η πυρηνική περιφέρεια χρησιμεύει ως πλατφόρμα δέσμευσης για περιοχές της χρωματίνης ετεροχρωματινικής φύσεως, ενώ η ετεροχρωματίνη μπορεί επίσης να βρεθεί στην επιφάνεια των πυρηνίσκων ή σε διακριτές εστίες μέσα στο νουκλεόπλασμα. Από την άλλη πλευρά, η ευχρωματίνη βρίσκεται διασκορπισμένη στο υπόλοιπο νουκλεόπλασμα και κοντά στα ανοίγματα των πυρηνικών πόρων. Η διερεύνηση κυτταρικών τύπων, όπως τα ραβδία του αμφιβληστροειδούς των νυκτόβιων θηλαστικών, που παρουσιάζουν αντιστροφή της συμβατικής αρχιτεκτονικής της χρωματίνης, αποκάλυψε δύο κύριους μηχανισμούς πρόσδεσης στην πυρηνική περιφέρεια που διατηρούν την περιφερειακή τοποθέτηση της ετεροχρωματίνης: τον A-tether, ο οποίος αποτελείται από την Lamin A/C και τις πρωτεΐνες που αλληλεπιδρούν με αυτήν, και τον B-tether, που αντιστοιχεί στον LBR.

Η παρούσα εργασία στόχευε στη διερεύνηση του ρόλου που ενδέχεται να διαδραματίζουν ο LBR και η Lamin A/C στη διατήρηση της ακεραιότητας του πυρήνα

και της αρχιτεκτονικής της χρωματίνης, με τη χρήση NIH/3T3 ινοβλαστών ποντικού στους οποίους είχε γίνει απαλοιφή των δύο αυτών βασικών συστατικών της πυρηνικής περιφέρειας, είτε μεμονωμένα είτε συνδυαστικά. Πιο συγκεκριμένα, διερευνήθηκαν οι ιδιότητες του πυρηνικού φακέλου και η δυναμική της χρωματίνης χρησιμοποιώντας κυρίως μεθόδους μικροσκοπίας. Τα αποτελέσματα που έχουν προκύψει έως τώρα έδειξαν ότι η ταυτόχρονη απουσία αυτών των δύο πρωτεϊνών μπορεί να προκαλέσει την ασύμμετρη κατανομή κύριων συστατικών της πυρηνικής περιφέρειας, αλλά και αλλαγές στην κατανομή της χρωματίνης στο εσωτερικό του πυρήνα, χωρίς ωστόσο να επηρεάζεται η δυναμική της χρωματίνης ή άλλες κυτταρικές λειτουργίες, όπως η κινητικότητα των κυττάρων. Από την άλλη πλευρά, τα κύτταρα που είχαν υποστεί μεμονωμένη απαλοιφή μιας εκ των δύο πρωτεϊνών (LBR ή Lamin A/C) φάνηκαν να επηρεάζονται μόνο ελαφρώς. Παρά τις εν λόγω ατυπίες, όλοι οι πληθυσμοί κυττάρων που είχαν υποστεί κάποια μετάλλαξη αποδείχθηκαν ικανοί στο να επιβιώνουν και να πολλαπλασιάζονται. Αυτές οι παρατηρήσεις υποδηλώνουν την ύπαρξη άλλων μηχανισμών που μπορεί να έχουν αντισταθμιστικό αποτέλεσμα και να αναπληρώνουν την απουσία των LBR και Lamin A/C. Ωστόσο, υπάρχουν ακόμη πολλά ερωτήματα που πρέπει να διευκρινιστούν προκειμένου να αποκτήσουμε μία καλύτερη εικόνα της αιτιώδους σχέσης μεταξύ της έλλειψης αυτών των δύο πρωτεϊνών και των φαινοτύπων που προκύπτουν, καθώς και των αρχών που διέπουν την αρχιτεκτονική της χρωματίνης σε γενικότερο πλαίσιο.

Abbreviations

3C: Chromatin Conformation Capture

cHC: constitutive Heterochromatin

DKO: Double Knock Out

EC: Euchromatin

ER: Endoplasmic Reticulum

fHC: facultative Heterochromatin

FRAP: Fluorescence Recovery After Photobleaching

HC: Heterochromatin

HP1: Heterochromatin Protein 1

INM: Inner Nuclear Membrane

KO: Knock Out

LAD: Lamina Associated Domain

LBR: Lamin B Receptor

LINC: Linker of Nucleoskeleton and Cytoskeleton

LLPS: Liquid-liquid Phase Separation

NE: Nuclear Envelope

NL: Nuclear Lamina

NPC: Nuclear Pore Complex

ONM: Outer Nuclear Membrane

ROI: Region Of Interest

TAD: Topologically Associated Domain

Introduction 

1. Introduction

1.1. The Eukaryotic Nucleus

The cell nucleus (Fig.1) is a membrane-bound organelle common amongst eukaryotic cells, most widely known as the compartment that contains the genetic material of the cell. However, the role of the eukaryotic nucleus extends beyond being a DNA storage organelle. This membranous structure also serves as the “command” center of the cell, inside which important cellular processes, such as replication, transcription and repair of the genetic material, take place (Foisner, 2003).

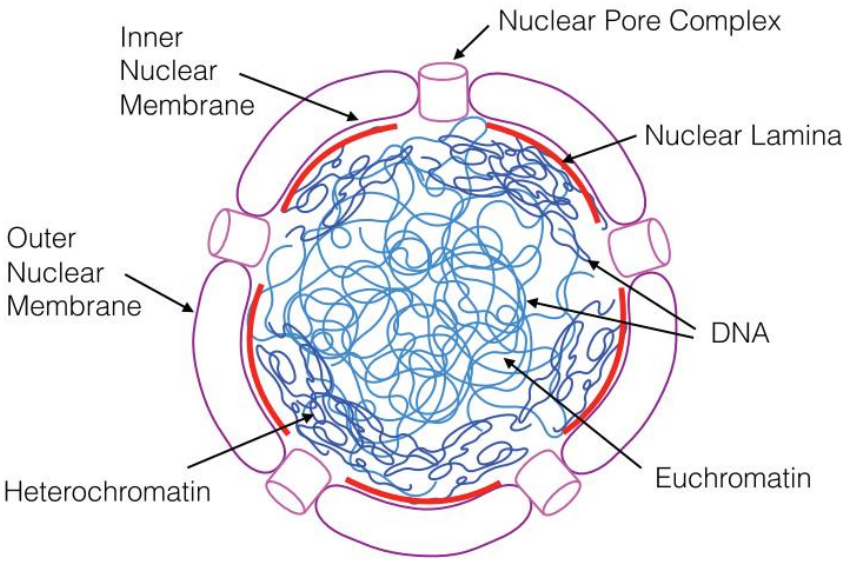

Figure 1. Schematic representation of the eukaryotic nucleus (arrows indicate the main features of the nucleus) (Sazer &Schiessel, 2017).

The inside of the nucleus, which is known as the nucleoplasm, is enclosed by a double-layered membrane called the Nuclear Envelope (NE). The NE is comprised of the Inner Nuclear Membrane (INM), which faces the nucleoplasm, the Outer Nuclear Membrane (ONM), which faces the cytoplasm and is continuously connected to the rough Endoplasmic Reticulum (ER), the nuclear pores and their corresponding membrane (Hetzer, 2010). The nuclear pores host large protein complexes called

Nuclear Pore Complexes (NPCs) that regulate the communication between the nuclear interior and the cytoplasm by facilitating large molecule transport from and to the cytoplasm (Hoeltz *et al.*, 2011).

The very fragile and sensitive genetic material of the cell is stored in the nucleoplasm, organized in a non-stochastic manner, serving the need for a very strict regulation of gene expression. In addition, the inside of the nucleus provides space for DNA-free structures, called nucleoli, that are separated from the rest of the nucleoplasm by liquid-liquid phase separation, since they exhibit liquid-like behavior. Nucleoli can be two or more in number per nucleus and their function lies in ribosome synthesis and assembly, as well as other cellular processes, such as response to stress conditions (Dubois & Boisvert, 2016).

1.2. The Nuclear Lamina

The Nuclear Lamina (NL) is an extensively studied and critical feature of the nuclear periphery. The main building blocks of this structure are proteins known as lamins. These proteins assemble into type V intermediate filaments which extend right beneath the nuclear envelope (Herrmann & Aebi, 2016). This meshwork along with its associated proteins forms the nucleoskeleton which plays a critical role in the regulation of nuclear mechanics, while it also offers a binding platform for DNA (Dechat *et al*., 2010).

In mammals, there are three genes that encode for two distinct types of lamins: A and B-type lamins. A-type lamins are all products of the alternative splicing of a single gene. The LMNA gene encodes for the two major type-A isoforms, Lamin A and Lamin C, as well as for the tissue-specific AΔ10 and C2. Lamin B1 and Lamin B2, which fall into the B-type category, are products of the LMNB1 and LMNB2 genes, respectively (Adam, 2017). LMNB2 also encodes for the rare germ-line-specific isoform Lamin B3 (Schütz *et al*., 2005). Lamins are also present in nuclei of other species, such as *Caenorhabditis elegance* (Liu *et al*., 2000) and *Drosophila melanogaster* (Döring & Stick, 1990).

Structurally, lamins are comprised of an N-terminal head, a central rod domain, which contains 4 a-helical coils (1A, 1B, 2A, 2B) separated by linker regions of high

flexibility, and a C-terminal tail that contains a nuclear localization signal (NLS), a domain that belongs to the immunoglobin family of protein domains and a CaaX motif (C: cysteine, a: aliphatic amino acid, X: any amino acid) (Gruenbaum & Medalia, 2015). The latter is present in all lamin isoforms except for Lamin C and offers a farnesylation site that is critical for the maturation process of lamins. This multiple-step process includes the addition of a prenyl moiety at the cysteine residue of pre-lamin A, pre-lamin B1 and pre-lamin B2. Prenylation is followed by the proteolytic removal of -aaX and the methylation of cysteine by an isoprenyl carboxy methyltransferase. The maturation process of Lamin A includes an additional step, at which the last fifteen C-terminal amino acids are proteolytically removed by the ZMSTE24/FACE1 enzyme (de Leeuw *et al*., 2018). Thus, mature B-type lamins remain farnesylated, in contrast to the mature Lamin A. The retention of the prenyl moiety on B-type lamins has been associated with their interaction with the INM (Gruenbaum & Foisner, 2015), while the absence of farnesylation combined with the phosphorylation of Lamin A in specific steps of the cell cycle increases the protein's solubility (Torvaldson *et al*., 2015).

Both types of lamins are mainly located at the nuclear periphery, where they oligomerize (Fig. 2) to create flexible, 3.5nm thick filaments. Each type forms distinct (Fig. 3) and spatially distinguishable meshworks (Fig. 4), as it has been proven by the use of modern high-resolution microscopic techniques (3D-structured illumination microscopy (3D-SIM), stochastic optical reconstruction microscopy (STORM)) (Shimi *et al.*, 2015; Xie *et al.*, 2016; Nmezi *et al.*, 2019). Yet, studies have shown that in the absence of one isoform, the meshworks of the rest of the lamins undergo structural changes, implying that, even though distinct, these filaments extensively interact with each other (Shimi *et al.*, 2015).

Except for their localization in the nuclear periphery, a fraction of A-type lamins is also present in the nucleoplasm. There, Lamin A and Lamin C form more loose filaments, as well as dense foci in the nuclear interior and have been associated with the organization of chromatin and other nuclear processes, such as DNA replication and repair (Dechat *et al.*, 2011; Naetar *et al.*, 2017). Interestingly, there are studies that associate the nucleoplasmic fraction of Lamin A/C with euchromatic regions that also contain the lamina-associated polypeptide 2α (LAP2α). Loss of LAP2α has been found to cause alterations regarding the binding of Lamin A/C to euchromatic regions,

as well as the euchromatin epigenetic markers. More specifically, regions that lose or gain Lamin A/C binding exhibit a decrease or an increase in euchromatic histone modifications, respectively, implying a role of Lamin A/C in the regulation of gene expression (Gesson *et al*., 2016).

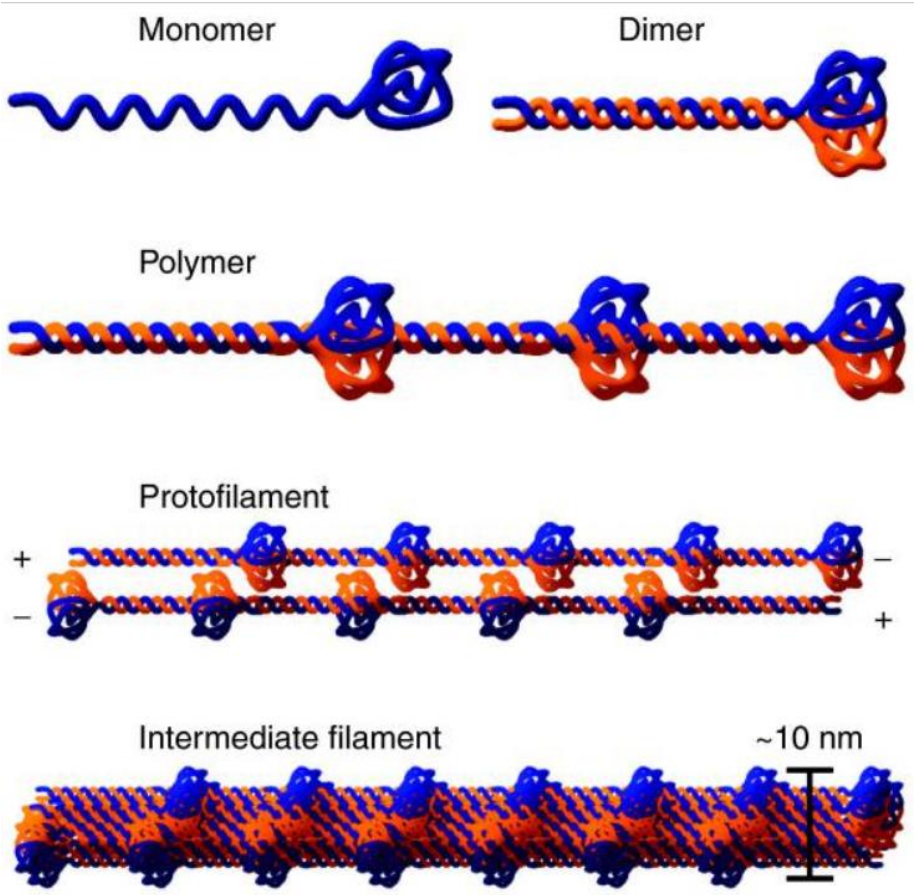

Figure 2. Schematic representation of how lamin filaments are formed. Lamin monomers arranged in parallel assemble into coiled-coil dimers, which in turn can interact in a head-to-tail manner to form polymers. Lamin polymers are then arranged antiparallel to each other and build what is called a protofilament. Three or four protofilaments are laterally associated and form intermediate filaments with a diameter of about 10nm (Dittmer & Misteli, 2011).

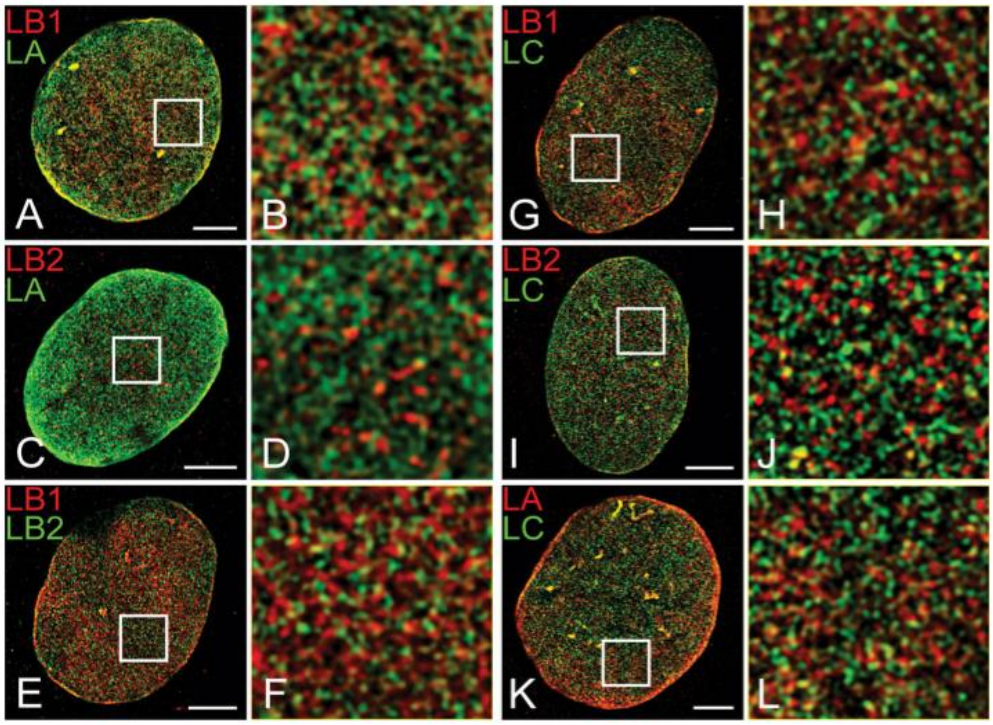

Figure 3. Reconstructed 3D-SIM images of MEFs nuclei labelled with antibodies against all possible combinations of the different lamin isoforms. The images show that different isoforms form mostly distinct meshworks with only a few overlapping areas (Shimi *et al.*, 2015).

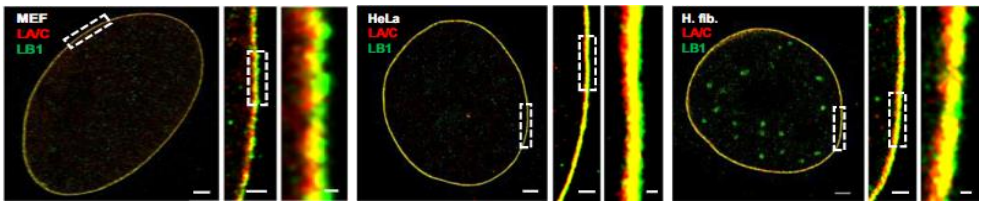

Figure 4. STORM images of 3 distinct cell types (MEFs, HeLa, human fibroblasts) labelled with antibodies against Lamin A/C and Lamin B1, showing the concentric and spatially distinguishable networks of these two lamin isoforms (Nmezi *et al.*, 2019).

The different types of lamins exhibit specificity regarding the cell types and developmental stages in which they are present. In particular, B-type lamins are ubiquitous in all nucleated mammalian cell types, while A-type lamins are expressed at low levels in pluripotency in comparison with the higher expression that characterizes more differentiated cell types (Eckersley-Maslin *et al.*, 2013; Wong & Stewart, 2020). In addition, different types of lamins form filaments of different physicochemical properties. As a result, changes in the stoichiometric ratio of A-/B-

type lamins can change the structural characteristics of the nucleus, such as stiffness and contractility. Through their interaction and cooperation with multiple proteins of the nuclear envelope and the nuclear periphery, lamins can act as multifunctional factors that participate, not only in the maintenance and regulation of the nuclear morphology and mechanics, but also in the regulation of chromatin states and organization (Vahabikashi *et al.*, 2022),

1.3. Chromatin

1.3.1. The Nucleosome and the Histone Code

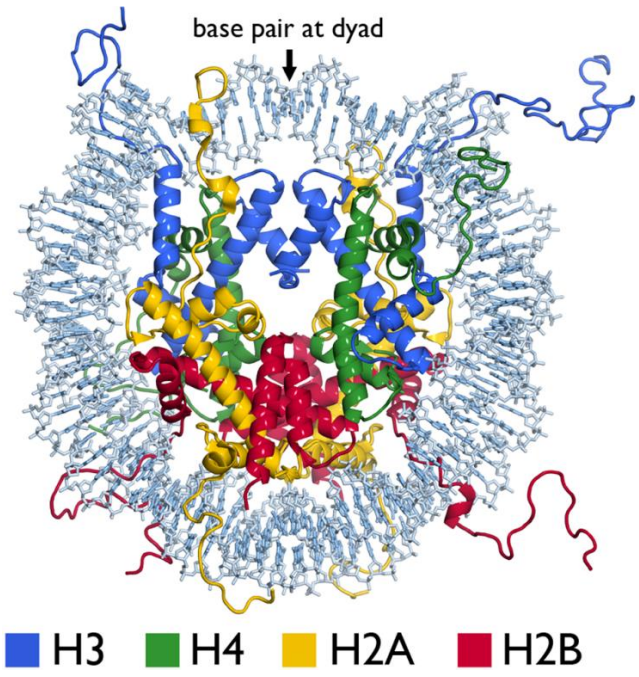

Figure 5. Schematic representation of the nucleosome particle structure (McGinty & Tan, 2015).

The genetic material is tightly packed inside the eukaryotic nucleus in the form of chromatin. The word chromatin refers to a complex that contains the DNA along with its structural and regulatory protein partners (Gilbert *et al.*, 2005). The fundamental structural component of the chromatin fibre is the nucleosome, which consists of an octamer of histone proteins and 147 DNA base pairs wrapped almost twice around this protein core (McGinty & Tan, 2015). Four core histones participate in the histone octamer composition: H2A, H2B, H3, H4 (Fig. 5). These proteins are rich in arginine and lysine residues and, thus, they are positively charged. This feature facilitates their interaction with the negatively charged phosphates of the DNA backbone, serving the formation of the nucleosome particle. Inside the nucleosome core histones H3 and H4 form a tetramer that interacts with two H2A-H2B dimers via hydrogen bonds. The nucleosome is

sealed with a single molecule of the linker histone H1, which stabilizes the nucleoprotein complex (Cutter & Hayes, 2015).

Histones are highly conserved among eukaryotes. Apart from the four core histones there are also histone variants which arose from gene duplication events and are expressed in specific differentiation and embryogenesis stages. A couple of examples are the H3.3 variant of histone H3 that is specific for testes, as well as H2A.x variant of histone H2A, which is present on double strand breaks and is a marker of DNA damage (Talbert & Henikoff, 2021).

Structurally, histones consist of a C-terminal hydrophobic histone fold, which is responsible for histone:histone and histone:DNA interactions, and an N-terminal tail that extends outside the nucleosome, offering spots for epigenetic chemical modifications (Mariño-Ramírez *et al.*, 2007; Zhang *et al.*, 2020). These modifications are associated with the regulation of chromatin accessibility and gene expression. They include methylation, acetylation, phosphorylation, ubiquitination and SUMOylation and they collectively constitute the “histone code”. According to the “histone code” hypothesis, different combinations of histone modifications on one or more histone tails can result in differences in the regulation of gene expression and cell fate (Turner, 2002). The epigenetic histone modifications are placed on and removed from specific residues of the histone tails by enzymes called “writers” and “erasers”, respectively. Enzymes called “readers” are able to recognise these chemical moieties and recruit other proteins that play a more active role in the regulation of gene expression (Nicholson *et al.*, 2015). The trimethylation of lysine 9 of histone H3 (H3K9me3) and the trimethylation of lysine 27 of histone H3 (H3K27me3), which are common heterochromatin markers and induce transcriptional repression (Araki & Mimura, 2017), as well as the acetylation of lysine 4 of histone H3 (H3K4ac) which has been found to be enriched on promoters of actively transcribed genes (Guillemette *et al.*, 2011), are only a few representative examples of the most common epigenetic histone modifications (Fig. 6).

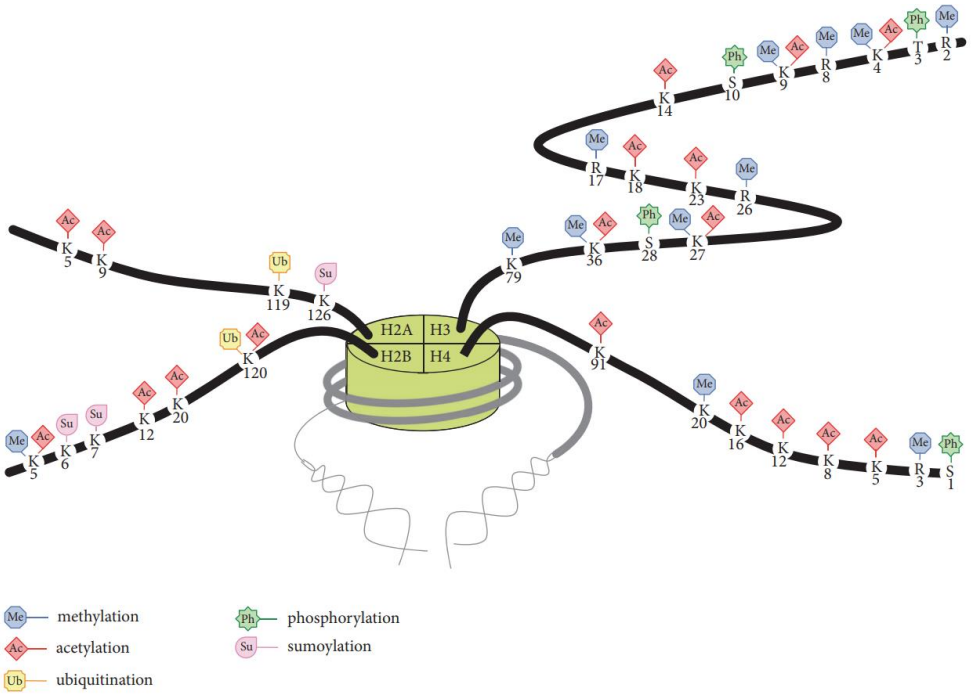

Figure 6. Schematic illustration of the main epigenetic modifications of histones' N-terminal tails (Araki & Mimura, 2017).

1.3.2. Chromatin organization in 3D space

During the past couple of decades, the development of modern tools for the investigation of chromatin architecture, such as Fluorescence in situ Hybridization (FISH), Chromatin Conformation Capture (3C) techniques and Chromatin Immunoprecipitation (ChIP) protocols, enabled scientists to make great progress in this field. Intensive studies led to gaining more insight into the principles of chromatin organization and revealed that the formation of the chromatin landscape happens at multiple levels, including inter- and intra-chromosomal interactions and chromatin loop formation, serving the need for efficient packaging and regulation of the genetic material (Fig. 8) (Kempfer & Pombo, 2020).

On the macroscale, chromosomes occupy specific locations inside the nucleus, called chromosome territories, as has been established by FISH experiments. The arrangement of chromosome territories appears to be radial, and the positioning of each chromosome is cell-type-specific while it also depends on the gene-density and chromosome size, as well as the stage of differentiation each cell undergoes. Thus,

large and gene-poor chromosomes tend to reside in the nuclear periphery, while small and gene-rich chromosomes accumulate in the nuclear interior, with this pattern being altered in case there are alterations in the transcriptional profile of the cell (Fritz *et al.*, 2019). Even though chromosomes are spatially distinct, inter-chromosomal interactions are present, with the most characteristic examples being the heterochromatic foci of murine nuclei where centromeres are gathered, as well as the "transcription factories", in which the transcription machinery concurrently acts on genes of different chromosomes (Fraser *et al.*, 2015; Szczepińska *et al.*, 2019).

At the chromatin level, there are two types of chromatin in interphase nuclei: euchromatin (EC) and heterochromatin (HC). The word euchromatin refers to the type of chromatin that is less condensed and more accessible to transcription factors and DNA / RNA polymerases, compared to heterochromatin, which is more condensed and is generally rendered "inactive" (Gilbert *et al.*, 2005). Heterochromatin is further distinguished into two subtypes: constitutive HC (cHC), which is mostly depleted of genes, includes centromere and telomere sequences and is constitutively repressed, and facultative HC (fHC), which is cell-type specific and can adapt the expression of its genes according to the developmental and differentiation stage of the cell (Saksouk *et al.*, 2015). Modern studies propose the classification of chromatin in two distinct nuclear compartments, in respect to euchromatin and heterochromatin. The "A compartment" is mostly euchromatic, is enriched for short interspersed nuclear elements (SINEs) and "active" histone markers and is accessible to transcription factors. The "B compartment" corresponds to domains of heterochromatic nature and contains mainly pericentromeric satellite repeats, long interspersed nuclear elements (LINEs) and long terminal repeats (LTRs) (Solovei *et al.*, 2016; Zheng & Xie, 2019).

Conventionally, the two types of chromatin occupy spatially distinct positions inside the nucleus. The highly condensed HC forms a dense layer that is in close proximity with the nuclear envelope, as well as a layer that covers the surface of the nucleoli. EC occupies the rest of the nucleoplasm while it is also located near the nuclear pores where it can interact with the NPCs (Fig. 7) (Solovei *et al.*, 2016; Feodorova *et al.*, 2020). The role of the nuclear periphery in the spatial organization of the genome is considered to be highly significant, with the binding of HC to the NE participating in the correct folding of chromosomes inside the nucleus and the maintenance of the conventional nuclear architecture (Rullens & Kind, 2021).

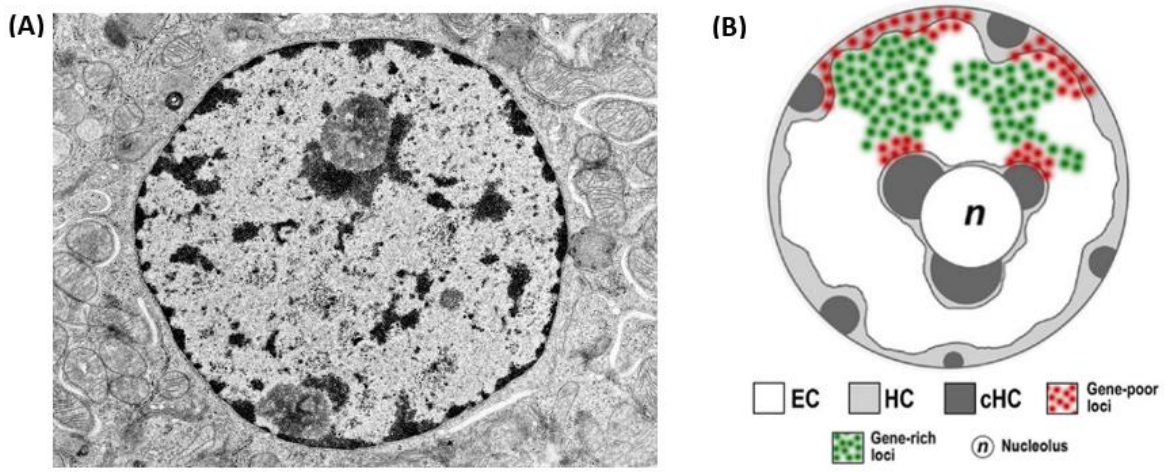

Figure 7. Representative images of the conventional nuclear architecture of the mammalian nucleus. (A) Electron microscopy image showing HC as darkly stained particles close to the NE, the nucleoli, as well as inside the nucleoplasm, and EC as lightly stained chromatin distributed in the rest of the nucleus and adjacent to the NPCs. (B) Schematic representation of the distribution of EC and HC inside the nucleus (Feodorova *et al.*, 2020).

On the microscale, distinct chromosomes can form internal loops, bringing distant loci in close proximity with each other and, thus, increasing the probability of their interaction. These architectural chromatin units are known as Topologically-Associated Domains (TADs) and are evolutionarily conserved across the animal kingdom. TADs have been found to facilitate the interaction of genes with distant cis-regulatory elements, while it has also been proposed that they participate in the coordinated expression of groups of genes specifically expressed in the various stages of differentiation. TADs are well-defined units, separate from each other, with only minor inter-TAD interactions, flanked by boundary regions with specific genetic identity and marked with CTCF and cohesin complexes (Dixon *et al.*, 2012; Szabo *et al.*, 2019; Rada-Iglesias *et al.*, 2018). These complexes are of high significance for the structural integrity of TADs, as well as for the maintenance of their borders (Zheng & Xie, 2019).

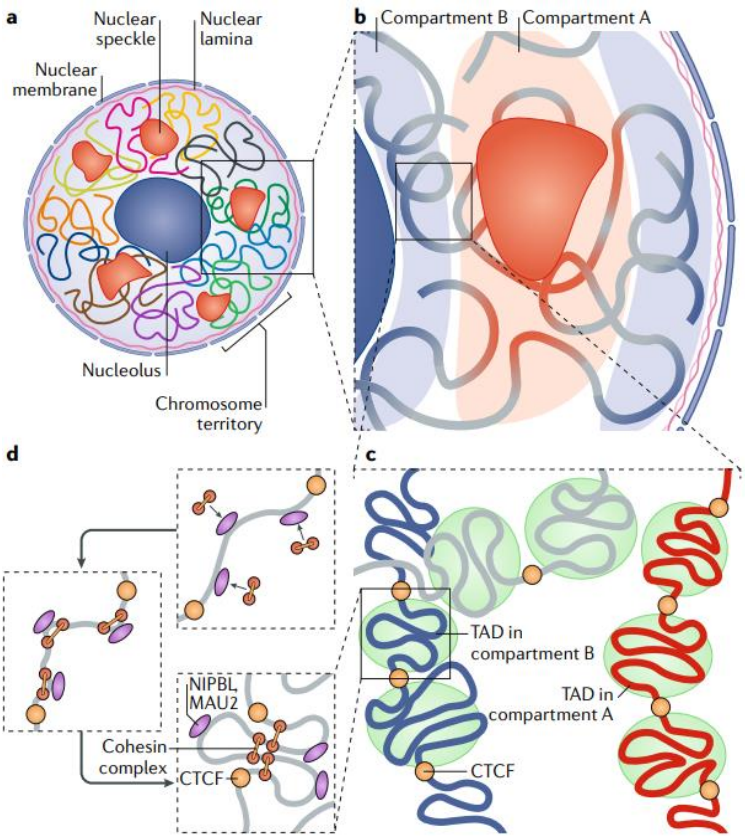

Figure 8. Schematic representation of the way genome is organized in 3D space. (a) Interphase chromosomes (depicted with different colors) occupy distinct territories. (b) In compartment A chromatin is dispersed inside the nucleoplasm, while compartment B preferentially interacts with the NE and the nucleolus. (c-d) Topologically - Associated domains (TADs) contain inter- and intra-chromosomal interactions that depend on cohesin-mediated chromatin looping. CTCF acts at TAD borders as an insulator, setting boundaries between the different TADs (Zheng & Xie, 2019).

1.3.3. Heterochromatin Protein 1 and the biophysics of chromatin organization

Extensive investigations that combine experimental and computational models have revealed that chromatin and its protein partners have the ability to act as polymers in a solution and form biomacromolecular condensates via liquid-liquid phase separation (LLPS) (Laghmach *et al.*, 2020). The theory suggests that the compartmentalization of chromatin could be attributed to chromatin binding factors, such as histone modification readers, or nucleosome arrays, that have the innate tendency to undergo phase separation. LLPS of such factors may lead to a chromatin compaction gradient and the subsequent transcriptional repression (Zhang *et al.*, 2020; Demmerle *et al.*, 2023).

A potential candidate that drives heterochromatin compaction via phase separation is Heterochromatin Protein 1 (HP1). The members of the HP1 family are evolutionarily conserved proteins that are involved in the establishment and

maintenance of genome organization. Their N-terminus carries a chromatin organization modifier (chromo-box) domain (CHD) that allows them to recognize and interact with di- and trimethylated lysine 9 of histone H3 (Nielsen *et al.*, 2002), while their C-terminus contains a chromo-shadow domain (CSD), responsible for their homo- and hetero-dimerization (Smothers & Henikoff, 2000). Three isoforms are present in mammals: HP1α and HP1β, which are mainly present in heterochromatin, and HP1γ, which can be found on both euchromatic and heterochromatic loci. Constitutively heterochromatic regions of chromatin, such as centromeres and telomeres, exhibit enrichment for HP1. These proteins are also found enriched in the nuclear periphery, with their interaction with major components of the NE, such as LBR, being a possible explanation for this localization pattern (Lomberk *et al.*, 2006).

HP1 is a well-studied “reader” of the histone epigenetic modification H3K9me3 and plays a major role in the establishment of a heterochromatic state in regions that contain this modification. More specifically, HP1 recognizes H3K9me3 via its CHD and attracts methyltransferases (SUV39H1 (mammals), Su(VAR)3-9 (*D. melanogaster*)), which, in turn, add more methyl moieties on adjacent nucleosomes, thus, promoting heterochromatin spreading. Additionally, HP1 has also been found to play an active role in other cellular processes, such as DNA replication and repair and the establishment of nuclear architecture, via its interaction with proteins involved in these functions (Kwon & Workman, 2008). Interestingly, HP1 has also been reported on euchromatic areas of the genome, implying a role of transcriptional regulation in those areas too. In fact, HP1 proteins act in a context, isoform and protein-partner-dependent manner and can have an activating or repressive impact in the expression of a gene (Schoelz & Riddle, 2022).

Regarding the involvement of HP1 in chromatin compartmentalization, it has been reported that HP1 tends to form condensates in vitro (Larson *et al.*, 2017; Strom *et al.*, 2017), while ectopic targeting of HP1α on specific genomic loci can lead to condensation of the targeted regions (Li *et al.*, 2003). These findings, along with the fact that HP1 can bind to DNA strongly and that HP1a dimers may be able to interact with neighboring dimers and form oligomers, provide more evidence that support the idea of it playing a role in chromatin condensation state via LLPS (Hildebrand & Dekker, 2020).

1.3.4. Chromatin – Nuclear Lamina Relationships

Studies using Chromatin Immunoprecipitation (ChIP) and DamID protocols to investigate the principles of chromatin organization revealed specific regions of chromatin that extensively interact with the NL. These regions are referred to as Lamina-Associated Domains (LADs) and form a dense heterochromatic zone that underlines the NE (Guerreiro & Kind, 2019). It is not yet known whether LADs directly interact with the NL components or not, but the investigation of the INM proteome and the proteins that are associated with LADs revealed an overlap between the two, implying that the proteins that are common in the two compartments may act as mediators of LAD binding to the NL (Fig. 9) (Wong *et al.*, 2021). LADs are gene-poor, late replicating, A/T-rich regions of chromatin that are enriched for Long Interspersed Nuclear Elements (LINEs) and heterochromatic histone markers, such as H3K9me2/3 (Rullens & Kind, 2021). A mammalian genome can contain approximately 1100-1400 LADs, with the latter corresponding to around 40% of the whole genome (Amendola & van Steensel, 2014).

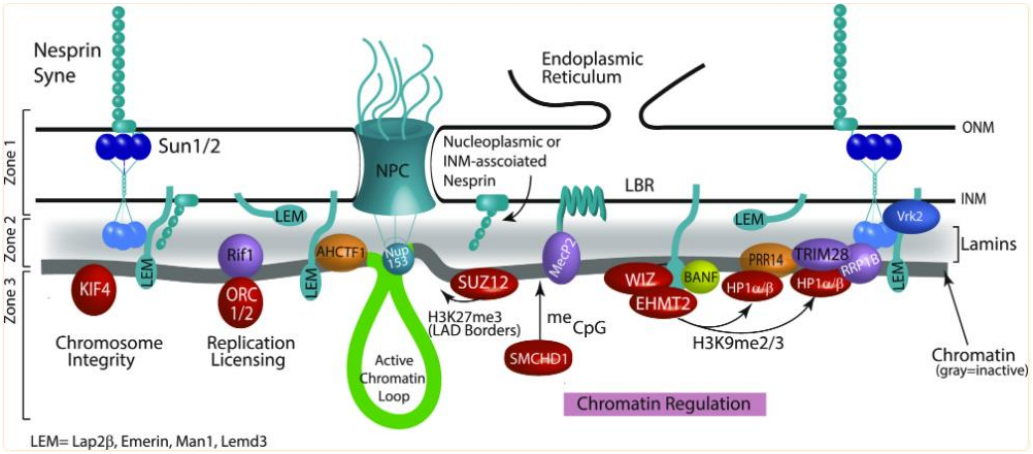

Figure 9. Depiction of a putative model of how proteins found in both the local INM and LAD proteomes (zone 1: NL proteome, zone 2: overlapping microproteome, zone 3: LAD proteome) may contribute to the maintenance of LADs in the nuclear periphery, as proposed by Wong *et al.*, 2021.

Same as chromatin, LADs can also be distinguished into two distinct categories: constitutive (cLADs) and facultative LADs (fLADs). cLADs are present in

all cell types and are mostly depleted of genes, while fLADs are cell type-specific and mainly contain developmental genes (Yánez-Cuna & van Steensel, 2017; Rullens & Kind, 2021). LADs are also highly heterogeneous. While cLADs' interactions with the NL are maintained, the subset of fLADs that contact the NL can differ from cell to cell (Briand and Collas, 2020). The heterogeneity of fLADs is reinforced by the stochastic distribution of fLADs in daughter nuclei after mitosis, when only a subset of them return to the nuclear periphery (Fig. 10) (Kind *et al.*, 2013).

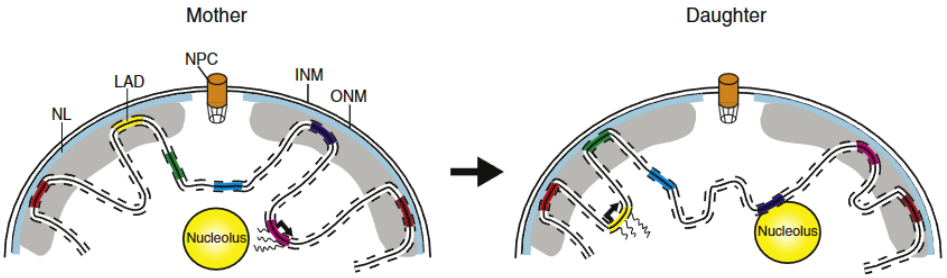

Figure 10. Graphical representation of the stochastic distribution of fLADs before and after mitotic division (Amendola & van Steensel, 2014).

The proteome of the nuclear periphery contributes to the formation of a local microenvironment, which was at first considered to be strictly repressive. However, this is not the case. Although the majority of LADs' genes are found to be repressed, there are several genes that are in a "poised state", ready to be expressed. In fact, the NL attracts transcriptional repressors, increasing their local concentration, while chromatin within the LADs is highly condensed and, thus, less accessible to chromatin related factors. Despite that, there is a fraction of genes that can move towards or from the NL, escape the repressive environment and change their expression potential. Nevertheless, detachment of a gene from the NL or translocation towards the NL does not always mean that the gene becomes activated or repressed, respectively (Briand & Collas, 2020). Actually, changing the position of a gene inside the nucleus can increase the possibility of the gene interacting with the appropriate factors that will facilitate its expression or silencing (Amendola & van Steensel, 2014).

The LAD borders are a very important feature of these domains. They are enriched for H3K27me3 and the CCCTC-binding factor (CTCF), a protein that acts as

an insulator that prevents euchromatin spreading from LAD-proximal euchromatic regions (Briand & Collas, 2020; Hoskins *et al.*, 2021). Interestingly, it has been shown that the variation observed between fLADs is mainly due to changes that occur in the LAD borders rather than in the entire LAD (Briand & Collas, 2020).

Apart from LADs and TADs, there are also other domains of chromatin that are associated with distinct nuclear compartments. Nucleoli-Associated Domains (NADs) are a great example of such domains. NADs are also heterochromatic and are in tight contact with the nucleoli surface, an interaction mediated by mechanisms that are not yet clear. NADs have been shown to overlap with fLADs. The stochastic nature of LADs may allow the shuffling of these domains between the NL and the nucleoli during the postmitotic reestablishment of chromatin architecture (Kind *et al.*, 2015). Another type of nuclear peripheral chromatin domains has recently been described: H3K9me2-Only Domains (KODs). These domains are enriched for H3K9me2, while they exhibit only limited interaction with Lamin B. They have been found to be enriched for tissue-specific enhancers that are able to escape the repressive NL environment. The histone modifications that mark these genomic loci are considered to maintain these enhancers in a poised state, allowing them to become rapidly activated when it is required and, thus, facilitating the spatiotemporal regulation of developmental genes or genes involved in differentiation (Fig. 11) (Smith *et al.*, 2021).

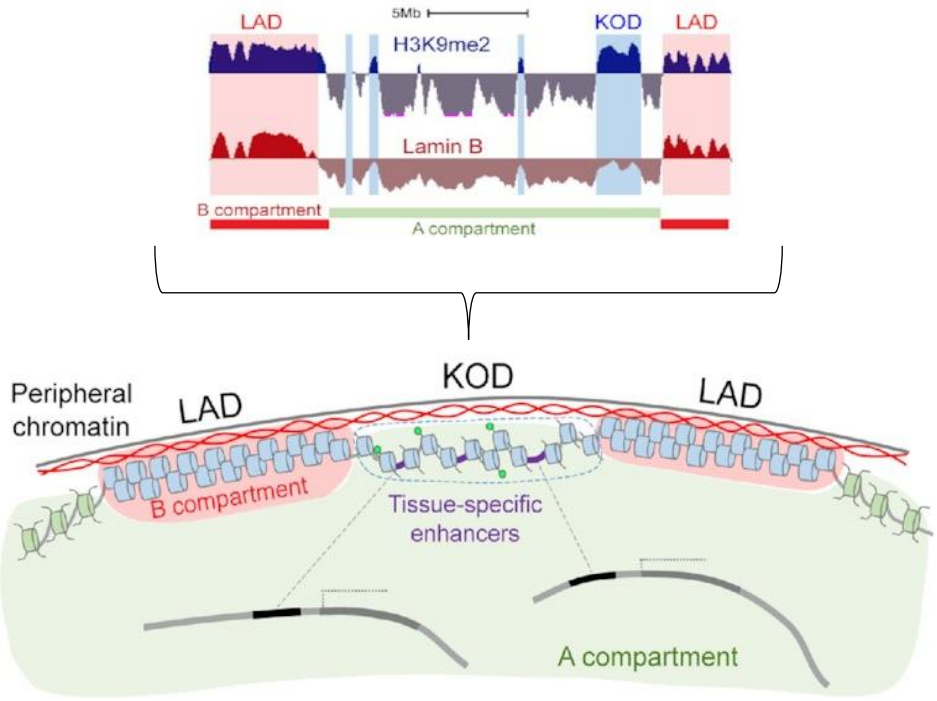

Figure 11. Graphical representation of H3K9me2-Only Domains (KODs). KODs are enriched for H3K9me2 and tissue-specific enhancers, while they display only limited contact with Lamin B (edited image, obtained by Smith *et al.*, 2021).

1.4. Proteins of the Nuclear Envelope

The nuclear envelope contains a large number of proteins with multiple and yet overlapping functions. After being synthesized in the ER, these proteins are specifically targeted to either the inner or the outer nuclear membrane. Thus, the distinct functions of the two nuclear envelope membranes are attributed to the different sets of proteins decorating each one of them (Schirmer & Foisner, 2009).

The proteins of the nuclear envelope share common domains and motifs that mediate their interaction with other components of the nuclear periphery. A very representative example of such domains is the LEM domain, a helix-loop-helix motif able to interact with chromatin via its binding of the DNA-bridging protein Barrier-to-Autointegration Factor (BAF). Its name is attributed to the three NE proteins it was firstly found to be present in: **L**amina-associated polypeptide 1/2 (Lap1/2), **E**merin and **M**an1 (Barton *et al.*, 2015). Other features of the nuclear envelope proteins include

their ability to form complexes, not only with one another, but also with nuclear lamina components, epigenetic markers, transcriptional regulators and proteins and enzymes related to chromatin, with these interactions serving the NE proteins' active role in targeting specific genomic loci to the nuclear periphery and shaping the genomic landscape (Briand & Collas, 2020; Mirza *et al.*, 2021).

1.4.1. LINC and NPC: two major features of the Nuclear Envelope

One of the most important complexes that is localized in the nuclear envelope is the Linker of Nucleoskeleton and Cytoskeleton (LINC) complex, which apart from its apparent role of connecting the inside of the nucleus with the rest of the cell, has also been found to play a role in the maintenance of NE's structural integrity. In more detail, the LINC complex is comprised of proteins that are members of two large families: SUN and KASH proteins (Jahed *et al.*, 2021). The proteins of the SUN family are transmembrane proteins of the INM with an N-terminal tail that protrudes towards the nucleoplasm where it binds the NL and chromatin-related factors, and a C-terminus that carries a SUN domain and protrudes towards the perinuclear space. These SUN domains interact with the KASH domains on the C-termini of proteins that belong to the KASH family, and which are mainly found crossing the ONM. The latter ones' N-terminal tails are found on the cytoplasmic side of the ONM, where they bind components of the cytoskeleton (Wang *et al.*, 2012). The LINC complex can thereby act as a link between the nucleoplasm and the rest of the cell, as well as its extracellular environment (Fig. 12). Via this complex, mechanical signals on the surface of the cell can be transmitted inside the nucleus where they are translated into changes in gene expression (Bouzid *et al.*, 2019).

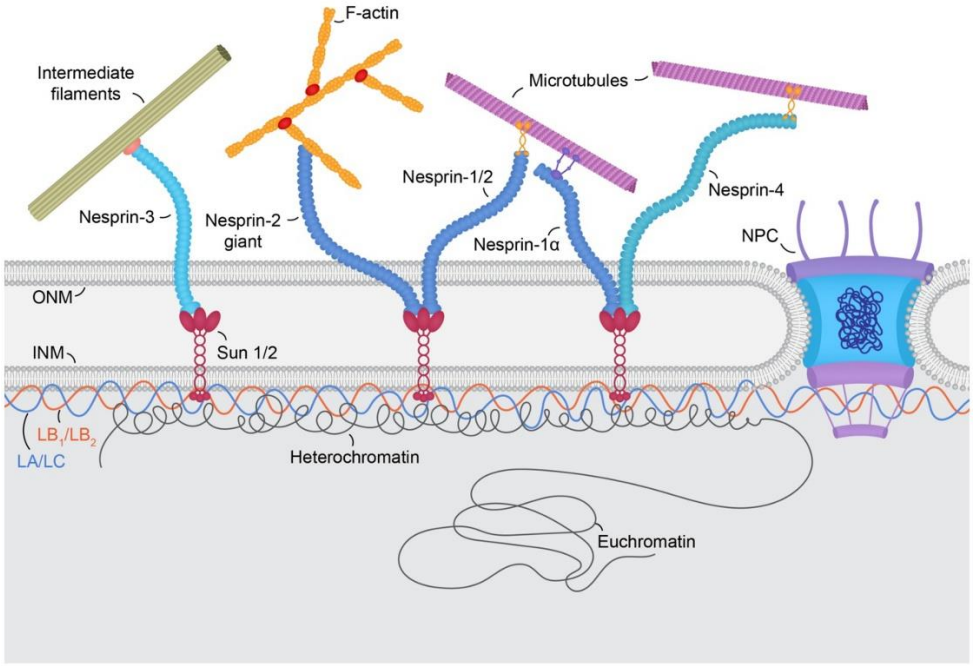

Figure 12. Schematic representation of the LINC complex. The KASH proteins of the ONM (Nesprin-1, Nesprin-2, Nesprin-3, Nesprin-4) interact with SUN protein trimers of the INM, forming bridges between chromatin and the nuclear lamina and different components of the cytoskeleton (Vahabikashi *et al.*, 2022).

Another complex of the nuclear envelope that is of high importance is the Nuclear Pore Complex (NPC), whose molecular weight can reach up to 120MDa in vertebrates. The NPC consists of a total of 30 proteins, referred to as Nucleoporins (Nups), which can form channels that run through the NE and play a rather significant role in the communication between the nuclear interior and the rest of the cell (Fig. 13) (Hoeltz *et al.*, 2011). During the last decade multiple studies have shown that apart from their regulatory role in the transport of large molecules from and to the nucleoplasm, NPCs also contribute to other nuclear processes, such as chromatin organization inside the nucleus and transcriptional regulation (Kuhn and Capelson, 2019).

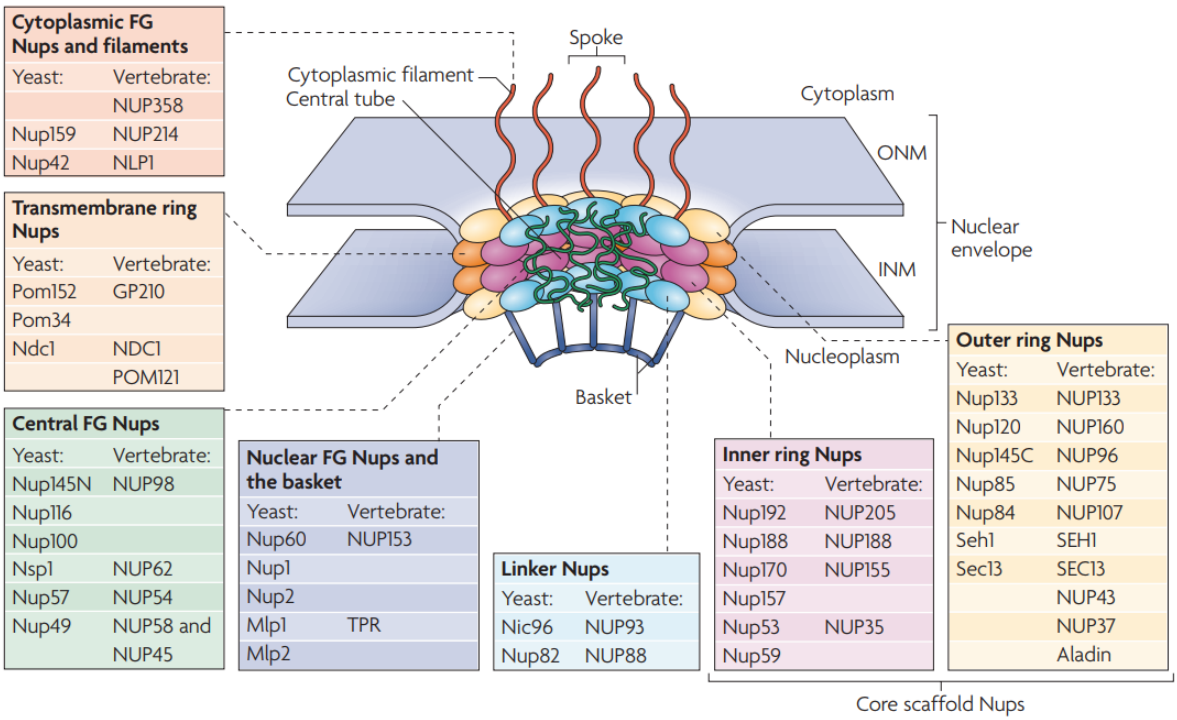

Figure 13. Schematic representation of the Nuclear Pore Complex. The individual subparts of an NPC consist of the nucleoporins shown in the corresponding tables (colour-coded) (Starmbio-De-Castillia *et al*., 2010).

Interestingly, a specific member of the SUN family, Sun1, has been found to interact with components of the NPC and is considered to participate in the NPCs' assembly in interphase nuclei (Liu *et al.*, 2007). Moreover, components of the LINC complex appear to play a role in the right localization of the NPCs on the NE (Jahed *et al.*, 2016). A similar relationship between the NPCs and proteins of the NL has also been revealed. A couple of studies have shown that upon loss of Lamin A major components of the NE exhibit asymmetric localization patterns, which also happen to coincide with abnormalities in the NE, such as areas of widened perinuclear space (Sullivan *et al*., 1999; Thanisch *et al*., 2017). Such studies pinpointed the potential functional relationships between the numerous proteins of the nuclear envelope, underlining the fact that they act cooperatively for the maintenance of NE's integrity.

1.4.2. The Lamin B Receptor, LBR

The Lamin B Receptor (LBR) is one of the most well-studied nuclear envelope proteins. It resides in the INM as a multifunctional transmembrane protein, while a fraction of it can also be found in the endoplasmic reticulum (ER), where it is composed (Holmer and Worman, 2001). LBR was first recognized in 1988 by Worman *et al*., in turkey erythrocytes, as a 58kDa protein (p58) that is localized at the NE and displays a high affinity for Lamin B. It is now known to be evolutionary conserved and expressed in all metazoans.

LBR is structurally comprised of a region that contains eight transmembrane domains, flanked by a long amino-terminal tail and a short carboxy-terminal end, both protruding into the nucleoplasm (Fig. 14) (Worman *et al.*, 1990).

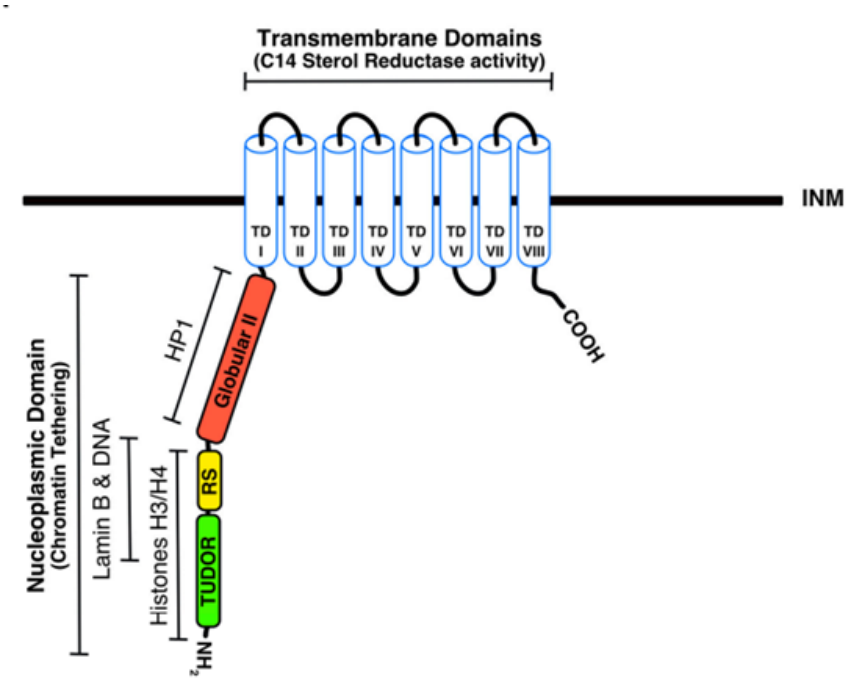

Figure 14. Schematic representation of full-length Lamin B Receptor's main domains, as well as some of its main interactors and their binding sites (edited image, obtained by Nikolakaki *et al.*, 2017).

The transmembrane segments of LBR display high homology and gene structure similarity with yeast and plant C14-sterol reductases, as well as ER enzymes

that have sterol reductase activity (Holmer *et al.*, 1998). In addition, human LBR was found to be capable of restoring the sterol biosynthetic pathway in C14-sterol reductase-defective yeast cells. These imply that LBR itself exhibits C14-sterol reductase activity as well (Silve *et al.*, 1998). Interestingly, a study in 2016 showed that LBR seems to be essential for cholesterol synthesis in human cells, despite the existence of an ER enzyme, called TM7SF2, which catalyzes the same reaction of the cholesterol biosynthetic pathway (Tsai *et al.*, 2016).

Apart from its enzymatic activity, LBR has also been found to interact with components of the nuclear periphery, a function that is mainly attributed to its amino-terminal tail. This amino-terminal tail is comprised of three distinct structural domains and serves as a docking site for other proteins of the nuclear periphery, such as the nuclear lamins and proteins related to chromatin. More specifically, these three structural components are: a Tudor domain, a region containing arginine-serine dipeptides (RS motif) and a second globular domain. The Tudor domain obtains a barrel-like structure and has been found to bind free, unmethylated histone H3 molecules, implying a potential role in histone chaperoning and nucleosome assembly (Liokatis *et al.*, 2012). Regarding the second part, it is a domain rich in RS repeats, which provides sites for phosphorylation by kinases such as SRPK1, PKA and $p34^{cdc2}$. SRPK1 is a kinase that phosphorylates RS motifs, which are commonly found in splicing factors. The phosphorylation of LBR by SRPK1 and PKA regulates its oligomerization as well as its interaction with other proteins of the nuclear periphery, via changes in its conformation, as has been shown by in silico molecular dynamics experiments (Papoutsopoulou *et al.*, 1999; Nikolakaki *et al.*, 1996; Sellis *et al.*, 2012). $P34^{cdc2}$ is a mitotic kinase that regulates LBR's phosphorylation state during the cell cycle (Nikolakaki *et al*., 1997). The RS motif has been found to be offered as a binding platform not only for lamin B, but also for H3-H4 oligomers and fully assembled nucelosomes (Liokatis *et al.*, 2012). Interestingly, the lack of ELYS, a major component of the NPC, has been found to lead to the phosphorylation of certain residues within the RS domain, causing defective LBR localization. This can be translated in a compromised nuclear envelope integrity (Mimura *et al.*, 2016). The last part of LBR's amino terminal tail is a second globular domain, which belongs to no specific conformation category. This domain has been reported as the one responsible for LBR's indirect interaction with Heterochromatin Protein 1 (HP1), which is mediated by

histone H3/H4 oligomers (Ye *et al.*, 1997; Polioudaki *et al.*, 2001). LBR can also interact with Methyl CpG-binding protein 2 (MeCP2). The relationship between these two proteins underlines the role of the nuclear envelope proteins in the maintenance of heterochromatin in the nuclear periphery and the regulation of gene silencing during cell differentiation (Guarda *et al.*, 2009).

LBR can also be modified by O-β-N-Acetylglucosaminyltransferase (OGT), an enzyme known for adding O-GlcNAc moieties on serine and threonine residues of a wide variety of proteins. The biological importance of this LBR modification is not yet clear, but what has been shown by Smet-Nocca *et al*. in a study of 2018 implies a potential crosstalk between O-GlcNAcylation and phosphorylation of LBR, which can affect its DNA-binding ability (Smet-Nocca *et al.*, 2018).

LBR's biosynthesis takes place in the ER, as was previously mentioned. Subsequently, the protein is laterally diffused across the membranes of the nuclear envelope until it reaches the INM where it is established via its interactions with other intranuclear components (diffusion-retention mechanism) (Ungricht *et al.*, 2015). Regarding LBR's mobility, it is far from homogenous, since the protein can be found not only as a free molecule in the ER and the INM, but also as a part of distinct microdomains of LBR molecules that are self-oligomerized and accumulate in the INM. Giannios et al. in 2017 showed that LBRs' dynamics are compartment-dependent, with the ER fraction of LBR being the most mobile, followed by the non-uniformly distributed LBR molecules of the INM (free molecules and microdomains) (Giannios *et al.*, 2017).

Another rather important role of LBR is the regulation of mitotic NE disassembly and post-mitotic NE reassembly. In interphase, LBR appears to be localized on the INM of the NE giving a clear nuclear rim, while a more mobile fraction of this protein is also found on the ER membranes, where its biosynthesis occurs. In mitosis, mitotic kinases phosphorylate LBR on certain residues, causing its detachment from nuclear components, that participate in its retention in the INM, thus promoting its redistribution into the ER and the NE breakdown. In late anaphase, LBR regains its DNA-binding ability and brings ER membranes in close proximity to the condensed chromatin, resulting gradually in its compartmentalization from the rest of the cell and in the NE reassembly (Ellenberg *et al*., 1997).

Taking LBR's bifunctionality into consideration, it has been proposed by Schuler *et al.* that the gene that encodes for LBR may have risen from the recombination of two distinct primordial genes, giving the protein its chimeric nature (Schuler *et al.*, 1994). In 2017 Nikolakaki *et al*. also proposed a model that could explain these characteristics of LBR. According to this provisional model, LBR takes part in the creation of lipid rafts in the INM via its sterol reductase activity. These lipid rafts are offered for the accommodation of the complexes LBR forms with other proteins of the nuclear periphery and may serve as heterochromatin docking sites on the nuclear envelope (Nikolakaki *et al.*, 2017).

Interestingly, in recent studies, LBR has been found to be causally related to cellular senescence, a cellular state characterized by irreversible growth arrest in mammalian cells. More specifically, knock-down of functional LBR seems to facilitate cellular senescence, by inducing changes in chromatin architecture, including the formation of senescence-associated heterochromatic foci (SAHF), and the loss of interaction with senescence-associated genes' (SAGs) promoters, which leads to their activation and the promotion of the senescence-associated secretory phenotype (SASP) (En *et al*., 2020; Arai *et al*., 2019; Lukášová *et al*., 2017).

1.5. Nuclear Envelope-associated pathologies

The nuclear envelope integrity and the maintenance of the genomic landscape are often compromised as a result of mutations in genes encoding for nuclear envelope and nuclear lamina components. These mutations can lead to a series of human pathological conditions, collectively termed as "nuclear envelopathies". The high number and the multifunctionality of the proteins located at the nuclear periphery are translated to an extensive spectrum of phenotypic alterations that characterize these diseases. Envelopathies are mainly tissue-specific and they have been found to affect the heart and skeletal muscles, adipose tissue and peripheral nervous system (Janin *et al.*, 2017).

An important subcategory of envelopathies is "laminopathies", a group of diseases caused by mutations in the genes encoding for Lamin A/C or proteins that interact with the nuclear lamina, for example LBR. Such mutations can lead to

muscular dystrophies, cardiomyopathies, lipodystrophies, as well as progeroid syndromes. Collectivelly, these diseases are characterized by nuclear abnormalities, including changes in the nuclear shape and the epigenetic landscape, as well as in the distribution of chromatin (Chi *et al.*, 2009; Worman, 2012). Such an example is the Hutchinson-Gilford Progeria Syndrome (HGPS), a rare progeroid syndrome caused by a mutation in the LMNA gene that leads to the production of a prelamin A variant, called progerin. On the cellular level, the accumulation of progerin leads to alterations in the heterochromatin positioning on the nuclear periphery, the epigenetic landscape, as well as gene expression (Marcelot *et al.*, 2020). On the organismal level, patients present early ageing features and usually die at an early age from cardiovascular complications (Kang *et al.*, 2018). Mutations in the LBR gene have also been associated with laminopathies in humans, such as Pelger-Huët anomaly and Greenberg skeletal dysplasia. Pelger-Huët anomaly patients who are heterozygous for LBR mutations exhibit neutrophils with hypolobulated nuclei, while for those who are homozygous for LBR mutations the phenotype appears to be much more severe. The neutrophils of these patients exhibit deformed, unsegmented nuclei and patients suffer from a wide range of defects, such as cardiac defects and cognitive impairment. Greenberg skeletal dysplasia is associated with mutations in the C-terminus of LBR and is developmentally lethal. It is considered to be a cholesterol metabolism disease, since the transmembrane domains of the protein are affected and lead to cholesterol synthesis deficiency (Nikolakaki *et al.*, 2017).

Multiple studies have been focused on gaining mechanistic insights into how mutations of the proteins of the nuclear lamina can cause the irregularities that characterize laminopathies. Two main explanations have been given so far. The first one suggests that defects of the nuclear lamina or the nuclear envelope can lead to defective gene expression profiles, underlining the role of the nuclear periphery in the regulation of transcription. The second one is based on the involvement of the nuclear lamina in mechanotransduction and signalling, proposing that abnormalities of the nuclear lamina meshwork may cause mechanical stress sensitivity. A third possible explanation could be a combination of the first two. According to this one, impaired reaction to mechanical stress can cause increased activation of stress-responsive signalling pathways, which can be translated into altered transcriptional profiles (Shin and Worman, 2020).

Although such diseases are quite rare, they provide a very helpful model for investigating the roles of the nuclear periphery in shaping the nucleus and regulating chromatin architecture and gene expression. Novel findings regarding the roles of lamins in health and disease can also find applications in the study of modern diseases such as cardiomyopathies and metabolic syndromes, as well as in the investigation of the molecular basis of tissue and organ alterations that occur during the normal aging process (Wong and Stewart, 2020).

1.6. Inverted Chromatin Architecture

Apart from the abnormalities in chromatin architecture that have been described by scientists so far in several pathological conditions, including laminopathies, chromatin landscapes that deviate from conventional nuclear architecture can also be found in nature. The most representative example of such alterations is the inverted chromatin architecture of the rod photoreceptors in the retina of nocturnal mammals (Feodorova *et al.*, 2020). The nuclei of these cells are characterized by the dissociation of heterochromatin from the nuclear periphery and its assembly in one major focus in the center of the nucleus. Specifically, in murine rod cells constitutive heterochromatin is tightly packed in a central heterochromatic core, covered by a shell of facultative heterochromatin, followed by euchromatin, which extends towards the nuclear envelope (Fig. 15) (Solovei *et al.*, 2009). This single chromocenter is characterized by high density, as well as refractivity, resembling a lens that prevents light from scattering and, thus, facilitates night vision (Solovei *et al.*, 2009; Kreysing *et al.*, 2010).

The inverted nuclear architecture is rendered disadvantageous compared to the conventional nuclei, since changes in the positioning of specific genomic loci inside the nucleus as well as changes in the accessibility of chromatin may lead to alterations in gene expression and inefficient DNA double-strand break repair (Frohns *et al.*, 2014). This may explain why chromatin inversion is only present in very specific cell types, in which it serves other purposes, such as nocturnal animals' vision in the dark.

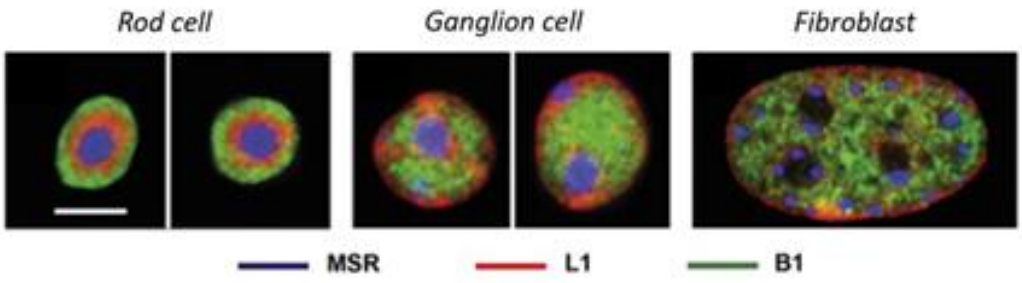

Figure 15. FISH images of three different cell types showing differences in the distribution of constitutive heterochromatin, facultative heterochromatin and euchromatin. Three probes were used for the purposes of this experiment: (1) MSR (major satellite repeats) – representative of cHC, shown in blue, (2) L1 (the major class of the long interspersed repetitive sequences) – representative of fHC, (3) B1 (the major class of the short interspersed repetitive sequences related to human *Alu* sequences) – representative of euchromatin, shown in green (edited image, obtained by Solovei *et al.*, 2009).

Mouse rod cells have been extensively used as models of this chromatin state, in studies that attempted to investigate the importance of and mechanistically explain the spatial organization of the genome. These studies revealed that there are two major peripheral tethers for heterochromatin binding to the nuclear periphery: the A- and the B- tether. The A-tether is comprised of Lamin A/C along with other proteins of the nuclear periphery with whom A-type lamins cooperate, while the B-tether refers to the Lamin B Receptor (Solovei *et al.*, 2013).

Murine rod cells lack both peripheral heterochromatin tethers: LBR and Lamin A/C. In fact, rod cells express LBR during embryogenesis and the first postnatal days. This is normally followed by LBR downregulation, which is gradually substituted by the expression of Lamin A/C, with the exception of a few terminally differentiated cell types that express both proteins. In rod cells, even though LBR expression levels are gradually declined, Lamin A/C never starts being expressed. The lack of both heterochromatin tethers leads to a global spatial chromatin reorganization that results in the complete inversion of chromatin (Fig. 16A) (Solovei *et al.*, 2013). Similar alterations in chromatin architecture have also been reported for other cell types, such as mouse olfactory neurons. In this type of cells, downregulation of LBR during differentiation coincides with the partial merging of chromocenters and the positioning

of certain alleles in specific locations in the nucleus, which will determine if they are going to be expressed or not. However, the initiation of Lamin A/C expression allows these cells to maintain the conventional chromatin landscape (Fig. 16B) (Clowney *et al.*, 2012).

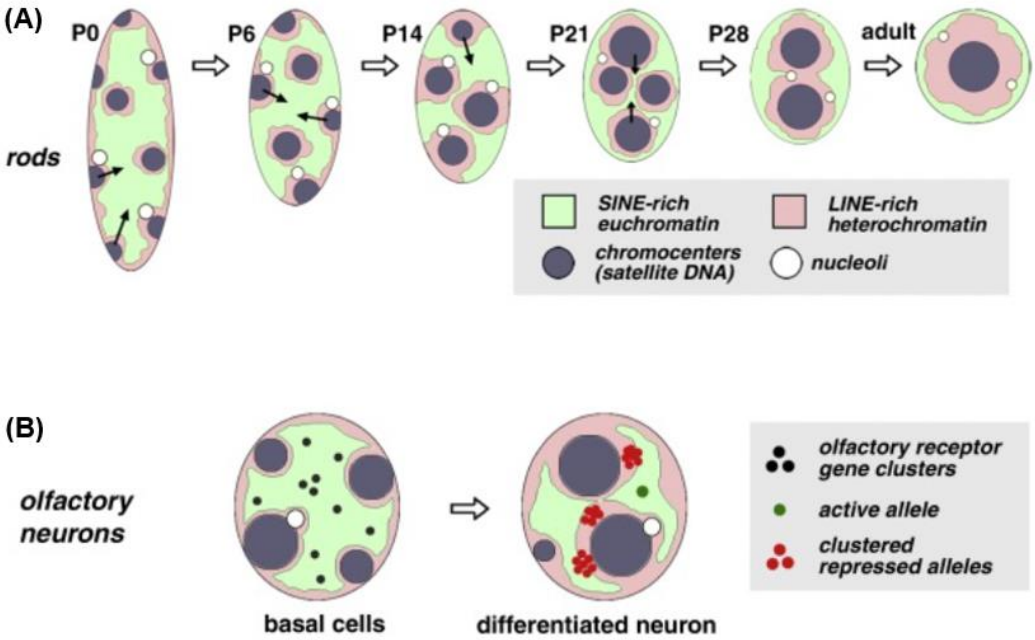

Figure 16. Schematic representation of the alterations in chromatin organization, as they occur during the differentiation of (A) mouse rod cells, (B) mouse olfactory neurons (edited image obtained by Solovei *et al.*, 2016).

Interestingly, studies have shown that nuclei of LBR-null mice that do not normally express Lamin A/C are inverted, while nuclei of cells derived from Lamin A/C-null mice that do not endogenously express LBR can be either inverted or conventional. Moreover, ectopic expression of LBR in mouse rod cells can rescue the inverted phenotype. On the other hand, ectopic expression of Lamin A/C in this cell type cannot fully restore the conventional nuclear architecture. These findings imply that the A-tether's heterochromatin binding ability also depends on Lamin A/C's partners, which may not be expressed themselves in mouse rod cells (Solovei *et al.*, 2013). Despite the continuous research on the field of chromatin inversion, these A-type lamins' partners have not been recognized to date. Also, the mechanism through

which chromatin inversion occurs as well as the conditions under which it occurs remain to be elucidated.

Aim

The main goal of this study was to investigate the role of major components of the nuclear envelope and the nuclear lamina in the maintenance of nuclear integrity and the regulation of chromatin architecture. The interest was focused on the phenotypes generated in NIH/3T3 mouse fibroblasts upon loss of LBR and/or Lamin A/C regarding the nuclear envelope properties and chromatin dynamics, as well as on the mechanistic aspects of these effects. More specifically, this work aimed to:

i. Investigate how major components of the nuclear periphery behave upon loss of LBR and/or Lamin A/C.

ii. Assess whether there are any alterations regarding the chromatin landscape and dynamics in the cells that lack LBR and/or Lamin A/C.

iii. Examine how cell motility and migration ability might be affected in the absence of LBR and/or Lamin A/C.

Materials & Methods 

2. Materials and Methods

2.1. Experimental model

All experiments were conducted in NIH/3T3 cells. NIH/3T3 LBR KO, LMNA KO, LBR-LMNA DKO and LMNA-LBR DKO stable cell lines were generated using the CRISPR/Cas9 gene editing technology and characterized by other members of the lab (Martzios Panagiotis, Soupsana Katerina, Tassou Vassiliki).

2.2. Cell Culture

NIH/3T3 cells were cultured in Dulbecco's Modified Eagles Medium (DMEM)–high glucose with sodium pyruvate (Gibco, 41966-029), supplemented with 2mM L-glutamine (Biosera, MS014N100P), 2mM penicillin/streptomycin (Biosera, MS012B100A) and 10% or 15% fetal bovine serum (FBS) (Gibco, 10270-106). Cells were kept in an incubator with the appropriate humidity at 37^{o}C, supplemented with 5% CO_2. They were split approximately every 2 days, when they reached a confluency percentage of 80%. This procedure included rinsing cells twice with Dulbecco's Phosphate Buffered Saline (DPBS) (Biosera, MS018S1002) and detaching them using a Trypsin/EDTA solution (Biosera, MS00WA100M), diluted in PBS (1:2). Trypsin was deactivated by the addition of fully supplemented growth medium and the appropriate amount of cells were seeded into new cell culture dishes. For long-term storage, cells were detached from the plate as above, centrifuged at 1000 rpm for 3 minutes and resuspended in Freezing Medium, which contained 30% v/v FBS and 10% v/v Dimethyl-Sulfoxide (DMSO) in DMEM. They were then transferred into cryovials, slowly frozen down at -80^{o}C and stored in liquid nitrogen. Cells were recovered from the liquid nitrogen by quickly being thawed in a 37^{o}C waterbath. Fresh warm medium was added and they were transferred into cell culture dishes. All cell lines were regularly tested for mycoplasma contamination.

2.3. Plasmids

All plasmids used in this work were designed and constructed by other members of the lab (Soupsana Katerina) using standard cloning procedures. The constructs used for the rescue experiments were the following: pEGFPN1-huLaminA (Fig. 17), pEGFPN3-huLaminB1 (Fig. 18) and pEGFPN2-mLBR (Fig. 19). pPycagip-eGFP-huHP1a (Fig. 20) was used for FRAP experiments.

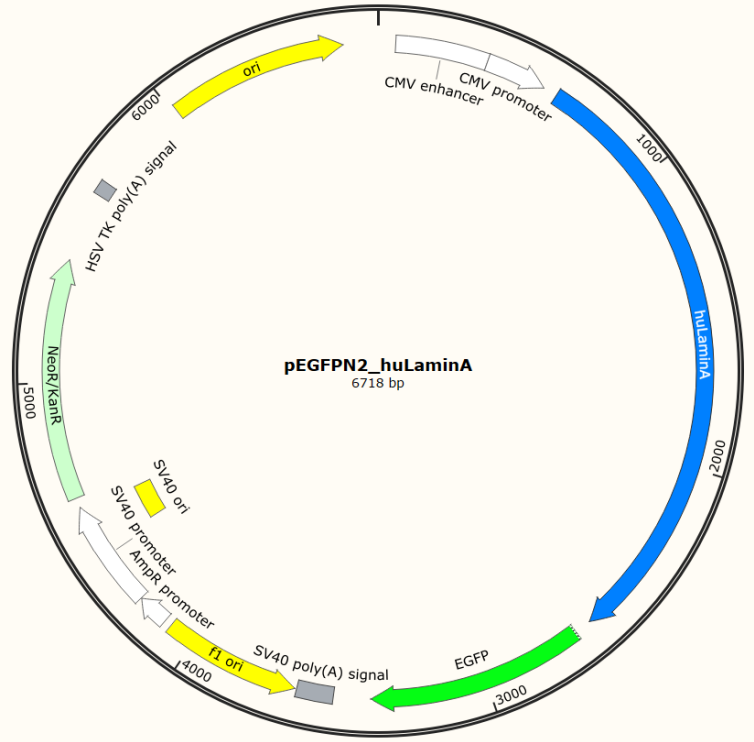

Figure 17. pEGFPN2-huLaminA plasmid map.

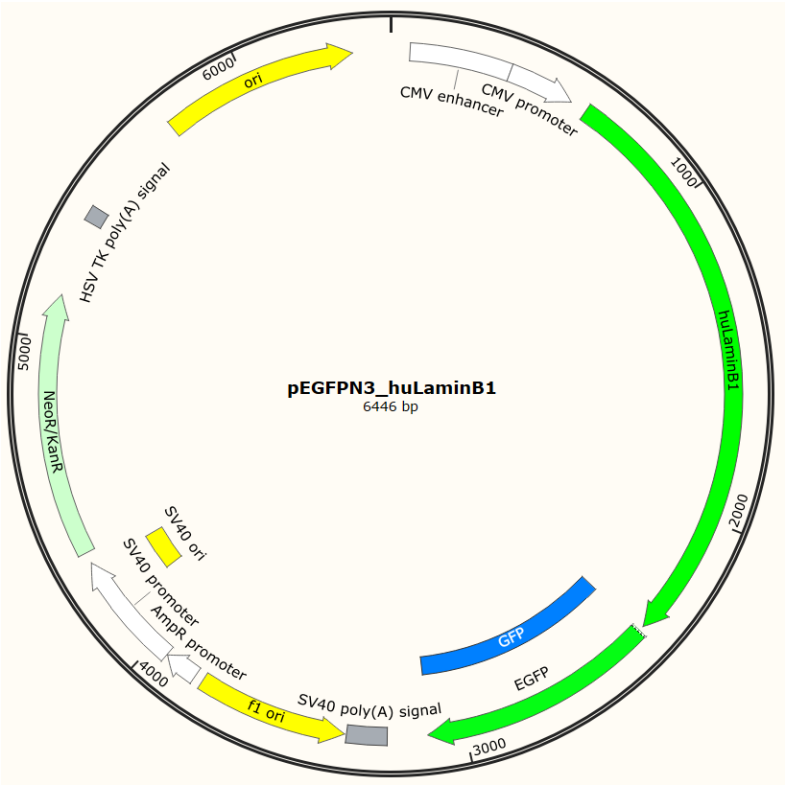

Figure 18. pEGFPN3-huLaminB1 plasmid map.

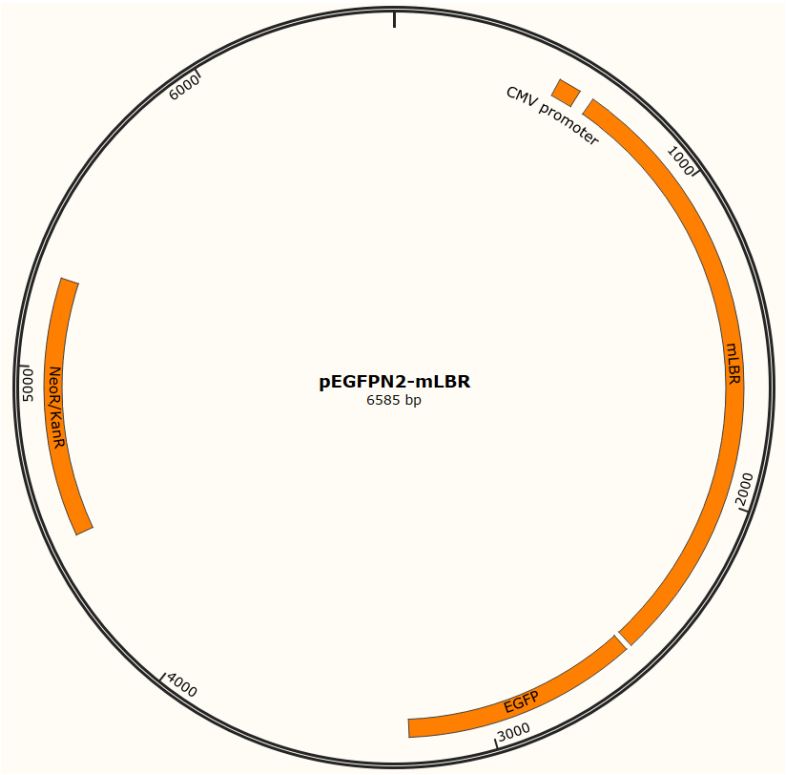

Figure 19. pEGFPN2-mLBR plasmid map.

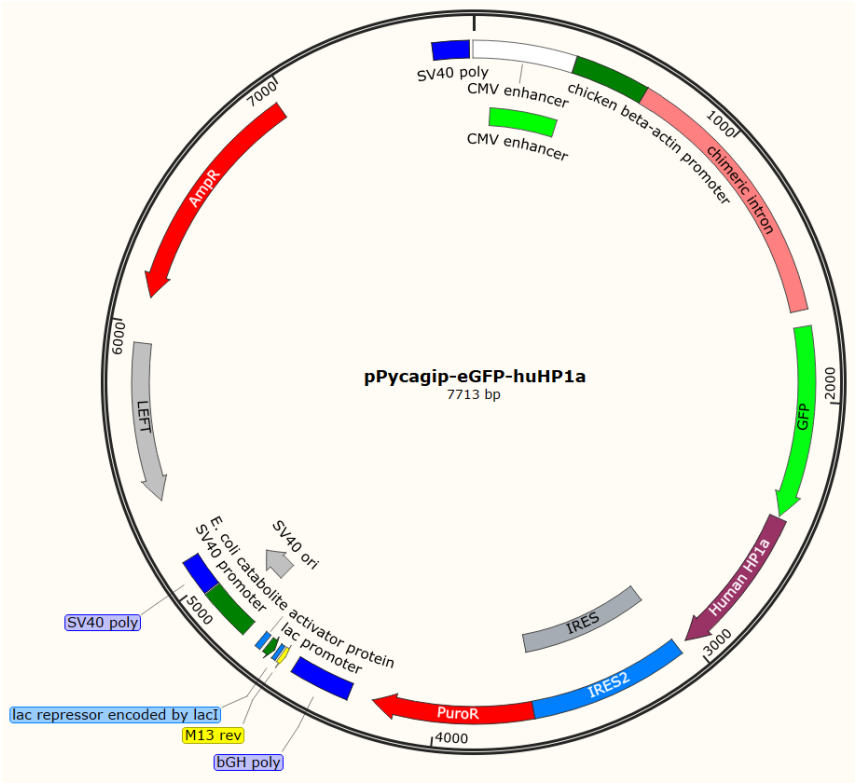

Figure 20. pPycagip-eGFP-huHP1a plasmid map.

2.4. Plasmid Isolation

Plasmids were isolated using the NucleoBond Xtra Midi kit (Macherey-Nagel 740410.50).

2.5. Transfection

Transfection of NIH/3T3 cells was performed using polyethyleneimine (PEI). PEI is a synthetic polymer that can form complexes with the negatively charged DNA backbone, due to its positive nature, and introduce it to the cells by endocytosis. More specifically, 2 ug of plasmid DNA (for a 35mm dish) were diluted in 25ul of free DMEM (Mix 1) and 0.9ul of working PEI solution (9ul PEI in 500ul sterile cell culture water (Biosera, MS00Q2100A)) were diluted in 75ul free DMEM (Mix 2). Mix 1 and Mix 2 were combined in a third tube, mixed by pipetting and incubated for 30min at room temperature. Cells were seeded the previous day so that the day of the transfection

they had reached approximately 50% confluency. Their medium was changed immediately before the transfection procedure. For a 35mm dish, 1ml fresh fully supplemented growth medium was used. Mix 3 was added dropwise. An incubation of 4.5 hours at 37ºC followed. At the end of the incubation period, the medium was changed again. This time, 2 ml of fresh fully supplemented growth medium was added to the cells and they were incubated for 24-48hrs at 37ºC, depending on the experiment.

2.6. Indirect Immunofluorescence

Cells were grown on glass coverslips (#N1.5) until they reached the desired confluency. Then, they were rinsed three times with PBS and fixed for 5-10min at room temperature using a fixation solution containing 1-4% formaldehyde (FA) diluted in PBS. The concentration of the FA and the duration of the incubation depended on the antibody used. The fixation step was followed by two washes with PBS and an incubation with Quench buffer (0.07gr glycine in 50ml PBS) for 10min at room temperature. Samples were rinsed again once with PBS and they were permeabilized and blocked with Blocking Buffer (150mM NaCl, 20mM Hepes pH 7.4, 2mM MgCl2, 0.5% Fish Skin Gelatin, 0.2% Triton-X100, 0.1mM EGTA) for 15min at room temperature. Then, primary antibodies, diluted in blocking buffer, were added to the samples for 1hr at room temperature in a humified chamber, protected from light. Samples were washed three times with blocking buffer, leaving the last wash for 15min at room temperature. Secondary antibodies were added, incubated and removed as above. A rinsing step with PBS followed and samples were incubated with a TO-PRO-3 iodide (642/661) solution (Invitrogen, T3605) (diluted 1:10000 in PBS) for 1hr at room temperature, protected from light. Finally, samples were again rinsed five times with PBS and mounted on slides using an antifading mounting medium (Vectashield, H-1000). Samples were stored till examined at 4ºC, protected from light. All details regarding the antibodies used can be found in tables 1 and 2. All antibodies were previously tested for specificity and optimum fixation and dilution conditions.

Table 1. Primary antibodies.

Antibody	Species	Dilution	Fixation	Reference
a-LMNB2	Rabbit	1:200	1% FA, 10min	ProteinTech 10895-1-AP
a-Nesprin3	Rabbit	1:200	1% FA, 10min	ProteinTech 27132-1-AP
a-Nups	Mouse	1:500	1% FA, 10min	Millipore, MABS1267
a-TMPO	Rabbit	1:100	1% FA, 10min	ProteinTech 14651-1-AP

Table 2. Secondary antibodies.

Antibody	Dilution	Reference
Anti-Rabbit IgG, Alexa Fluor 488	1:400	Invitrogen A11008
Anti-Mouse IgG, Alexa Fluor 568	1:400	Invitrogen A11004

2.7. Confocal Microscopy

Unless stated otherwise, all images were acquired with a Leica SP5 TCSII confocal microscope using Argon laser at 10% of the maximum intensity, Diode-pumped solid-state laser (561nm), HeNe laser (633nm) and an HCX PL APO CS 63X/1.4 oil or an HCX PL APO CS 100X/1.4 oil objective. Bidirectional scanning with a speed of 400Hz was applied and the sequential image acquisition mode was used. Images were obtained as Z-stacks with 0.42um intervals and the line average was set as 2 or 4 (depending on the observed sample). The image analysis was 512 x 512 pixels. All confocal images were edited using LAS X, Adobe Photoshop CC 2015 and Fiji software.

2.8. Fluorescence Recovery After Photobleaching (FRAP)

2.8.1. Experimental procedure

FRAP experiments were conducted on a Leica SP5 TCSII confocal microscope using the Argon laser at 10% of the maximum power and an HCX PL APO CS 63X/1.4 oil objective. Pinhole and zoom factor were adjusted to 1.57 Airy Units and 10-12, respectively. Image analysis was set at 256x256 pixels (8bit). The 488nm laser line was at 15%, with an emission detection range of 500-550nm. The regions of interest (ROIs) were circular, 1um diameter, and they were bleached using the 488nm laser line at 100% of the maximum power. Bidirectional scanning with a speed of 1400Hz was applied. Fifty images (one image every 0.113s) were taken before three bleach pulses (one every 0.113s) were performed. After bleaching, 350 images were taken every 0.113s. At the end of the experiment, the following ROIs were also recorded: a) unbleached ROI (unfrap)- a circular ROI of 1um diameter in a similar region, b) the whole nucleus and c) background - a circular ROI of 1um diameter outside of the nucleus. Samples were kept at a constant temperature of 37°C and their medium was changed to Minimum Essential Eagle's Medium (Sigma Aldrich, M3024).

2.8.2. FRAP data analysis

The raw FRAP data were corrected for background fluorescence and photobleaching, by subtracting the background fluorescence intensity (F_{bk}) from the bleached ($F_{frap}(t)$) and the unbleached ($F_{unfrap}(t)$) region intensity for each time point and calculating the corrected fluorescence signal ($F_{corrected}(t)$) for each time point by:

$$Fcorrected(t) = \frac{Ffrap(t) - Fbk}{Funfrap(t) - Fbk}$$

(Kang et al., 2012).

The corrected data were then normalized into a 0-1 scale, using the following equation:

$$F(t) = \frac{Fcorrected(t) - F0}{Fi - F0}$$

Where F_0 is the postbleach initial fluorescence intensity and F_i corresponds to the average prebleach fluorescence intensity (Kang et al., 2015).

For the quantitative analysis of FRAP data several parameters had to be calculated. For this purpose, the normalized fluorescence intensities within the bleached ROIs were plotted as a function of time. The half time of recovery $t_{1/2}$ was readily extracted from the resulting fluorescence recovery curves, as the time required for a bleached spot to reach half of the steady state fluorescence intensity (plateau). The mobile fraction (*Mf*) of the fluorescently labelled protein corresponds to the plateau of the fluorescence recovery curve and was calculated as the average of the last 100 out of the 350 normalized postbleach fluorescence intensities of the bleached spot (postbleach steady state fluorescence intensity).

The diffusion coefficient (*Da*) for each bleached focus was calculated as proposed by Kang et al.:

$$Dconfocal = \frac{rn\text{^}2 + re\text{^}2}{8 * t1/2}$$

Where r_n is the nominal radius of the bleached spot as defined by the user (in this case r_n=0.5um) and r_e is the effective radius of a postbleach profile (here r_e=0.5755um, as determined by colleagues in previous experiments) (Kang et al., 2012).

The mean, the standard deviation and the coefficient of variation (CV) for each variable were calculated. All outliers were identified by calculating the Mahalanobis distance and removed from the data sets. The remaining data were plotted in violin plots in order to compare the mean and the distribution of data around the mean between each data set.

2.9. Wound Healing Assay

2.9.1 Experimental procedure

For the wound healing assay, cells were seeded onto 24-well cell culture dishes and incubated at 37^{o}C until they reached a confluent monolayer. Then, a cell-free gap was created by scratching the monolayer with the sharp end of a 200ul pipette tip. After the generation of wounds, cells were transferred at the IncuCyte ZOOM 2016B environmental chamber and they were incubated under standard conditions. Cells were monitored for a total of 48 hours using the IncuCyte ZOOM 2016B software. Photos of the cell-free areas were obtained at 2-hour time intervals (4 photos per well) using the phase contrast mode and the 4x objective. Five independent experiments were conducted for each clone. The images obtained were edited using Adobe Photoshop CC 2015 and the cell-free area of each time point was measured using the Fiji software.

2.9.2. Wound Healing assay data analysis

The analysis of the data obtained by the wound healing assay was performed as proposed in a paper published by Jonkman et al. in 2014. The cell free areas were measured by manually drawing lines along the leading edges of each cell front using the free-hand tool of Fiji software (Fig. 21).

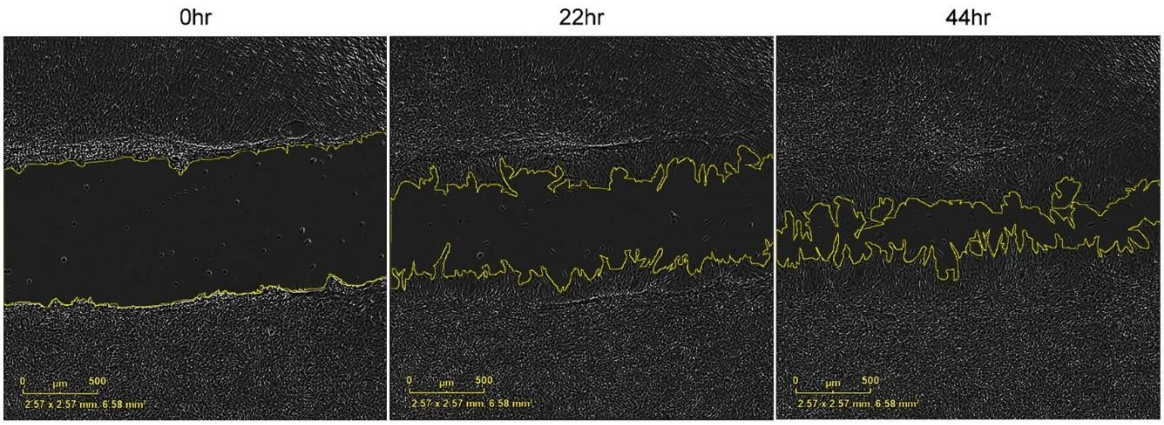

Figure 21. Representative images of the selected gap area (yellow line) that is measured over time (3 distinct time points), using Fiji software (scalebar: 500um).

The measurements of the gap area were then plotted as a function of time and the general equation of the trendline of the plotted values was generated:

$$A(t) = mt + b$$

Where A(t) is the gap area at each timepoint, m is the slope of the line and b corresponds to the initial gap area (t=0).

To determine the velocity at which cells migrate towards the cell free area, the following equation was used:

$$Vmigration = \ (|slope|)/(2\ x\ l)$$

Where l is the length of the gap area. The equation above was used assuming the following:

- $\mathrm{slope} = \mathrm{dA/dt}$
- $\mathrm{Initial\ Gap\ Area} = \mathrm{w\ x\ l}$ (where w is the width of the gap (Fig. 22))
- $\mathrm{dA/dt} = \mathrm{l\ x\ dw/dt}$ (Length is constant since cells do not migrate in from the edges of the wound)
- $\mathrm{dw/dt} = 2\ \mathrm{x\ Vmigration}.$

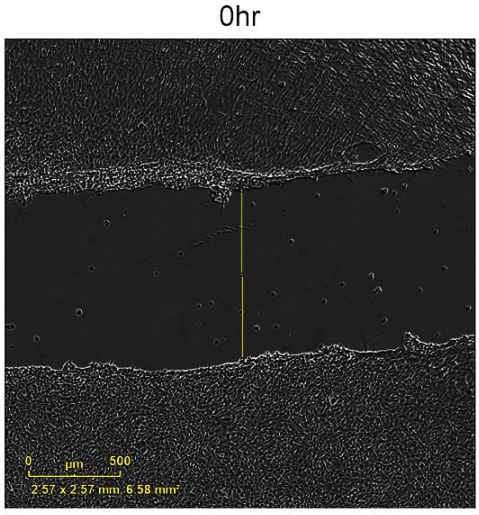

Figure 22. Representative image showing how the width of the initial gap area (yellow line) is measured, using Fiji software (scalebar: 500um).

2.10. Statistical Analysis

Statistical analysis of the data was performed by Gerta Qamili (Dr. Mpatsidis group, Department of Mathematics, University of Ioannina) and Soupsana Katerina. The statistical tests that were used and the calculated p-values can be found in Tables A1 – A5 in the Appendix section. Asterisks are used in the various plots that follow to indicate the statistical significance (*: $p<0.05$, **: $p\leq0.01$, ***: $p\leq0.001$).

Results 

3. Results

Background of the work

This work is part of a long-term project undertaken by Dr. Politou's laboratory. For the purposes of this project, the following stable cell lines of NIH/3T3 cells were generated by Soupsana Katerina, Martzios Panagiotis and Tassou Vassiliki, using the CRISPR-Cas9n technology (Fig. 23):

- LMNA Knock-Out
- LBR Knock-Out
- LMNA-LBR Double Knock-Out
- LBR-LMNA Double Knock-Out

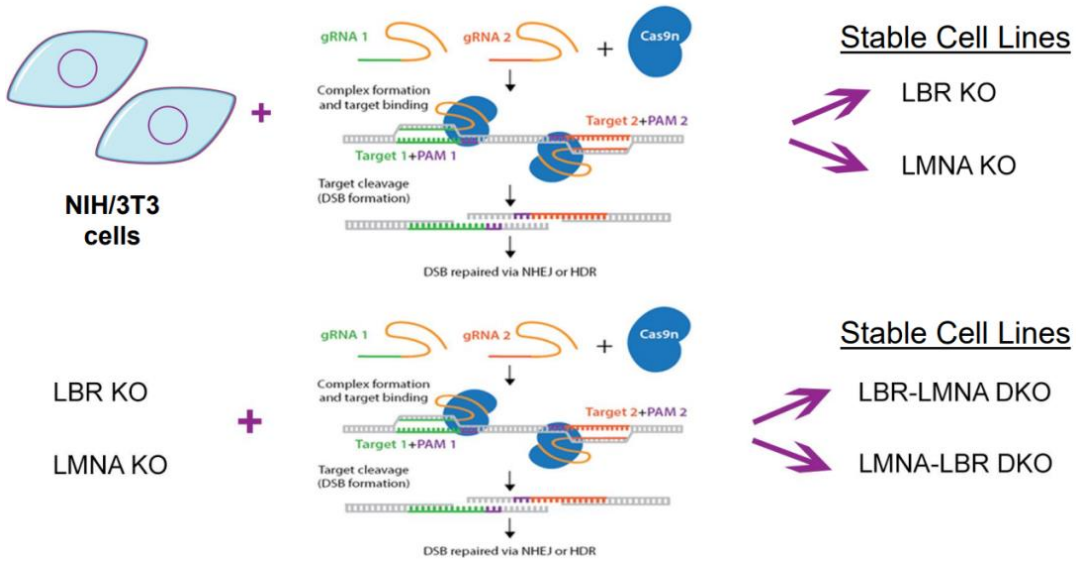

Figure 23. Schematic representation of the experimental design for the generation of stable cell lines (NIH/3T3) that do not express LBR and/or Lamin A/C, using the CRISPR-Cas9n gene editing technology.

Two clones from each cell line were studied in experiments that followed the cell line construction (LMNA KO1, LMNA KO2, LBR KO1, LBR KO2, LMNA-LBR DKO1, LMNA-LBR DKO2, LBR-LMNA DKO1, LBR-LMNA DKO2), along with their

respective controls (NIH WT 10% FBS, NIH WT 15% FBS). All six clones that lack LBR exhibited a very low growth rate compared to the rest of the clones, and, thus, they were cultured in growth medium with a higher FBS concentration (15% FBS). This required the additional use of wild-type cells that were being cultured under the same conditions as a control for these clones. The successful depletion of Lamin A/C and LBR in each case was confirmed by Western blot and immunofluorescence experiments with antibodies against the two proteins of interest, while the mRNA levels for each protein were also assessed by qRT-PCR. Moreover, the precise deletion caused in the LBR and LMNA genes by the CRISPR-Cas9n technology was identified using amplicon sequencing.

The characterization of the single KO and double KO clones started with the estimation of their growth rate. LBR KO, LBR-LMNA DKO and LMNA-LBR DKO clones appeared to grow slower compared to the LMNA KO clones and the wild-type controls. At the same time, the estimation of the mitotic index and the percentage of cells at each cell cycle stage (measured by FACS) revealed no significant differences between the clones tested.

The morphology of cells was mainly assessed by indirect immunofluorescence experiments, in which antibodies that recognised major components of the nuclear periphery were used. The assessment of these samples by confocal microscopy revealed alterations in the distribution of proteins located at the nuclear periphery as well as of main euchromatic and heterochromatic epigenetic markers. More specifically, a significant percentage of cells among the LMNA KO, LMNA-LBR DKO and LBR-LMNA DKO cell populations exhibited an uneven distribution of several protein markers of the nuclear periphery (all tested markers can be found in Table A6 in the Appendix section) (Fig. 24 and Fig. 25).

Concurrent labelling of nuclei with more than one protein revealed a tendency for the markers to follow the same pattern of uneven distribution in the affected nuclei. This phenotype was called “asymmetric” and appeared with a higher frequency in the LMNA-LBR DKO and LBR-LMNA DKO clones and with a lower frequency in the LMNA KO clones, while it was quite rare among the LBR null cells.

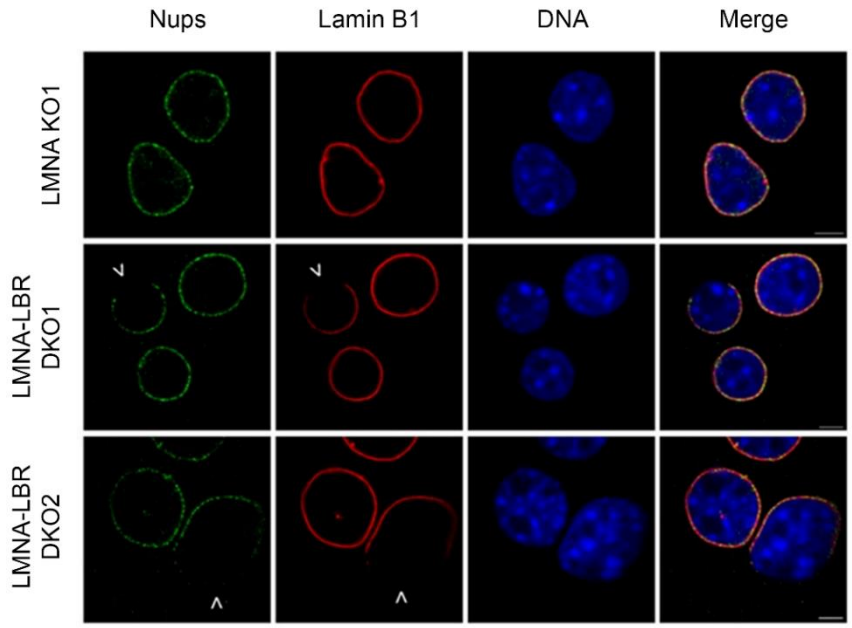

Figure 24. Indirect Immunofluorescence images of LMNA KO and LMNA-LBR DKO nuclei labelled with antibodies against Nups and Lamin B1 (DNA staining: TOPRO-3, scalebar: 5um). The DKO nuclei exhibit asymmetric distribution of the two markers tested (by Martzios Panagiotis).

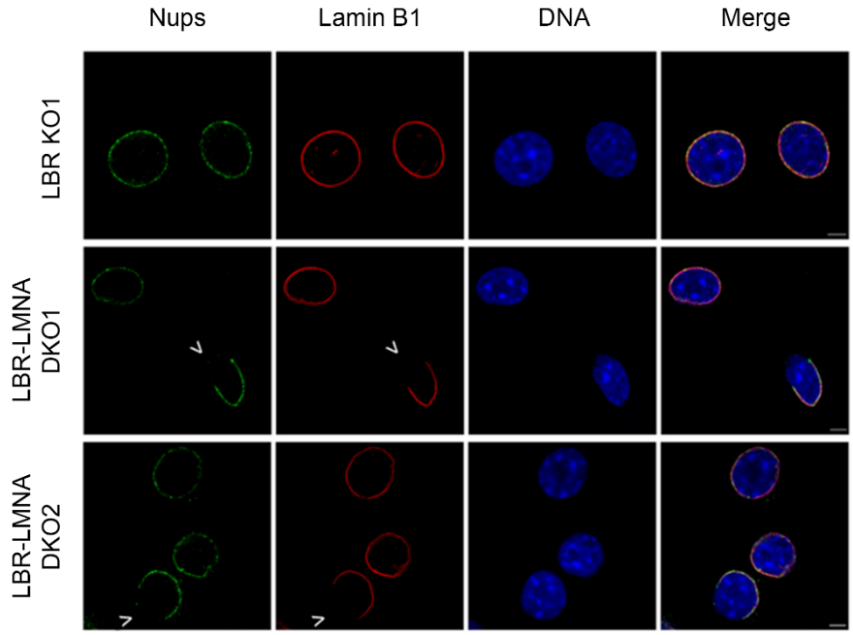

Figure 25. Indirect immunofluorescence images of LBR KO and LBR-LMNA DKO nuclei labelled with antibodies against Nups and Lamin B1 (DNA staining: TOPRO-3, scalebar: 5um). The DKO nuclei exhibit asymmetric distribution of the two markers tested (by Martzios Panagiotis).

The chromatin markers tested so far showed deviations from their normal distribution, that were mostly apparent in the DKO clones. Briefly, the heterochromatin proteins HP1α and HP1γ exhibited normal distribution in the single LBR or LMNA KO clones, while all the DKO clones (both LMNA-LBR and LBR-LMNA DKO) exhibited a decreased number of heterochromatic foci, compared to the respective control cell populations (Fig. 26). These were only preliminary observations supported by an overall visual assessment of the respective microscopic images, but no quantitative data had been obtained at that point.

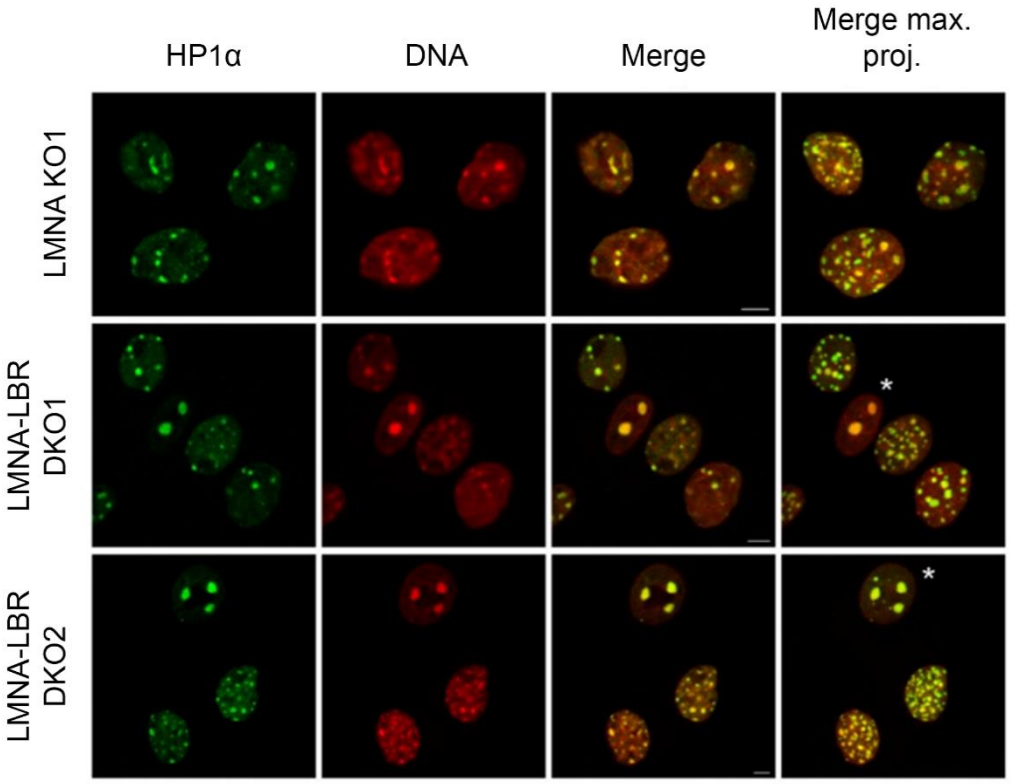

Figure 26. Indirect immunofluorescence images of LMNA KO and LMNA-LBR DKO nuclei labelled with an antibody against HP1α (DNA staining: TOPRO-3, scalebar: 5um). Asterisks mark the nuclei that exhibit a decreased number of heterochromatic foci. Similar observations have also been made for the clones that belong to the LBR-LMNA DKO cell line (by Martzios Panagiotis).

All these preliminary observations raised more questions regarding the causal relationship between loss of LBR and/or LMNA and the nuclear aberrations that had

been observed, as well as the way chromatin is affected upon loss of these two major heterochromatin tethers of the nuclear periphery.

3.1. Loss of LBR and/or Lamin A/C causes abnormal localization of major components of the nuclear periphery.

In the context of the present thesis, a thorough morphological analysis of the mutant clones was performed by conducting indirect immunofluorescence experiments using antibodies that recognize proteins of the nuclear envelope and the nuclear periphery.

Initially, all clones were concurrently labelled with antibodies against the nuclear pores and Lap2 (TMPO- Lap2α, Lap2β, Lap2γ isoforms). The antibody used against the nuclear pores identifies the Phenylalanin - Glycin repeats (FG-repeats) that are present in most of the nucleoporins of the NPC, ensuring that it captures the whole complex rather than single nucleoporin molecules. Lap2β and Lap2γ are transmembrane proteins of the INM whereas Lap2α is present in the nucleoplasm where it interacts with Lamin A. The transmembrane Lap2 isoforms form a distinguishable nuclear rim. Thus, as it becomes quite apparent from figures 27 and 28, Lap2 exhibits asymmetric nuclear envelope localization in the LMNA-LBR and LBR-LMNA DKO clones, while this phenomenon is not common among the single LBR or LMNA KO and wild-type cells. Nevertheless, the INM parts that seem to lack these proteins coincide with the parts of the NE where nuclear pores are also absent, in agreement with previous observations by colleagues (Martzios P.), regarding different combinations of NE markers.

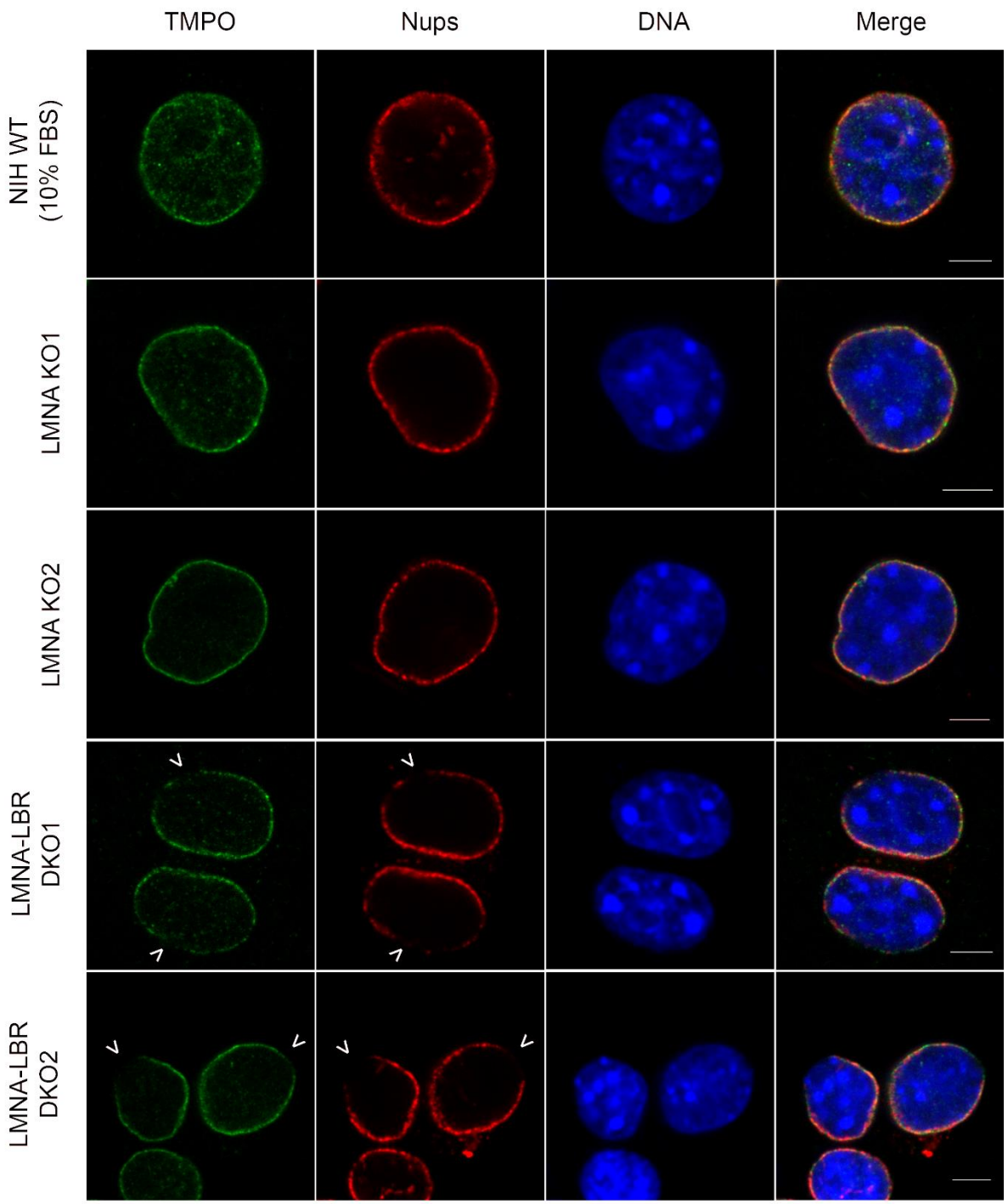

Figure 27. Indirect immunofluorescence images of NIH WT, LMNA KO and LMNA-LBR DKO nuclei labelled with antibodies against all three Lap2 isoforms and Nups (DNA staining: TOPRO-3, scalebar: 5um). Arrows indicate the parts of the NE from which both Lap2 and the NPCs are excluded.

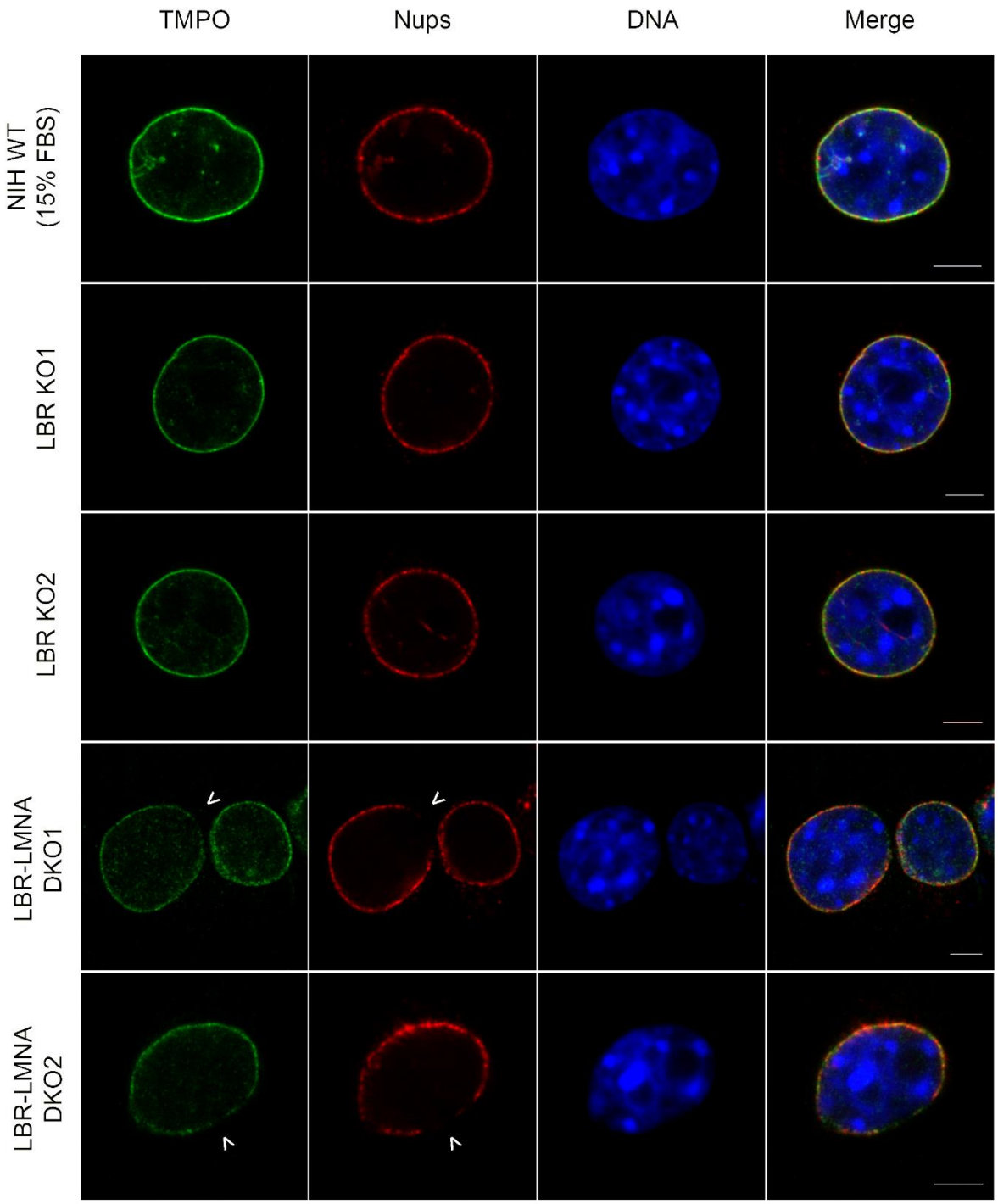

Figure 28. Indirect immunofluorescence images of NIH WT, LBR KO and LBR-LMNA DKO nuclei labelled with antibodies against all three Lap2 isoforms and Nups (DNA staining: TOPRO-3, scalebar: 5um). Arrows indicate the parts of the NE from which both Lap2 and the NPCs are excluded.

.

The phenomenon of asymmetric distribution of major components of the nuclear periphery, that has been observed with a high frequency in all four LMNA-LBR and LBR-LMNA DKO clones, could be attributed to a discontinuity or another type of morphological abnormality of the nuclear envelope membrane system. For this reason, it was considered useful to also investigate how a protein of the ONM behaves upon loss of LBR and/or Lamin A/C. For this purpose, Nesprin 3 was chosen. Nesprin 3 is a member of the KASH family and participates in the formation of the LINC complex. Cells of all clones were concurrently labelled with antibodies against Nesprin 3 and the nuclear pores, in order to detect the localization of the former in asymmetric cells. Interestingly, this protein was also found to frequently exhibit asymmetric localization in the LMNA-LBR and LBR-LMNA DKO clones, following the same distribution pattern as the NPCs (Fig. 29 and Fig. 30). The uneven distribution of all the markers that have been tested so far, regardless of whether they are localized in the INM (Lap2), the ONM (Nesprin 3), the nuclear pore membrane (NPCs) or the nuclear lamina (B-type lamins), could mean that loss of LBR and Lamin A/C affects the total set of membranes that comprise the NE, yet in a way that is still not clear.

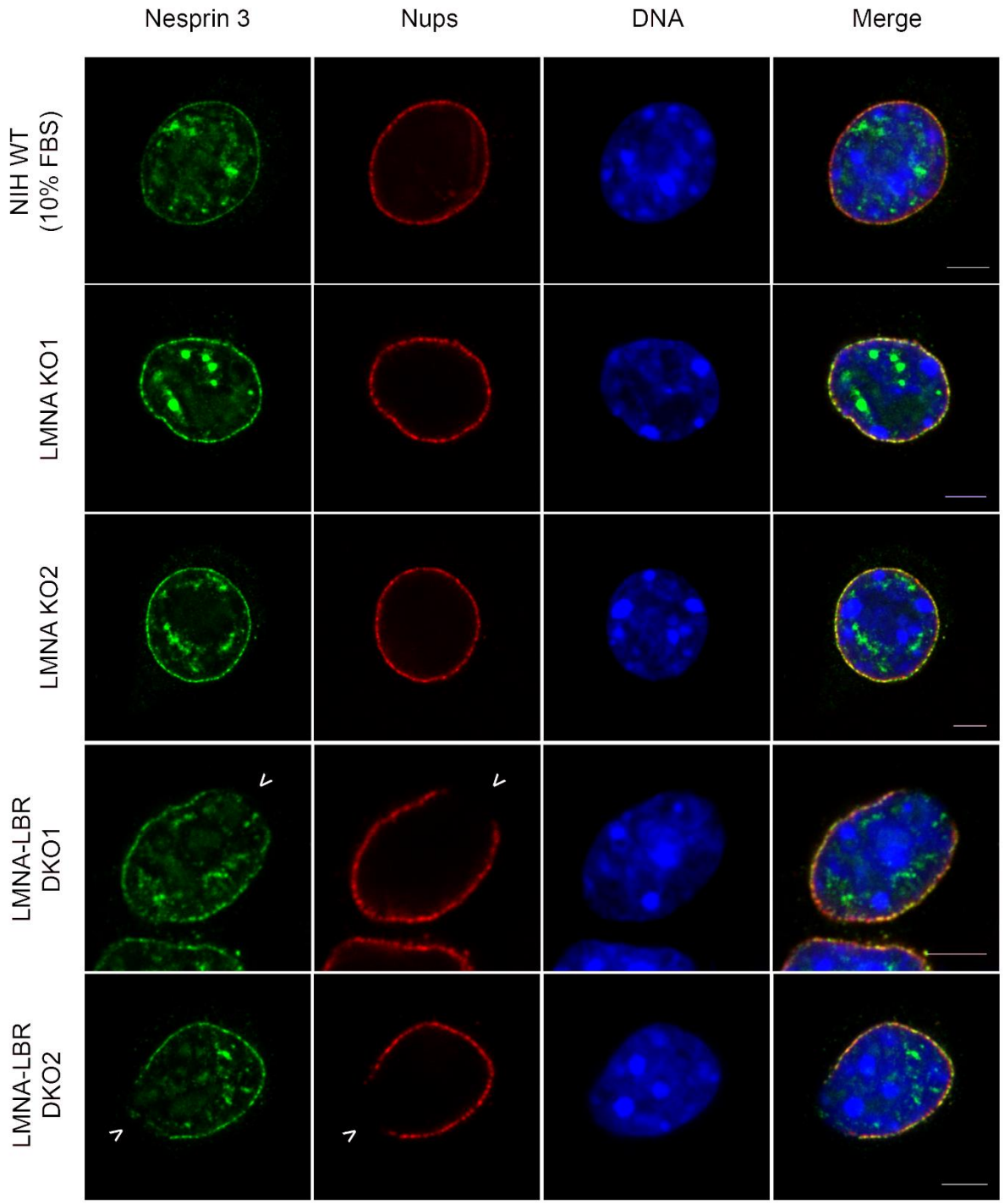

Figure 29. Indirect immunofluorescence images of NIH WT, LMNA KO and LMNA-LBR DKO nuclei labelled with antibodies against Nesprin 3 and Nups (DNA staining: TOPRO-3, scalebar: 5um). Arrows indicate the parts of the NE from which both Nesprin 3 and the NPCs are excluded.

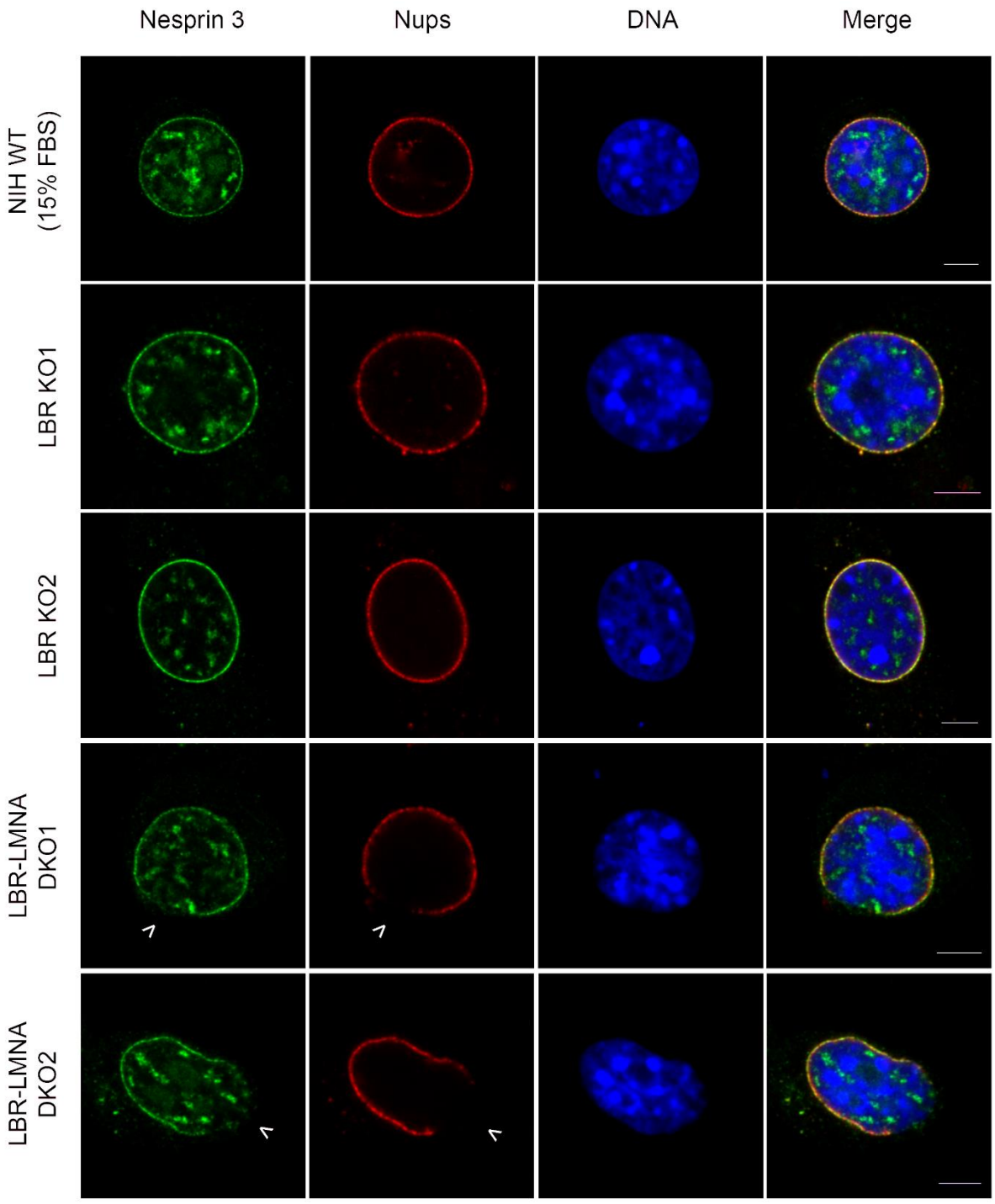

Figure 30. Indirect immunofluorescence images of NIH WT, LBR KO and LBR-LMNA DKO nuclei labelled with antibodies against Nesprin 3 and Nups (DNA staining: TOPRO-3, scalebar: 5um). Arrows indicate the parts of the NE from which both Nesprin 3 and the NPCs are excluded.

In order to further validate the existence of cells with asymmetric nuclei within the LMNA-LBR and LBR-LMNA DKO cell populations, all clones were stained with an antibody that recognizes Lamin B2, a major component of the nuclear lamina and a common marker of the nuclear periphery, that was previously found to be asymmetrically localized with a higher frequency in the DKO clones (Fig. 31 - 34). Then, the number of cells that exhibited the symmetric and asymmetric nuclear phenotype was determined for a total of 700 cells per clone, in 3 independent experiments, and the respective percentiles were calculated. The quantitative data obtained confirmed the visual observations of the asymmetries, with the latter being very frequent among the LMNA-LBR and LBR-LMNA DKO cell populations, while a small percentage of cells found within the LMNA KO clones was also asymmetric. In more details, 5% and 8% of the nuclei in the LMNA KO1 and LMNA KO2 cell populations, respectively, were found to be asymmetric, while this percentage reached 24.6% in the LMNA-LBR DKO1 clone, 12.6% in the LMNA-LBR DKO2 clone, 20.9% in the LBR-LMNA DKO1 clone and 13.4% in the LBR-LMNA DKO2 clone (Fig. 35). All differences between the tested clones and their respective controls were statistically significant (Table A1, Appendix). This was in agreement with previous quantification experiments performed by other members of the lab (Soupsana Katerina and Martzios Panagiotis).

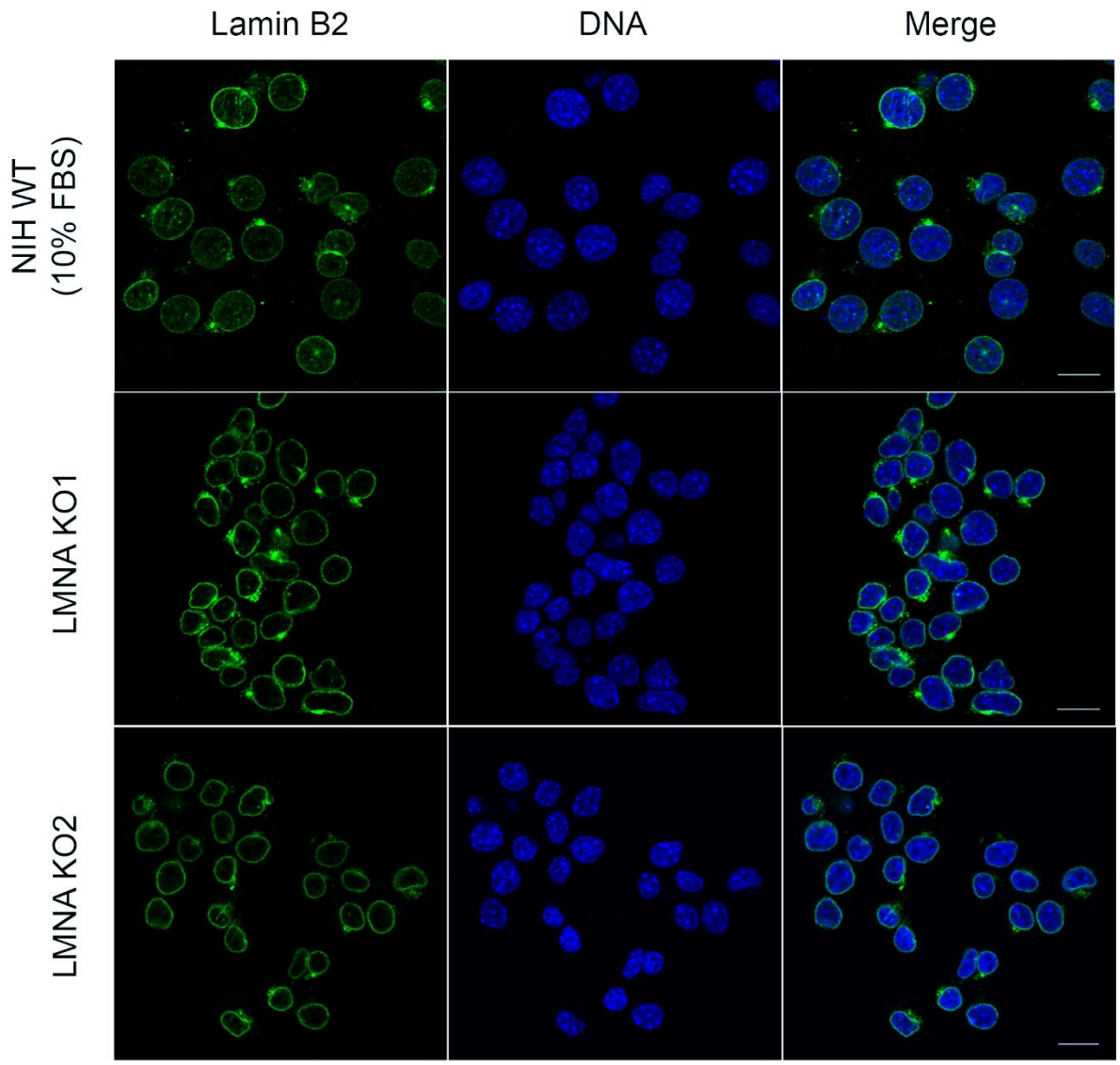

Figure 31. Indirect immunofluorescence images of NIH wild type and LMNA KO nuclei labelled with an antibody against Lamin B2 (DNA staining: TOPRO-3, scalebar: 15um).

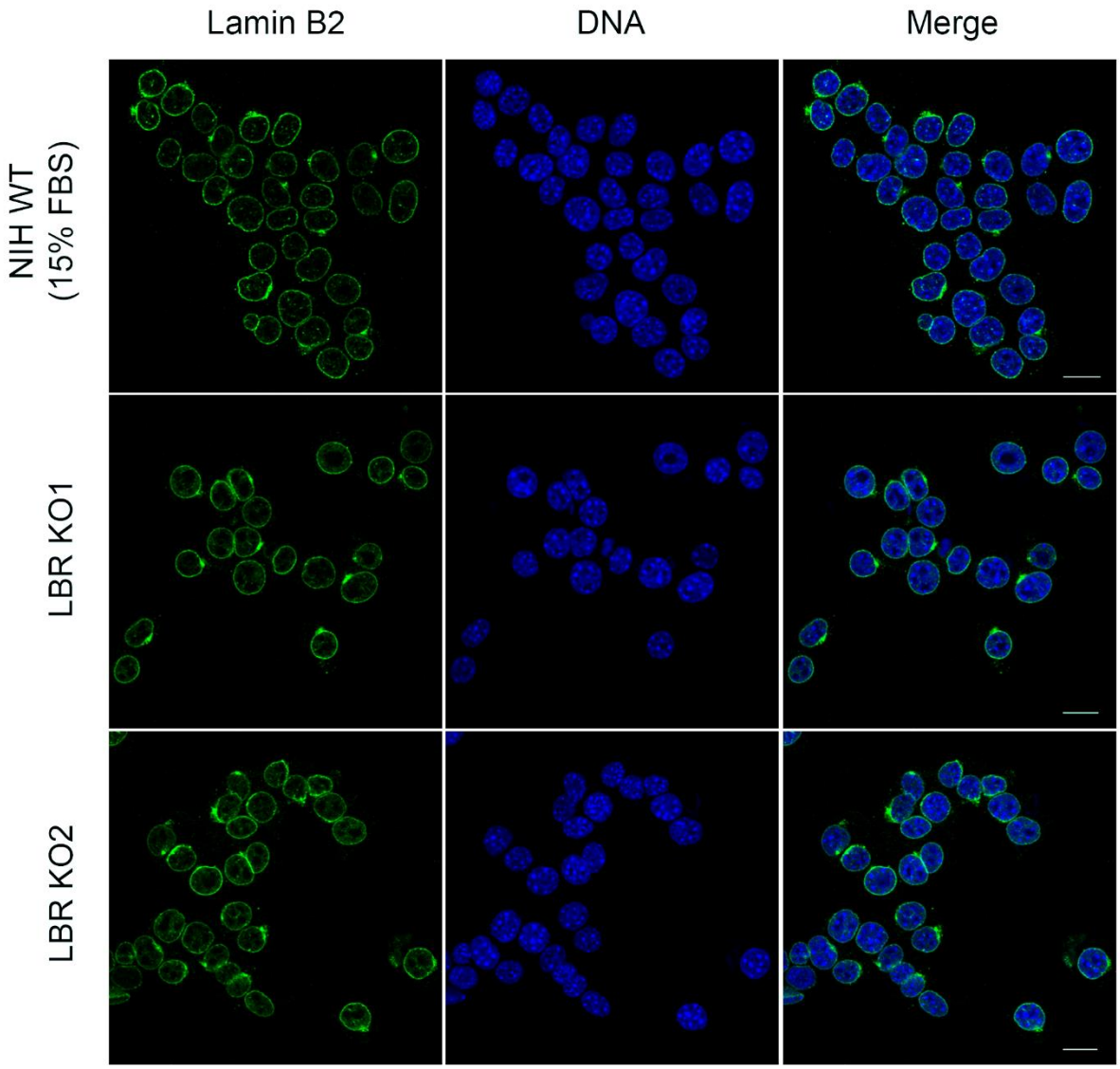

Figure 32. Indirect immunofluorescence images of NIH wild type and LBR KO nuclei labelled with an antibody against Lamin B2 (DNA staining: TOPRO-3, scalebar: 15um).

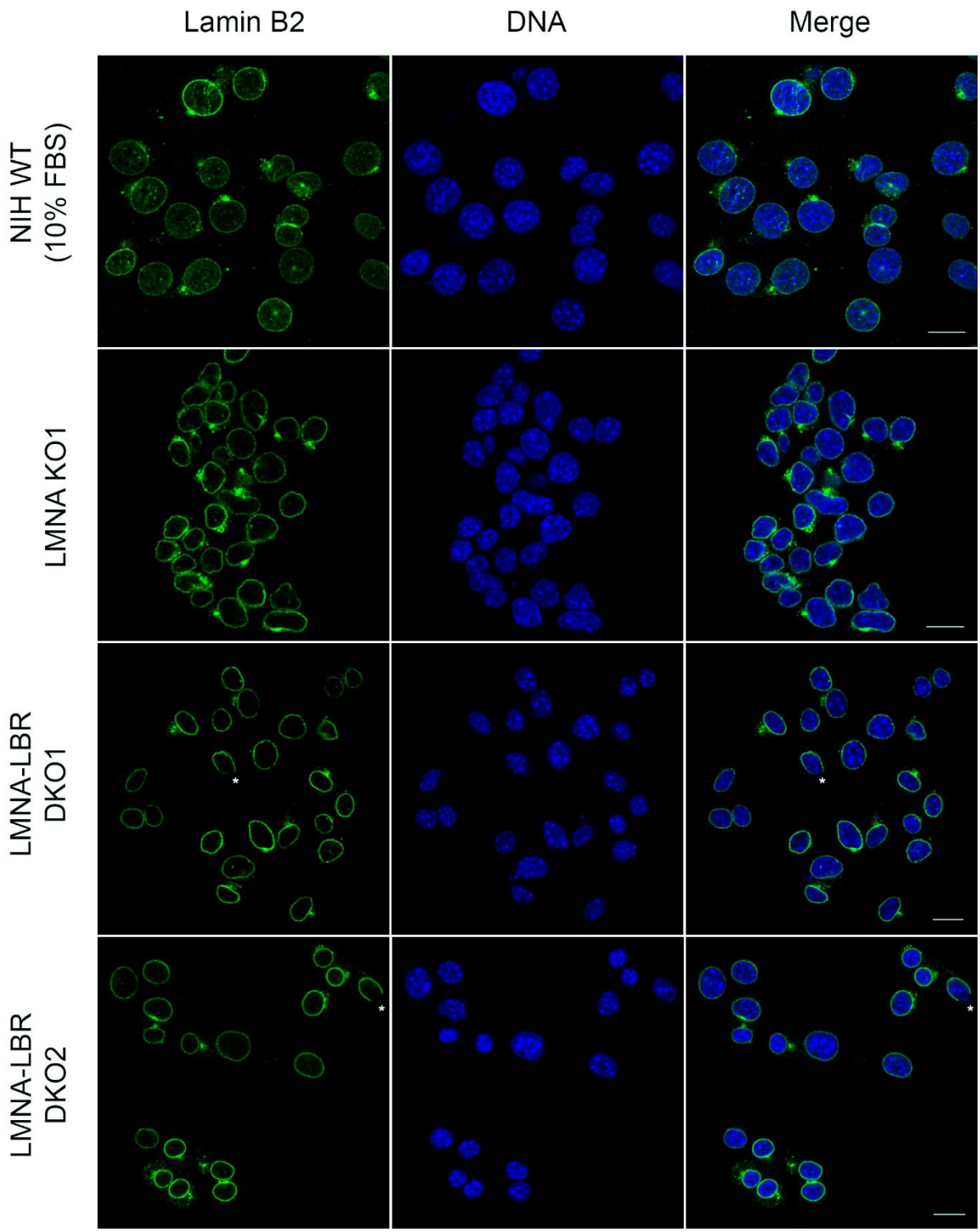

Figure 33. Indirect immunofluorescence images of NIH WT, LMNA KO and LMNA-LBR DKO nuclei labelled with an antibody against Lamin B2 (DNA staining: TOPRO-3, scalebar: 15um). Asterisks mark the nuclei that exhibit an asymmetric distribution of Lamin B2 in the nuclear periphery.

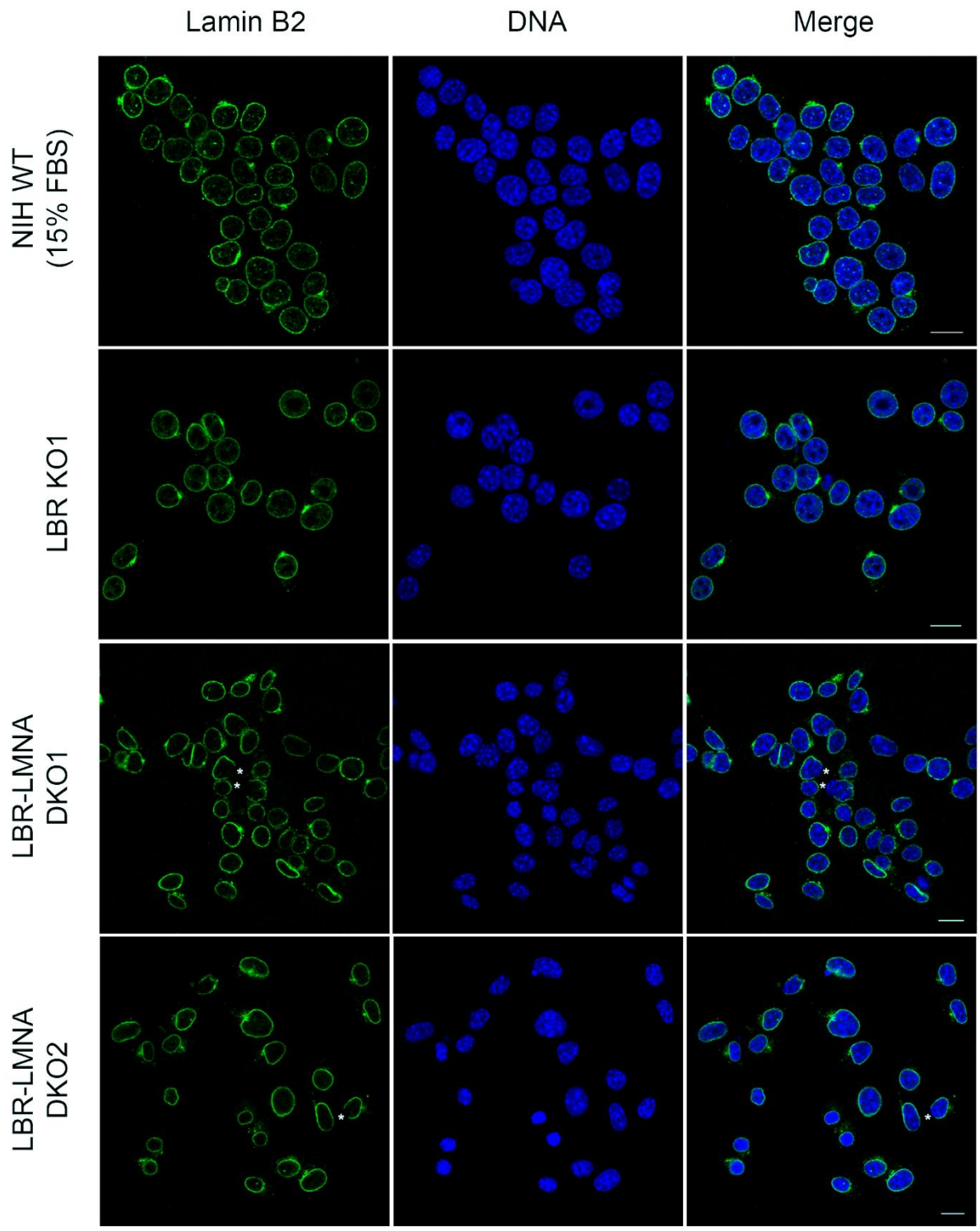

Figure 34. Indirect immunofluorescence images of NIH WT, LBR KO and LBR-LMNA DKO nuclei labelled with an antibody against Lamin B2 (DNA staining: TOPRO-3, scalebar: 15um). Asterisks mark the nuclei that exhibit an asymmetric distribution of Lamin B2 in the nuclear periphery.

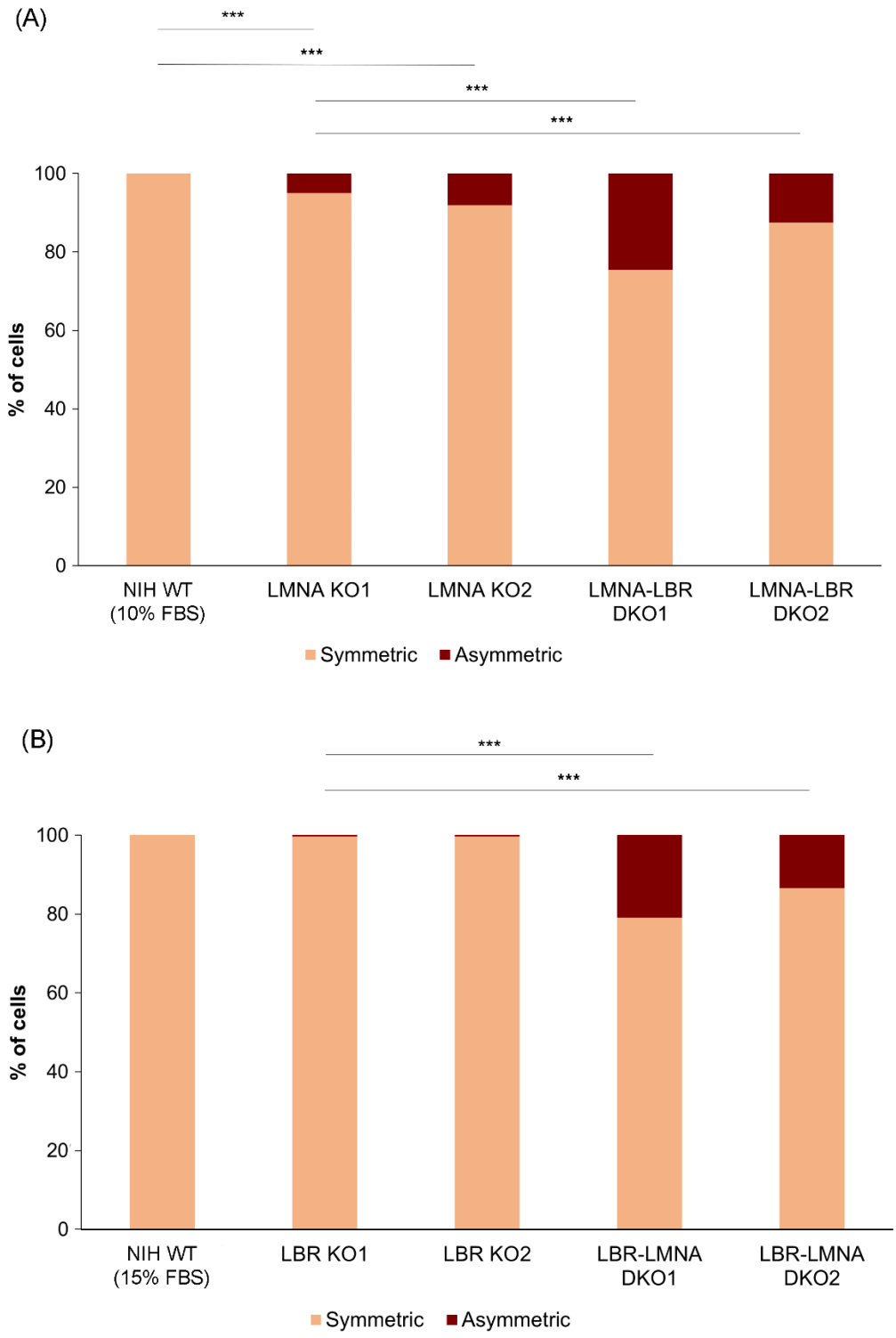

Figure 35. Percentiles of cells displaying symmetric and asymmetric localization of Lamin B2 in the following cell populations: (A) NIH WT (10% FBS), LMNA KO1, LMNA KO2, LMNA-LBR DKO1, LMNA-LBR DKO2, and (B) NIH WT (15% FBS), LBR KO1, LBR KO2, LBR-LMNA DKO1, LBR-LMNA DKO2. 700 cells (3 independent experiments) have been measured for each clone tested. All the differences between the mutant clones and their respective controls are statistically significant (***: $p<0.001$).

3.2. Overexpression of at least one of Lamin A/C or Lamin B1 or LBR is not sufficient to reverse the abnormal distribution of major components of the nuclear periphery observed in the double-knockout cells.

In 2014 a scientific study by Guo et al. provided evidence that when the protein levels of each lamin alone are sufficiently high, the respective lamin can form an NL meshwork that is able to maintain the normal distribution of NPCs on the INM (Guo *et al.*, 2014). Following these observations, other members of our lab (Martzios P.) carried out ectopic expression of either Lamin A/C, or Lamin B1, or LBR in all of the LMNA-LBR and LBR-LMNA double-knockout clones. These lines were transfected with the following plasmids: pEGFPN2-huLMNA (Fig. 17), pEGFPN3-huLMNB1 (Fig. 18) and pEGFPN2-mLBR (Fig. 19). 24 hours post-transfection cells were labelled with antibodies against the NPCs in order to investigate whether the asymmetric phenotype could be rescued. Interestingly, the overexpression of neither of these nuclear lamina components appeared to be sufficient to reverse the phenotype. In fact, even the proteins that were overexpressed in each case presented an uneven distribution in the nuclear periphery, which coincided with the one observed for the NPCs.

The incidence of cells in which the ectopically expressed proteins followed a normal distribution pattern, while the NPCs did not, could imply that cells might need more than 24 hours to fully reverse the abnormal phenotype. For this reason, we conducted another series of experiments, in which cells expressed the constructs mentioned above for 48 hours before being examined. These experiments provided no evidence on further phenotype reversal, since, even after 48 hours of Lamin A/C or Lamin B1 or LBR overexpression, cells with an asymmetric distribution of these proteins as well as of the NPCs were still present in all four double-knockout clones.

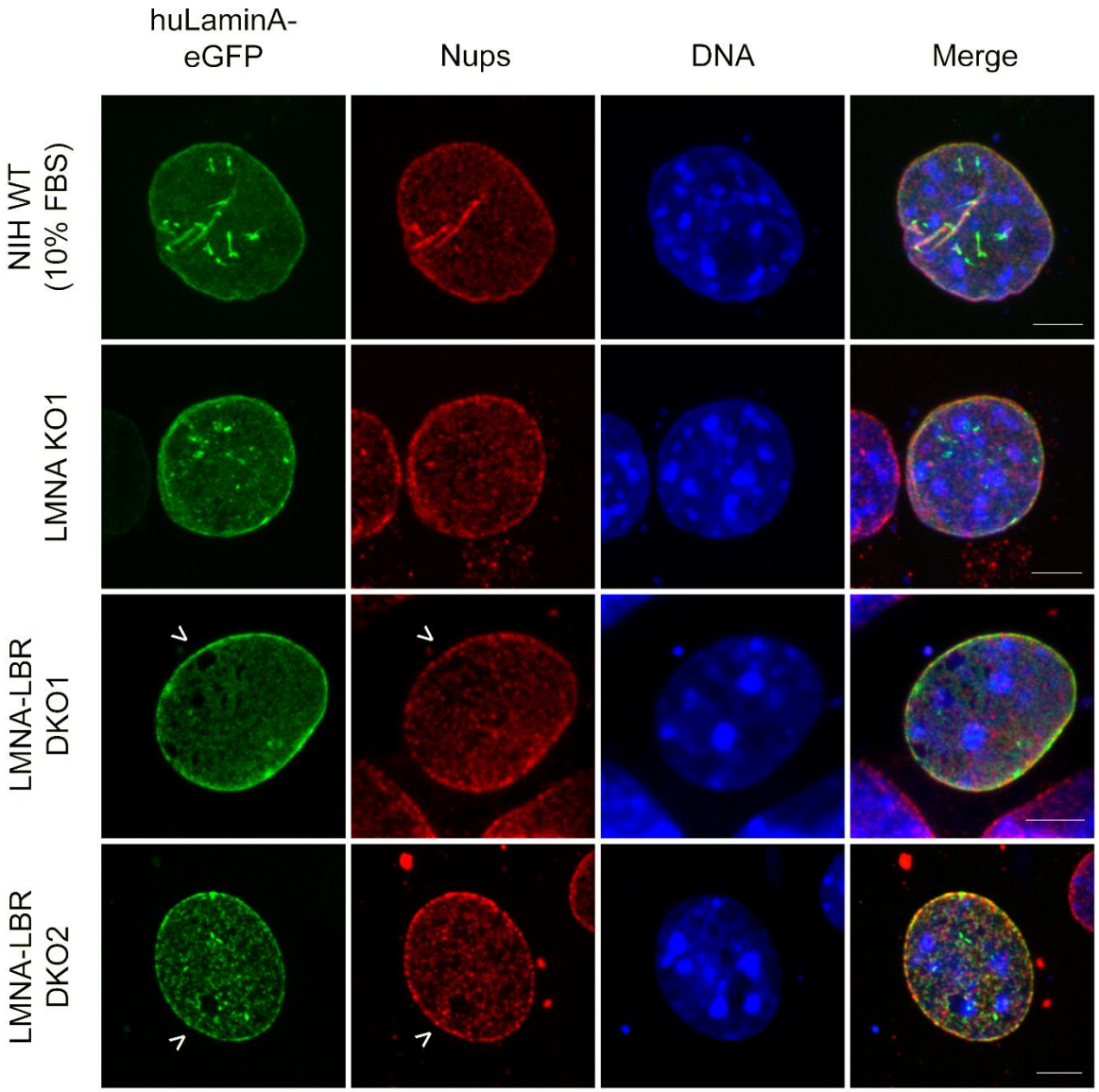

Figure 36. Indirect immunofluorescence images of NIH WT (10% FBS), LMNA KO and LMNA-LBR DKO nuclei of cells that overexpress pEGFPN2-huLMNA and are labelled with an antibody against Nups (DNA staining: TOPRO-3, scalebar: 5um). Arrows indicate the parts of the nuclear envelope where neither of Lamin A/C nor the NPCs are present.

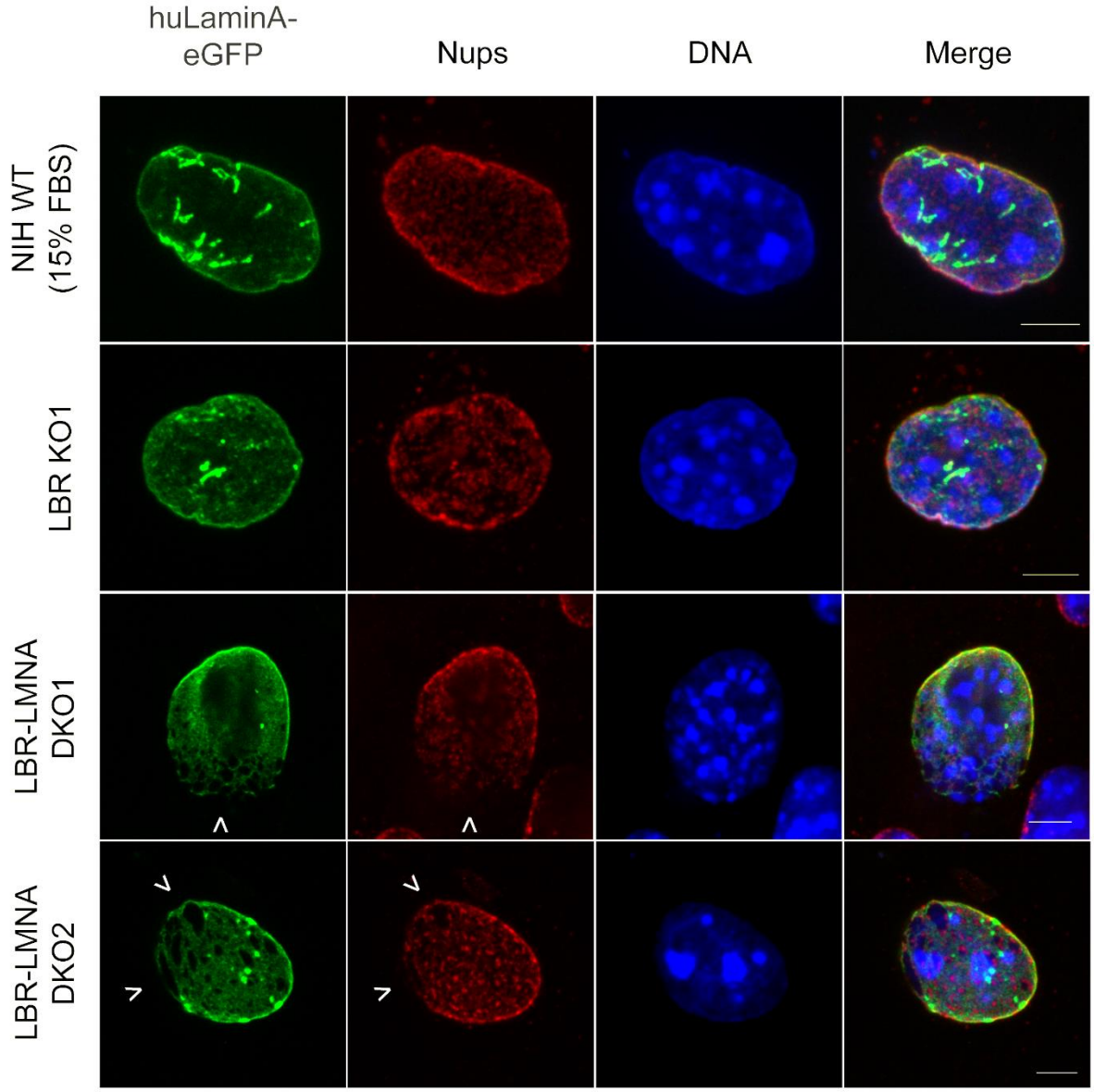

Figure 37. Indirect immunofluorescence images of NIH WT (15% FBS), LBR KO and LBR-LMNA DKO nuclei of cells that overexpress pEGFPN2-huLMNA and are labelled with an antibody against Nups (DNA staining: TOPRO-3, scalebar: 5um). Arrows indicate the parts of the nuclear envelope where neither of Lamin A/C nor the NPCs are present.

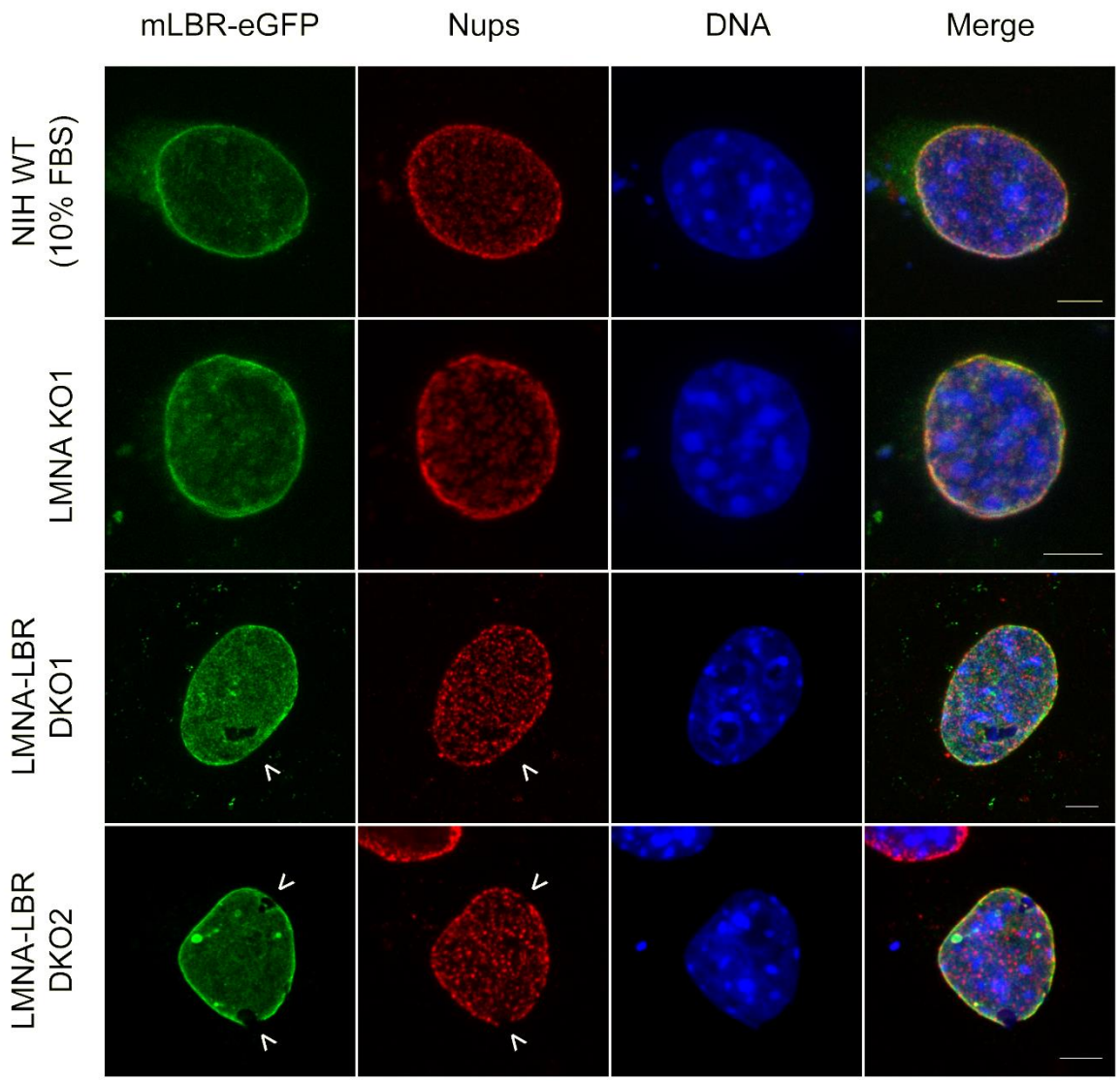

Figure 38. Indirect immunofluorescence images of NIH WT (10% FBS), LMNA KO and LMNA-LBR DKO nuclei of cells that overexpress pEGFPN2-mLBR and are labelled with an antibody against Nups (DNA staining: TOPRO-3, scalebar: 5um). Arrows indicate the parts of the nuclear envelope where neither of Lamin A/C nor the NPCs are present.

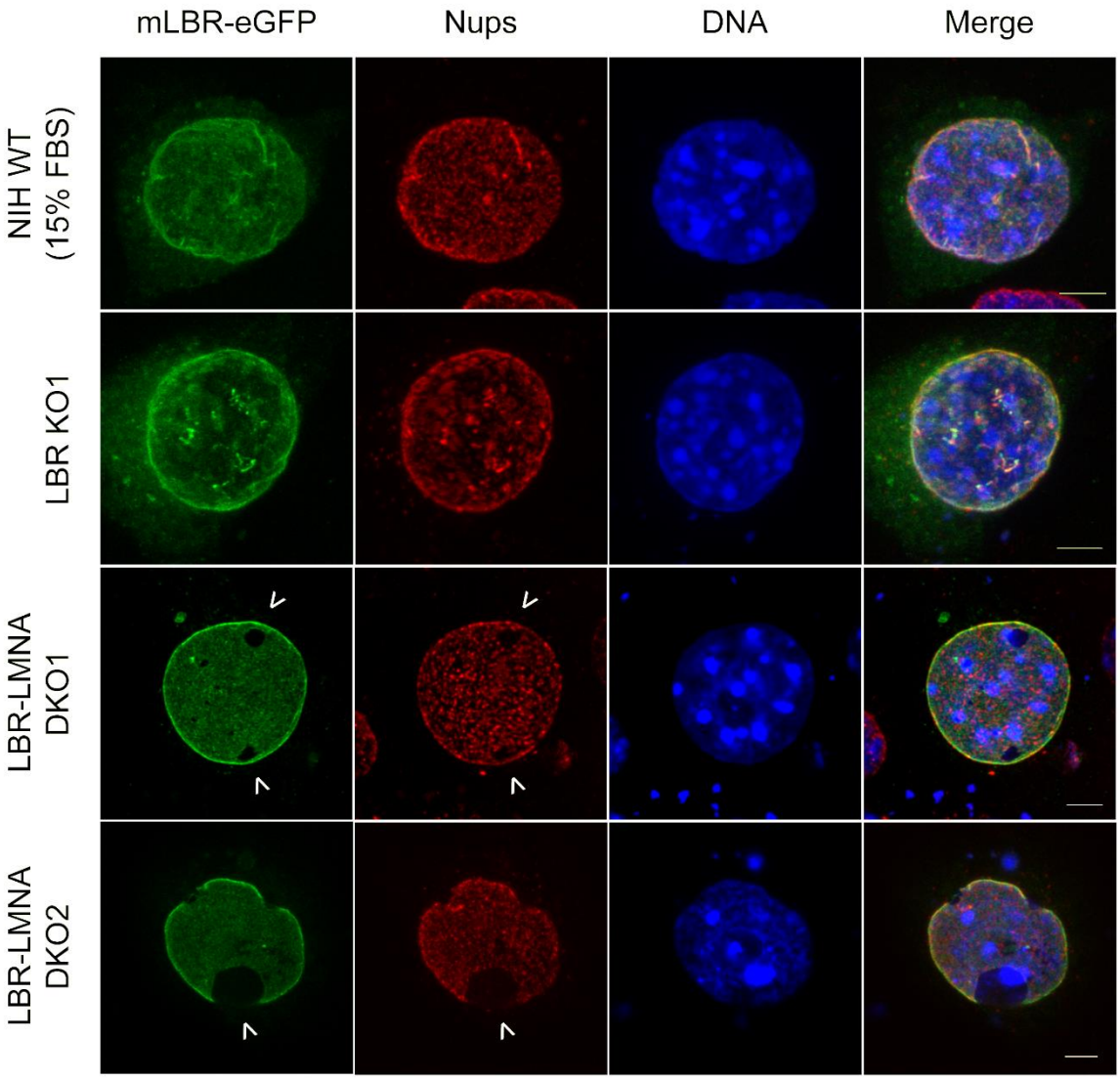

Figure 39. Indirect immunofluorescence images of NIH WT (10% FBS), LBR KO and LBR-LMNA DKO nuclei of cells that overexpress pEGFPN2-mLBR and are labelled with an antibody against Nups (DNA staining: TOPRO-3, scalebar: 5um). Arrows indicate the parts of the nuclear envelope where neither of Lamin A/C nor the NPCs are present.

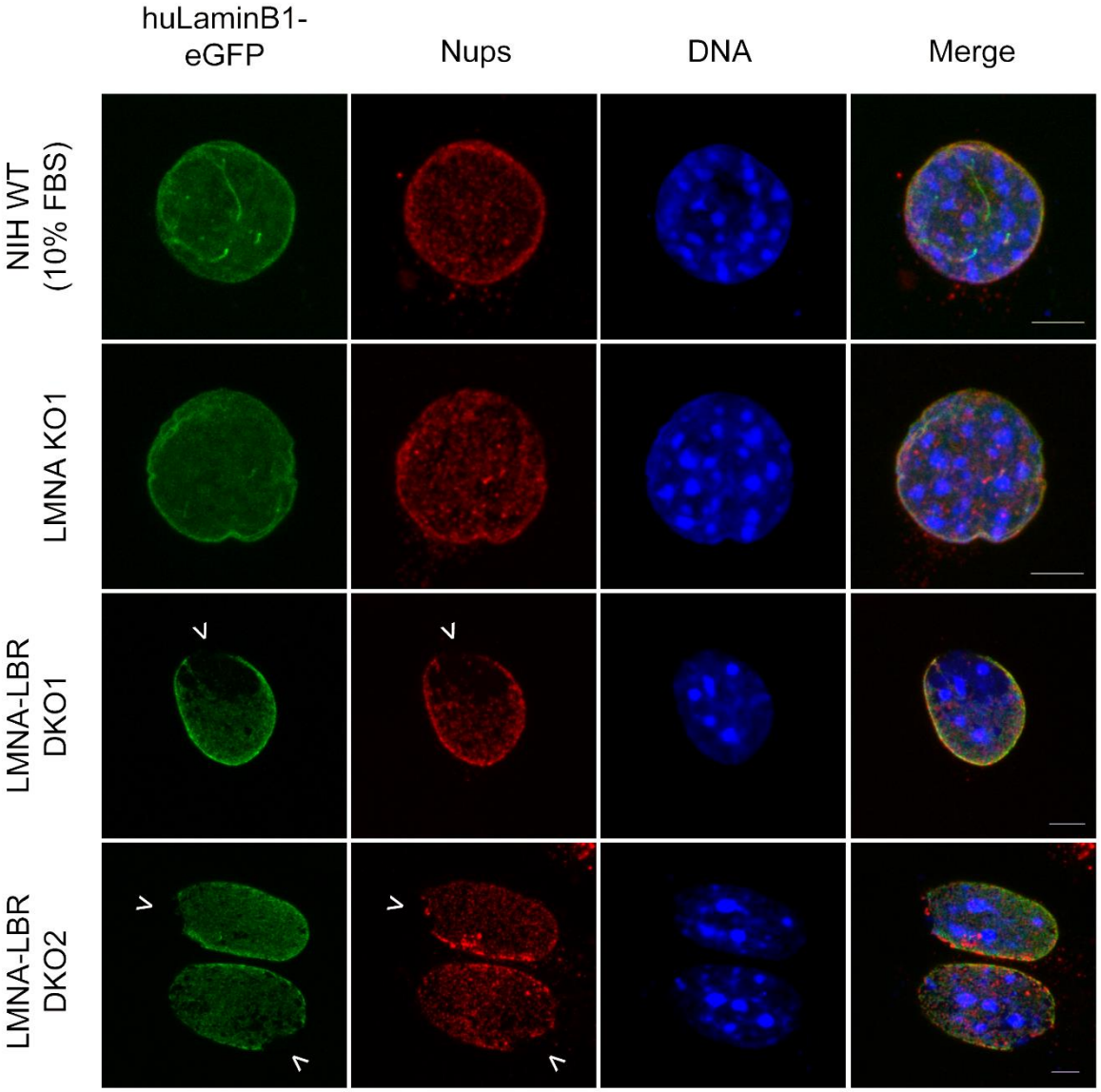

Figure 40. Indirect immunofluorescence images of NIH WT (10% FBS), LMNA KO and LMNA-LBR DKO nuclei of cells that overexpress pEGFPN3-huLMNB1 and are labelled with an antibody against Nups (DNA staining: TOPRO-3, scalebar: 5um). Arrows indicate the parts of the nuclear envelope where neither of Lamin A/C nor the NPCs are present.

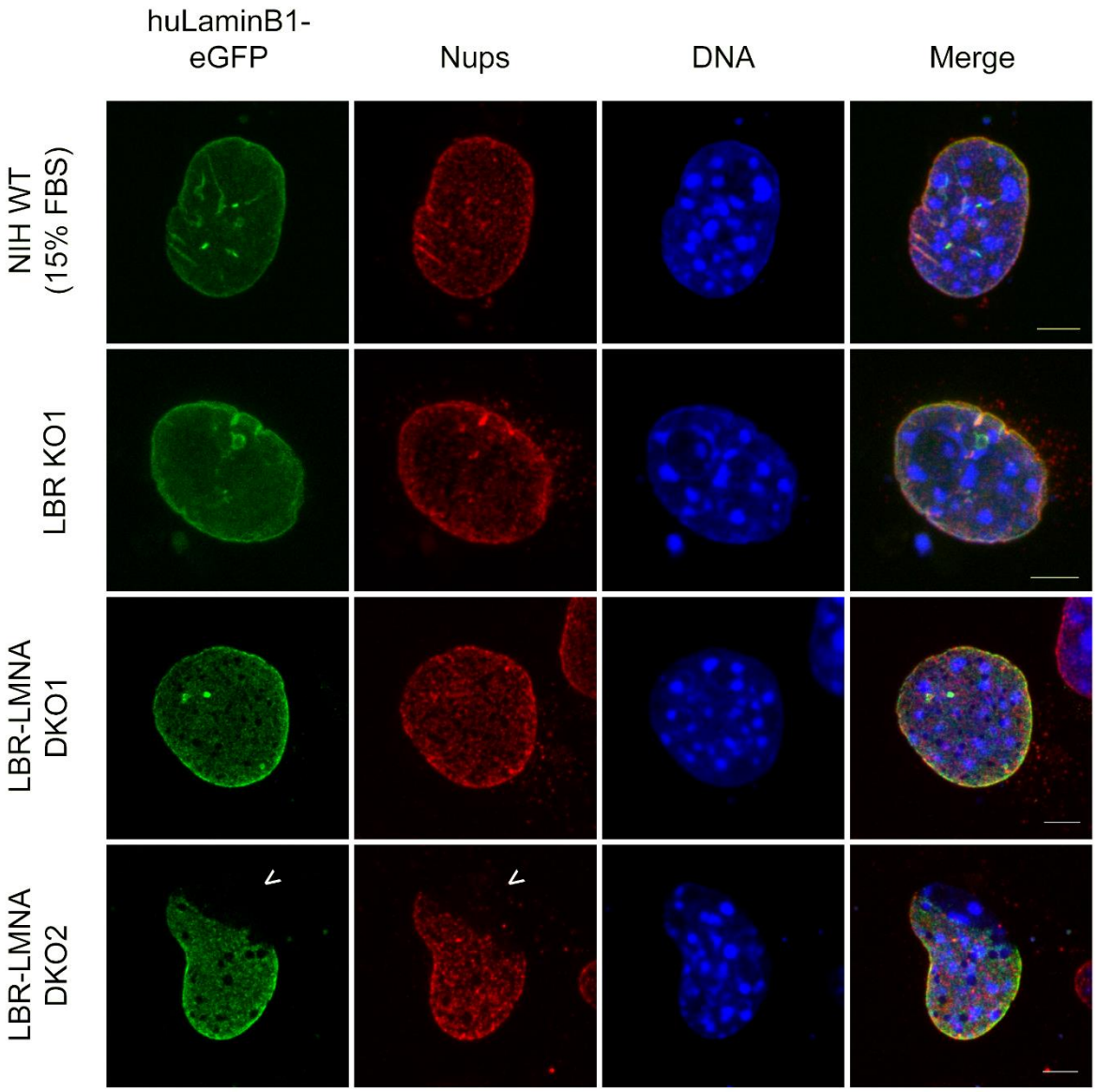

Figure 41. Indirect immunofluorescence images of NIH WT (10% FBS), LBR KO and LBR-LMNA DKO nuclei of cells that overexpress pEGFPN3-huLMNB1 and are labelled with an antibody against Nups (DNA staining: TOPRO-3, scalebar: 5um). Arrows indicate the parts of the nuclear envelope where neither of Lamin A/C nor the NPCs are present.

The asymmetric phenotype was more apparent when the maximum projection mode of the LASX software was used, which allows the visualization of the whole surface of the nucleus and not only its equatorial plate (Fig. 36 – 41). From the figures above it becomes clear that the ectopic expression of at least one of the Lamin A/C,

Lamin B1 or LBR fails to reverse the asymmetric phenotype that is frequently observed among nuclei of the DKO cell populations. In fact, nuclei that exhibit whole parts of the nuclear envelope that are emptied of nuclear pores as well as the protein that is overexpressed in each case were still present in all LMNA-LBR DKO and LBR-LMNA DKO clones. This finding does not agree with what was proposed by Guo *et al.* and it could imply that the aberrations caused upon loss of LBR and Lamin A/C are quite severe and might include the irreversible disruption of the membranes of the nuclear envelope.

3.3. The number of heterochromatic foci is decreased upon combinatorial loss of LBR and Lamin A/C

One feature that characterizes interphase nuclei of murine cells is the existence of foci of heterochromatic nature, which are dispersed throughout the nucleoplasm. These foci are called chromocenters and are the result of centromeric and pericentromeric heterochromatin coalescence (Saksouk *et al.*, 2015). Former members of the lab (Soupsana K. and Martzios P.) observed that cells which are depleted for both Lamin A/C and LBR exhibit nuclei with a decreased number of heterochromatic foci compared to single LBR or LMNA knockout and wild type cell populations.

To further validate these observations, the number of heterochromatic foci per nucleus was calculated for a total of 60 cells per clone in 3 independent experiments. From the violin plots in figures 42 and 43 it becomes quite clear that, even though the number of foci per nucleus is not affected upon loss of LBR or Lamin A/C alone, there is a noticeable difference between the number of foci in nuclei that lack both proteins (LMNA-LBR DKO and LBR-LMNA DKO) and that of their respective controls. Not only the mean values were different between the clones that were compared, but also the distribution of data points around the mean was altered. These differences were assessed by statistical analysis and were all found to be statistically significant (Table A2, Appendix).

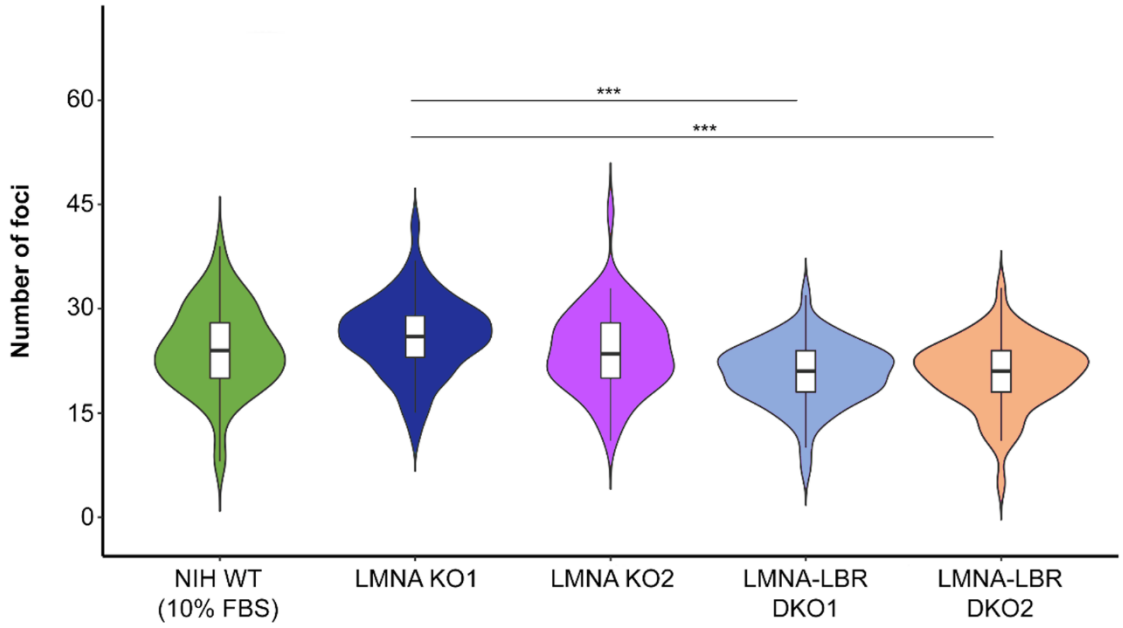

Figure 42. Violin plots depicting the number of heterochromatic foci per nucleus for the following cell populations: NIH WT (10% FBS), LMNA KO1, LMNA KO2, LMNA-LBR DKO1, LMNA-LBR DKO2. The decrease in the number of foci per nucleus in LMNA-LBR DKO1 and LMNA-LBR DKO2 compared to LMNA KO1 is statistically significant (***: $p<0.001$).

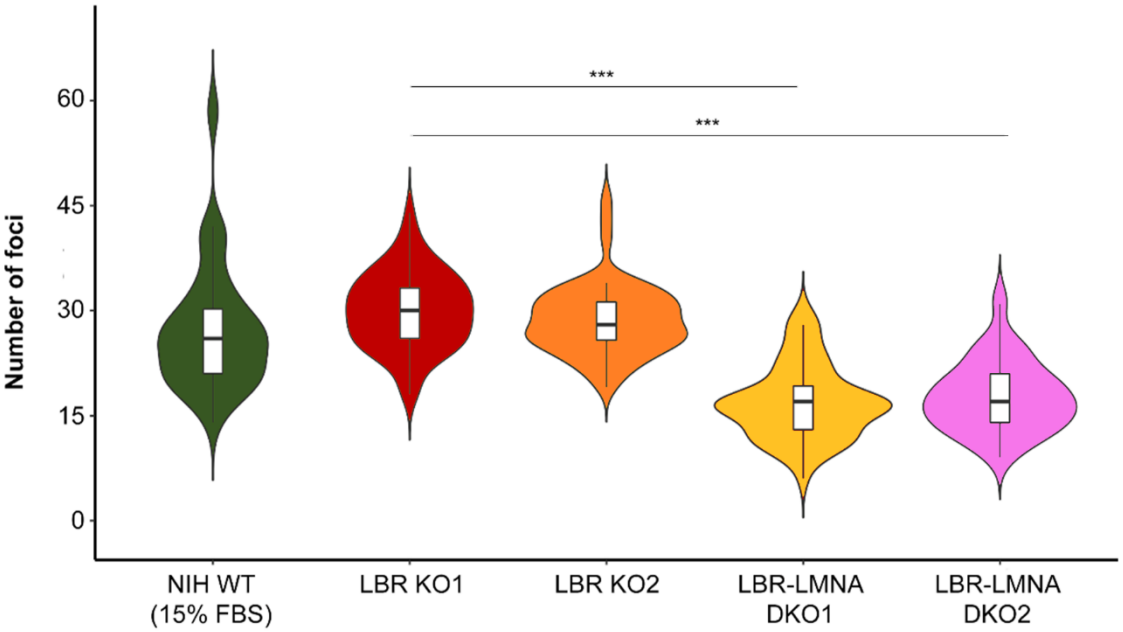

Figure 43. Violin plots depicting the number of heterochromatic foci per nucleus for the following cell populations: NIH WT (15% FBS), LBR KO1, LBR KO2, LBR-LMNA KO1, LBR-LMNA DKO2. The decrease in the number of foci per nucleus in LBR-LMNA DKO1 and LBR-LMNA DKO2 compared to LBR KO1 is statistically significant (***: $p<0.001$).

The presence of nuclei with fewer heterochromatic foci among the LMNA-LBR DKO and LBR-LMNA DKO cell populations implies an impairment of the mechanisms that maintain chromatin architecture of interphase nuclei. In fact, such nuclei resemble the inverted nuclei of the rod cells of nocturnal mammals (Solovei *et al.*, 2009). This could mean that loss of both LBR and Lamin A/C may lead to the partial merging of heterochromatic foci, but is not sufficient for the complete chromatin inversion.

3.4. Loss of LBR and/or Lamin A/C does not cause any irregularities regarding chromatin architecture and dynamics.

The decreased number of foci observed in the DKO clones is in agreement with the fact that Lamin A/C and LBR have been repeatedly associated with the regulation and maintenance of the chromatin landscape. For this reason, it was decided to investigate whether there are any alterations in chromatin organization and dynamics upon loss of Lamin A/C and/or LBR. In order to assess the possibility of such alterations, the distribution of the epigenetic marker H3K9me3 was studied by indirect immunofluorescence, while a full series of Fluorescence Recovery After Photobleaching (FRAP) experiments were also conducted. For the purposes of these experiments, cells from all the clones tested were transiently transfected with the plasmid pPycagip-eGFP-huHP1α (Fig. 20). HP1α is enriched in the heterochromatic foci of murine cell nuclei and its mobility and dynamics would serve as an indicator of the heterochromatin condensation. At the same time, H3K9me3, which is one of the epigenetic markers HP1a recognizes and binds, would allow the observation of any irregularities in chromatin organization upon loss of LBR and/or Lamin A/C.

3.4.1. Assessing the chromatin landscape using H3K9me3 as a heterochromatin marker.

For the investigation of any potential irregularities regarding the chromatin landscape, cells from all the clones examined were transiently transfected with the

plasmid pPycagip-eGFP-huHP1α (Fig. 20) and, 24 hours post transfection, they were labelled with an antibody that recognizes H3K9me3. Assessment of the samples by confocal microscopy (Fig. 44 – 47) did not reveal any visually observable alterations regarding the levels or localization pattern of H3K9me3 in any of the LMNA KO, LBR KO, LMNA-LBR DKO and LBR-LMNA DKO clones, when they were compared with their respective controls. The epigenetic marker was found to be present in the entire nucleoplasm with an enrichment in the chromocenters and the nuclear periphery, in agreement with the distribution pattern of HP1α-eGFP in all the clones tested. Since no conclusion about how the loss of the two peripheral HC tethers may affect the chromatin landscape could be drawn from this experiment, we proceeded to the assessment of HP1α dynamics at the level of heterochomatic foci, using the FRAP assay.

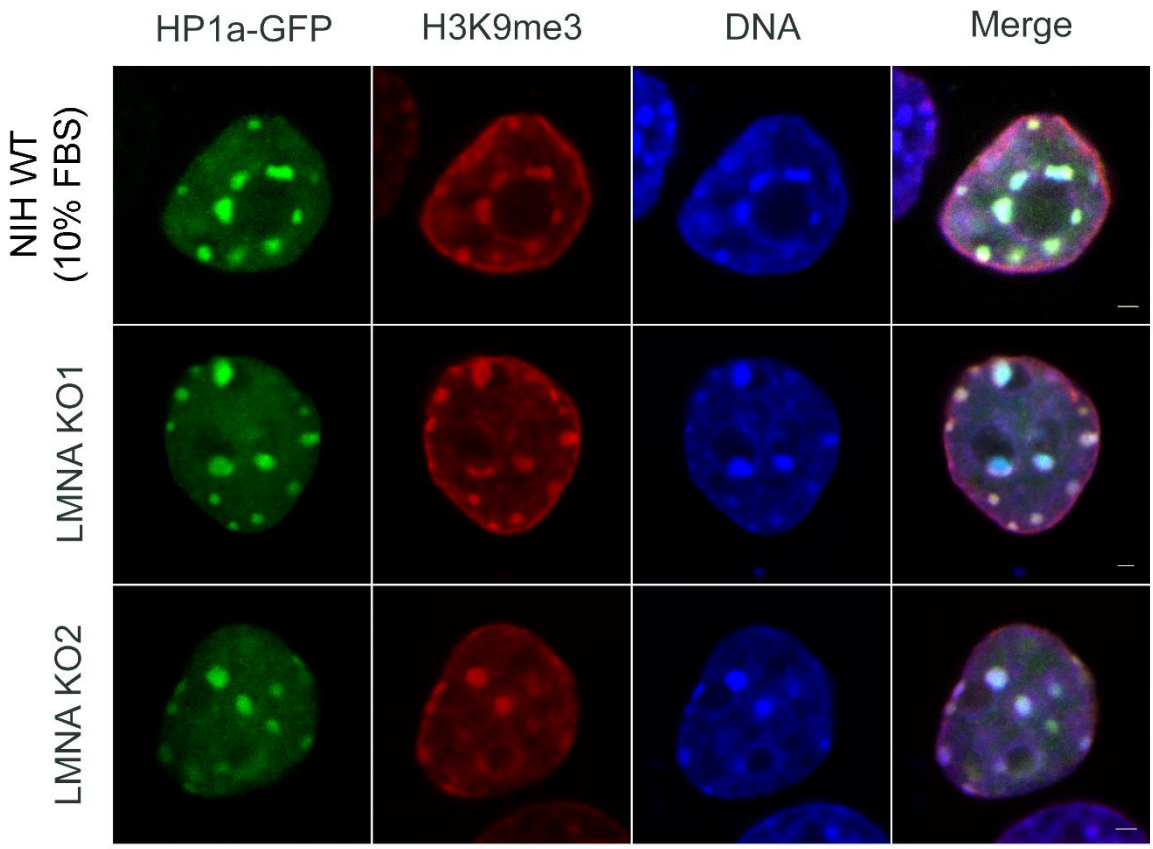

Figure 44. Indirect immunofluorescence images of NIH WT (10% FBS), LMNA KO1 and LMNA KO2 nuclei of cells that overexpress HP1a-GFP, labelled with an antibody against H3K9me3 (DNA staining: DAPI, scalebar: 3um).

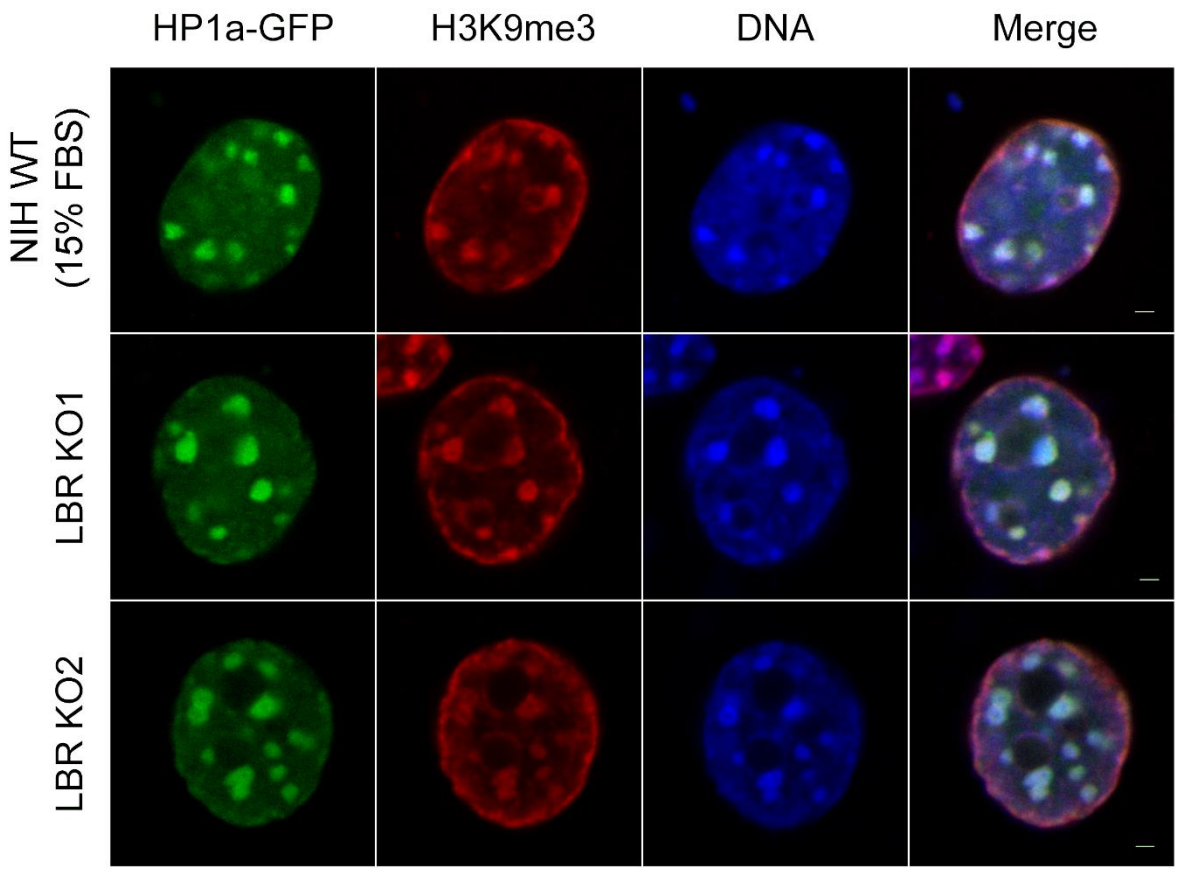

Figure 45. Indirect immunofluorescence images of NIH WT (15% FBS), LBR KO1 and LBR KO2 nuclei of cells that overexpress HP1a-GFP, labelled with an antibody against H3K9me3 (DNA staining: DAPI, scalebar: 3um).

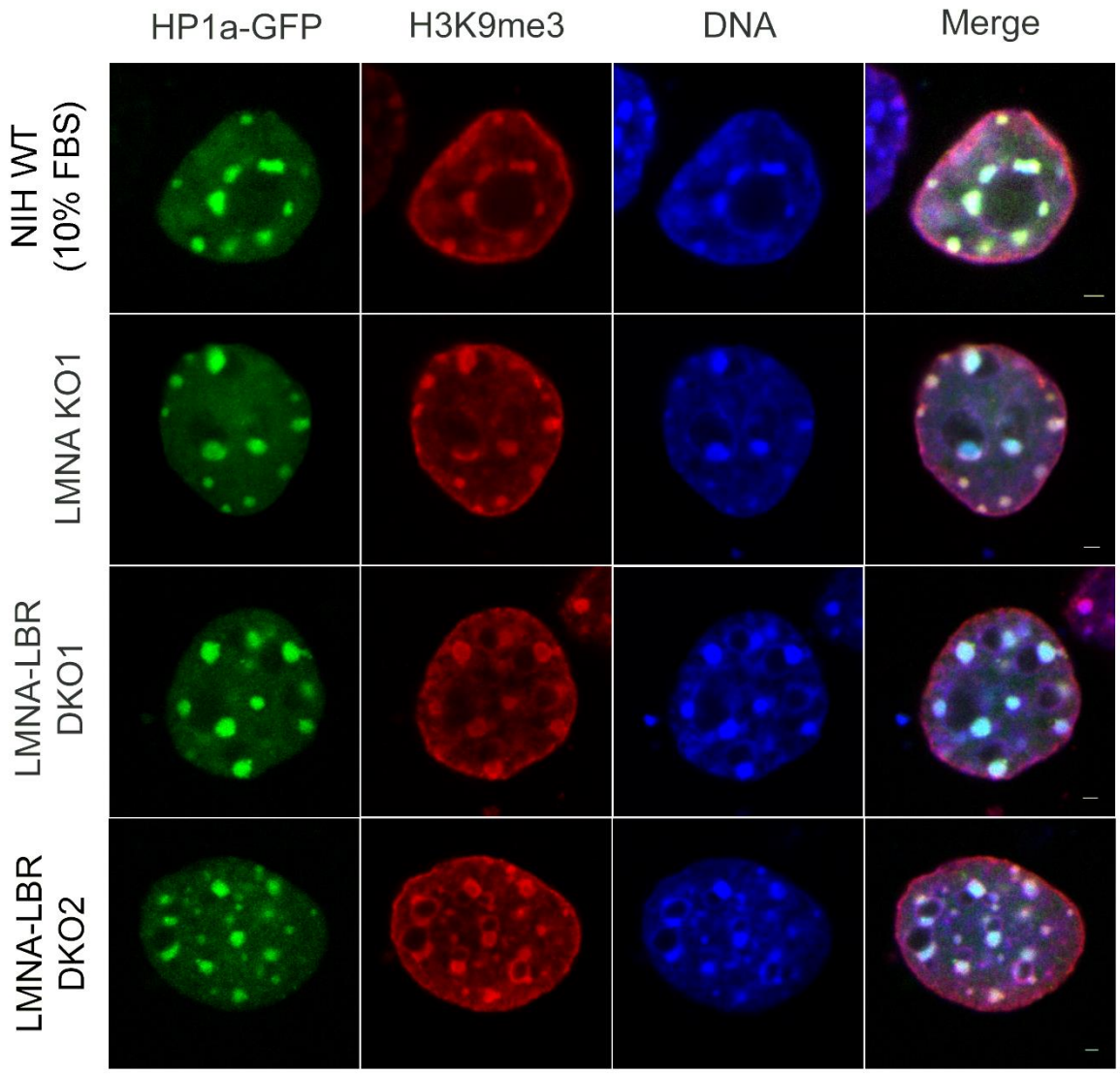

Figure 46. Indirect immunofluorescence images of NIH WT (10% FBS), LMNA KO1, LMNA-LBR DKO1 and LMNA-LBR DKO2 nuclei of cells that overexpress HP1a-GFP, labelled with an antibody against H3K9me3 (DNA staining: DAPI, scalebar: 3um).

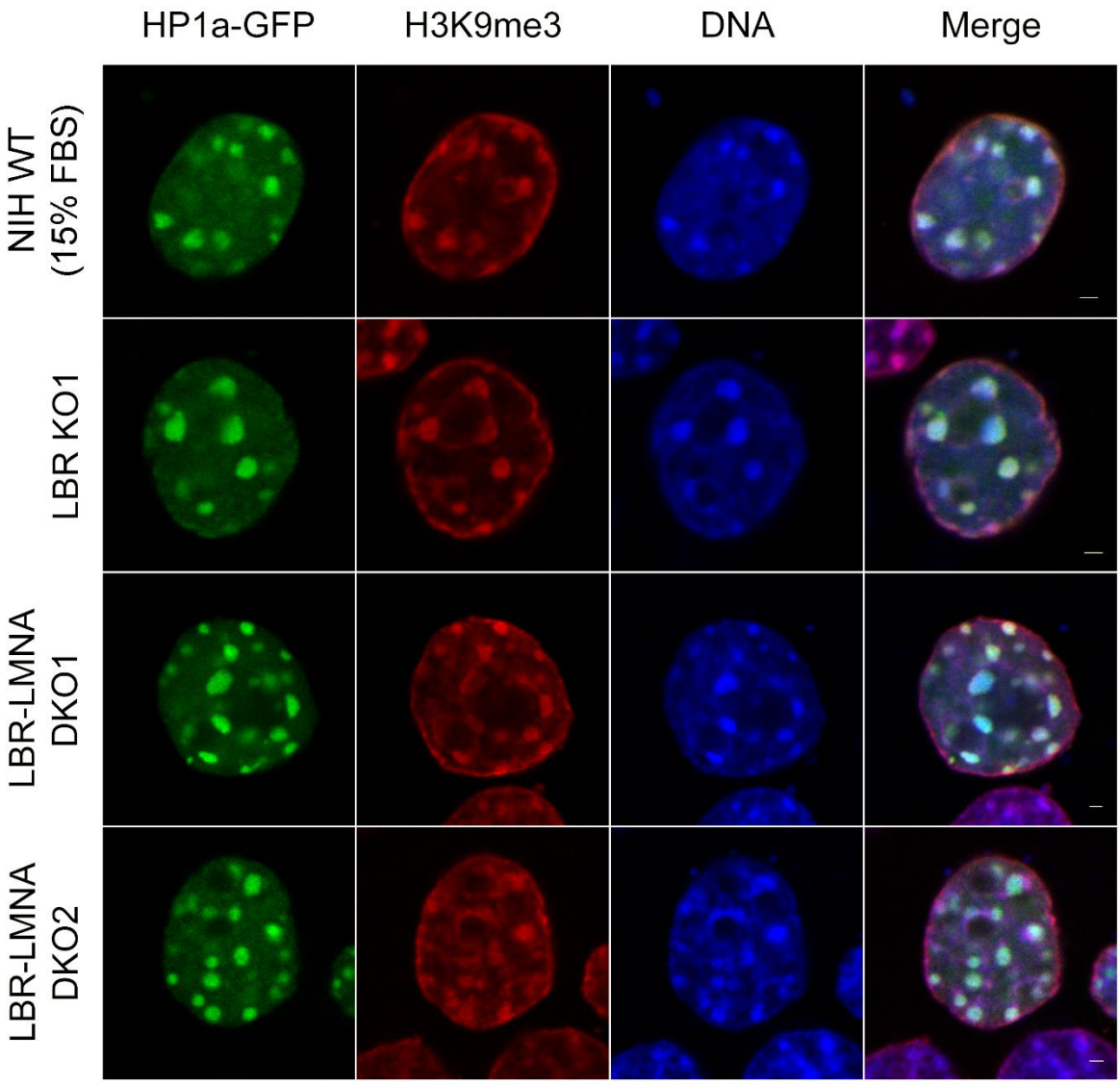

Figure 47. Indirect immunofluorescence images of NIH WT (15% FBS), LBR KO1, LBR-LMNA DKO1 and LBR-LMNA DKO2 nuclei of cells that overexpress HP1a-GFP, labelled with an antibody against H3K9me3 (DNA staining: DAPI, scalebar: 3um).

3.4.2. Assessing chromatin state and dynamics using the FRAP assay.

Prior to the FRAP experiments cells were transiently transfected with the plasmid pPycagip-eGFP-huHP1α (Fig. 20). After 24 hours the transfected cells were assayed. During the FRAP experiments one focus per nucleus was assayed at a time, for a total of 50 nuclei per clone tested. Circular regions of 1um diameter (regions of

interest: ROIs) were randomly selected and bleached with a high laser pulse (Fig. 48A – 48J (a)). From the recovery curves that were obtained (Fig. 48A – 48J (b)) the following parameters that are associated with the diffusional mobility of HP1α were measured: the mobile fraction (*Mf*) of the protein and the recovery halftime ($t_{1/2}$). The scatter plots obtained when the *Mf* and $t_{1/2}$ were plotted on the same graph (Fig. 48A – 48J (c)) showed that there is no covariance between the two variables (as suggested by the calculation of the R^2 for each dataset). The non-covariant relationship between the mobile fraction of HP1α and the exchange rate of the fluorescent and bleached molecules in each ROI implied the existence of a more complex type of a "state space".

"State space" refers to a concept introduced by Christogianni *et al.* (Christogianni *et al.*, 2017) based on plots of *Mf*/*Da* ratio against *Da.* The authors named the resulting curve "the state of chromatin (SC) curve" and described it as "the signature of dynamic ensembles in a dataset". This curve was considered to correspond to a spectrum of dynamic chromatin states, where the datapoints that exhibit a lower *Da* and a higher *Mf/Da* ratio correspond to highly condensed chromatin ensembles, while the datapoints that present a higher *Da* and a lower *Mf/Da* ratio correspond to a more accessible chromatin state. Thus, the comparison of this type of curves between the clones of interest could potentially reveal the alterations in the state of chromatin that may occur upon loss of LBR and/or Lamin A/C. To this end, the diffusion coefficient (*Da*) of HP1α was also calculated for each clone tested. Plotting the *Mf*/*Da* ratio against *Da* resulted in a continuum of data points that form a SC curve (Fig. 48A – 48J (d)).

(A)

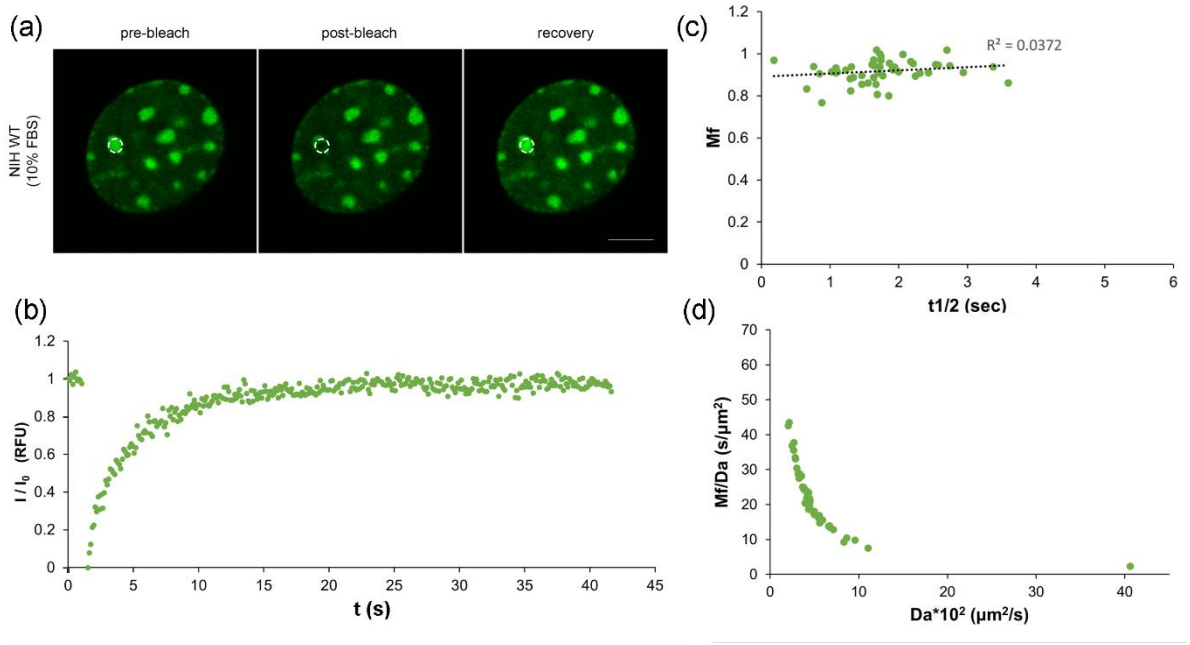
(a)
pre-bleach
post-bleach
recovery
NIH WT (10% FBS)
(b)
I / I0 (RFU)
t (s)
(c)
R² = 0.0372
Mf
t1/2 (sec)
(d)
Mf/Da (s/µm²)
Da*10² (µm²/s)

(B)

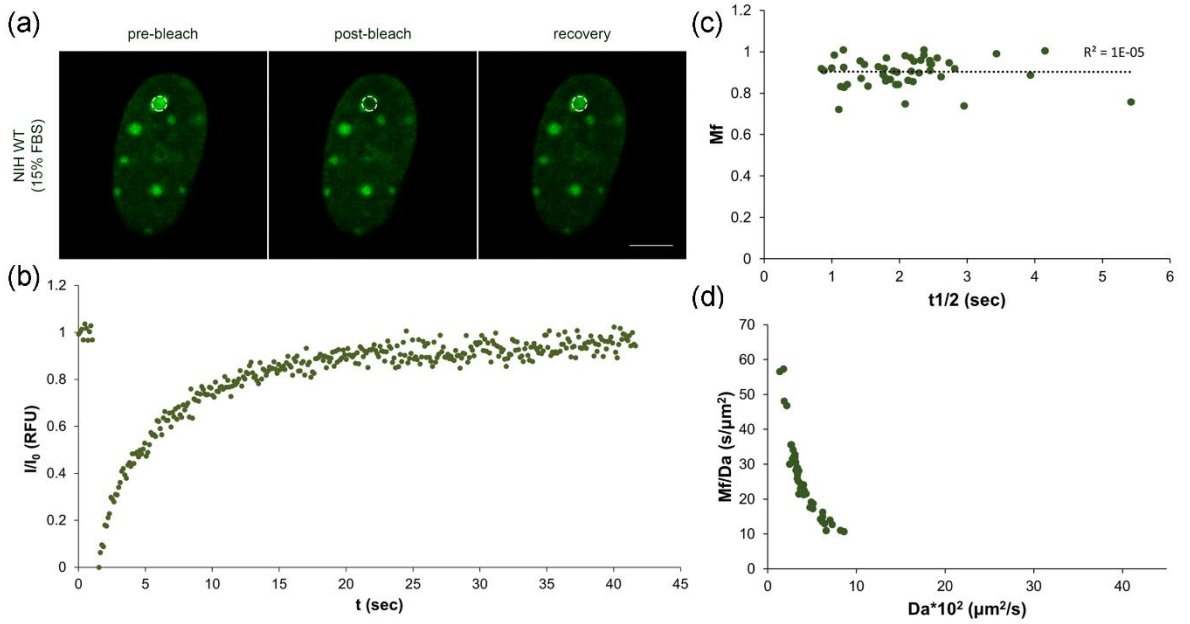
(a)
pre-bleach
post-bleach
recovery
NIH WT (15% FBS)
(b)
I/I0 (RFU)
t (sec)
(c)
R² = 1E-05
Mf
t1/2 (sec)
(d)
Mf/Da (s/µm²)
Da*10² (µm²/s)

(C)

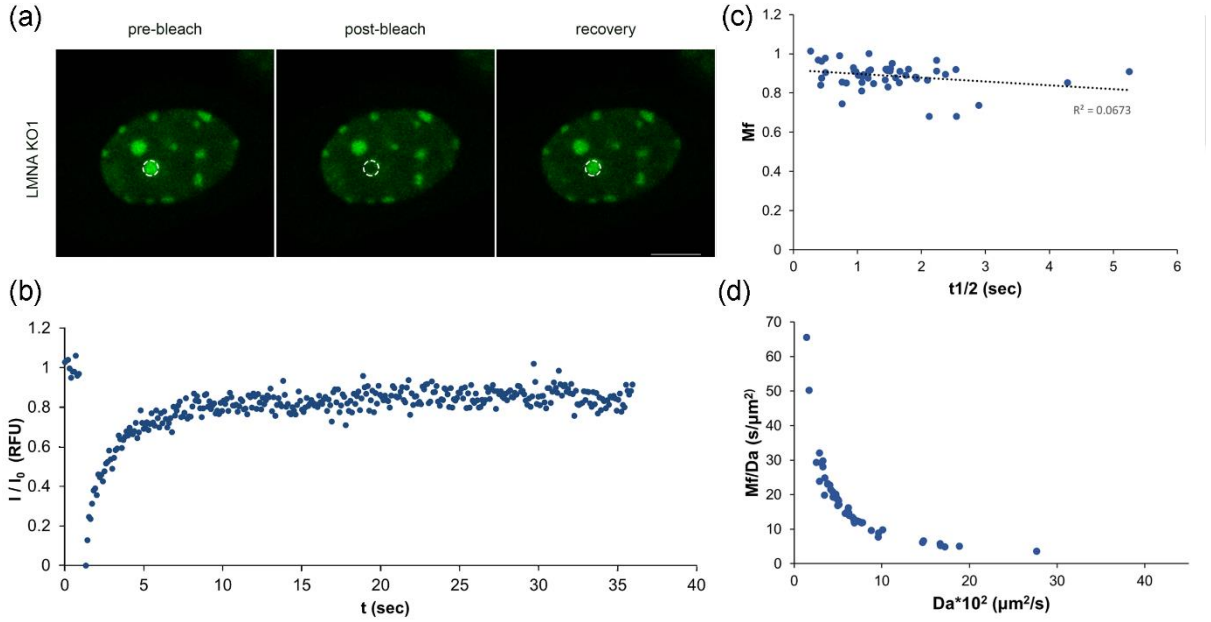
(a)
pre-bleach
post-bleach
recovery
LMNA KO1
(b)
I / I0 (RFU)
t (sec)
(c)
Mf
t1/2 (sec)
R² = 0.0673
(d)
Mf/Da (s/µm²)
Da*10² (µm²/s)

(D)

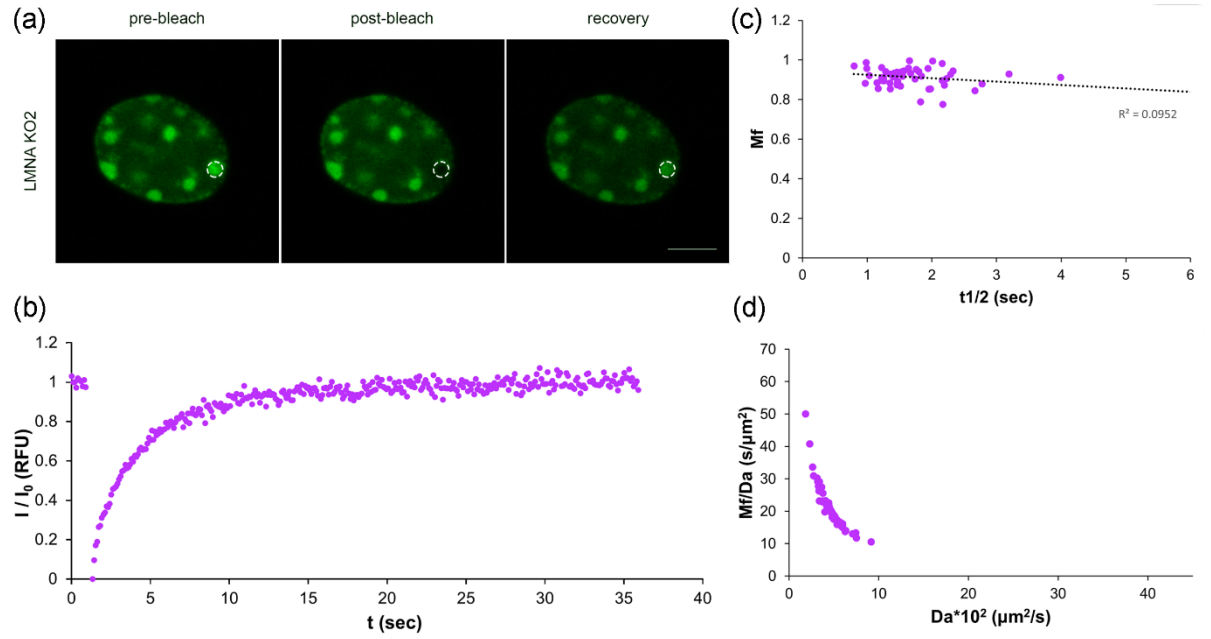
(a)
pre-bleach
post-bleach
recovery
LMNA KO2
(b)
I / I0 (RFU)
t (sec)
(c)
Mf
t1/2 (sec)
R² = 0.0952
(d)
Mf/Da (s/µm²)
Da*10² (µm²/s)

(E)

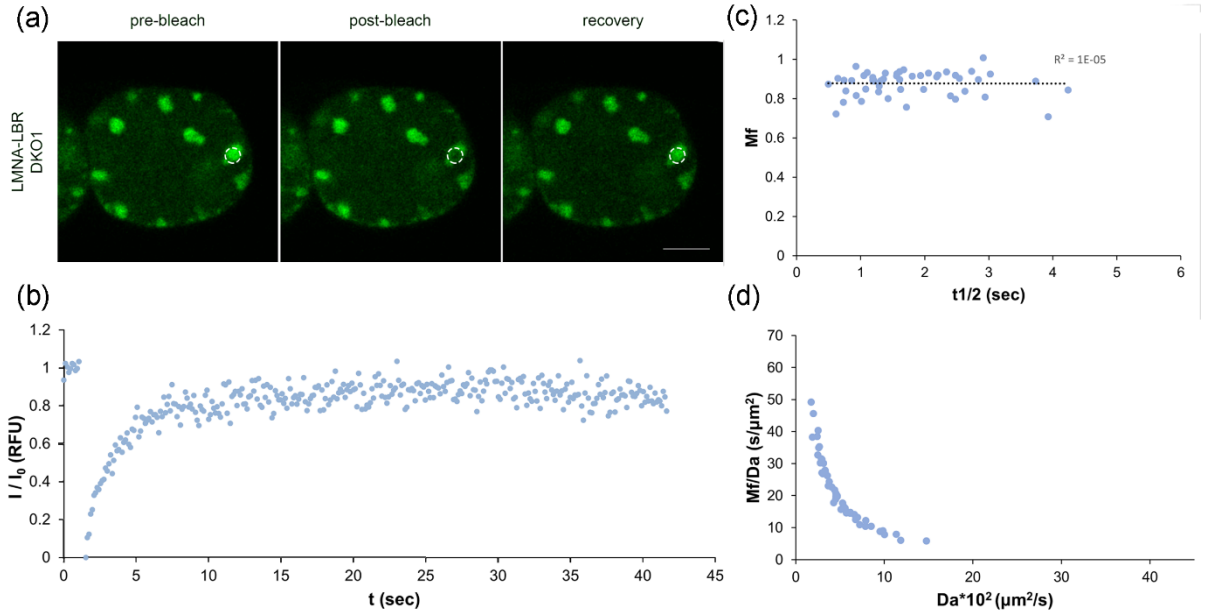
(a)
pre-bleach
post-bleach
recovery
LMNA-LBR DKO1
(b)
I / I0 (RFU)
t (sec)
(c)
Mf
t1/2 (sec)
R² = 1E-05
(d)
Mf/Da (s/µm²)
Da*10² (µm²/s)

(F)

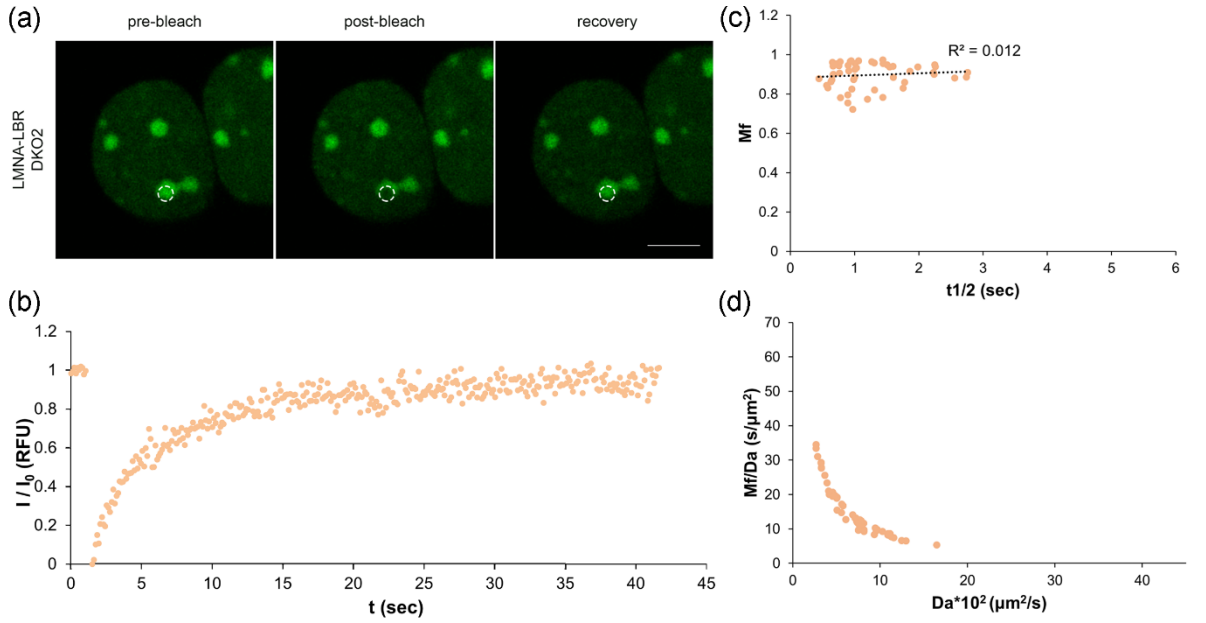
(a)
pre-bleach
post-bleach
recovery
LMNA-LBR DKO2
(b)
I / I0 (RFU)
t (sec)
(c)
Mf
t1/2 (sec)
R² = 0.012
(d)
Mf/Da (s/µm²)
Da*10² (µm²/s)

(G)

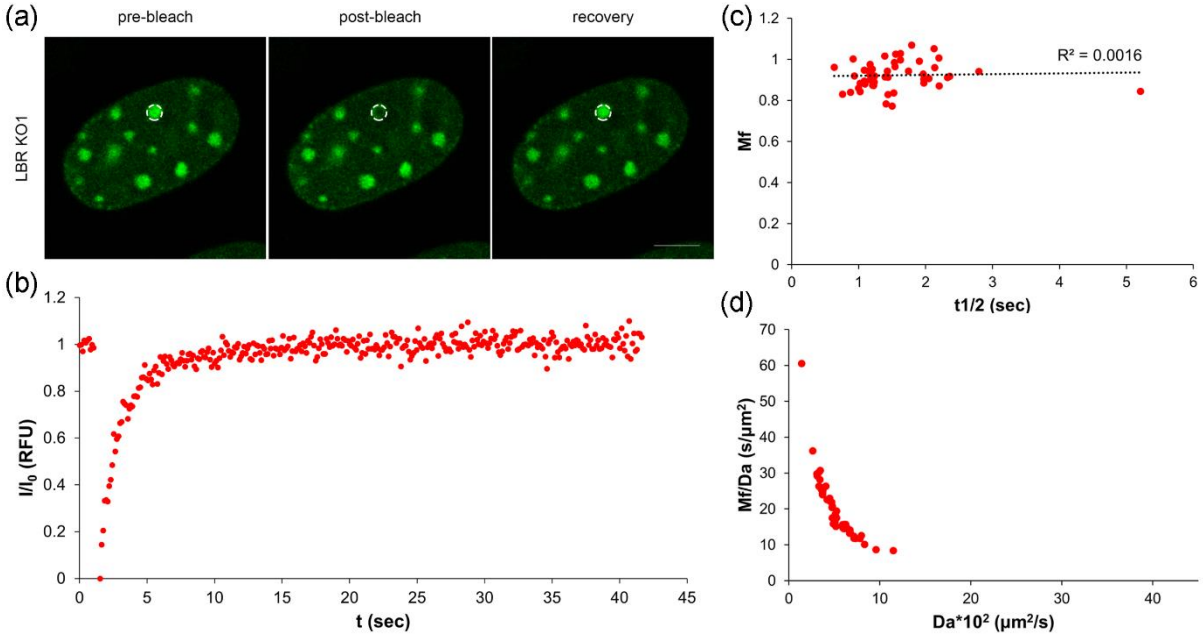
(a)
pre-bleach
post-bleach
recovery
LBR KO1
(b)
I/I0 (RFU)
t (sec)
(c)
Mf
t1/2 (sec)
R² = 0.0016
(d)
Mf/Da (s/µm²)
Da*10² (µm²/s)

(H)

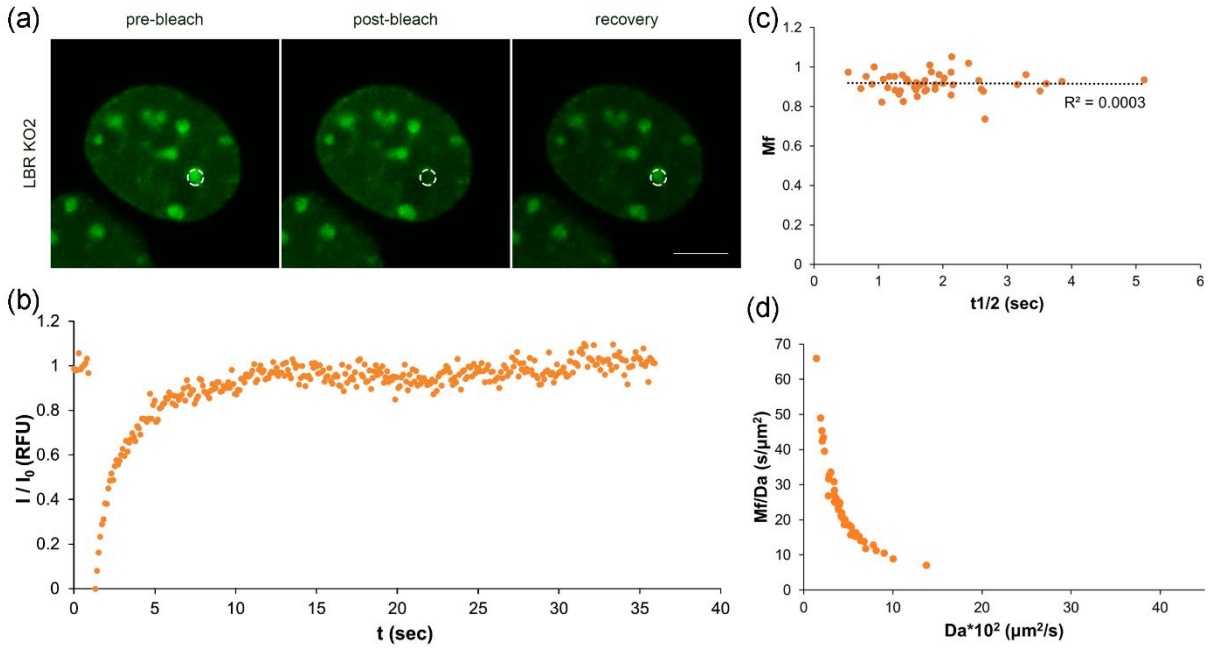
(a)
pre-bleach
post-bleach
recovery
LBR KO2
(b)
I / I0 (RFU)
t (sec)
(c)
Mf
t1/2 (sec)
R² = 0.0003
(d)
Mf/Da (s/µm²)
Da*10² (µm²/s)

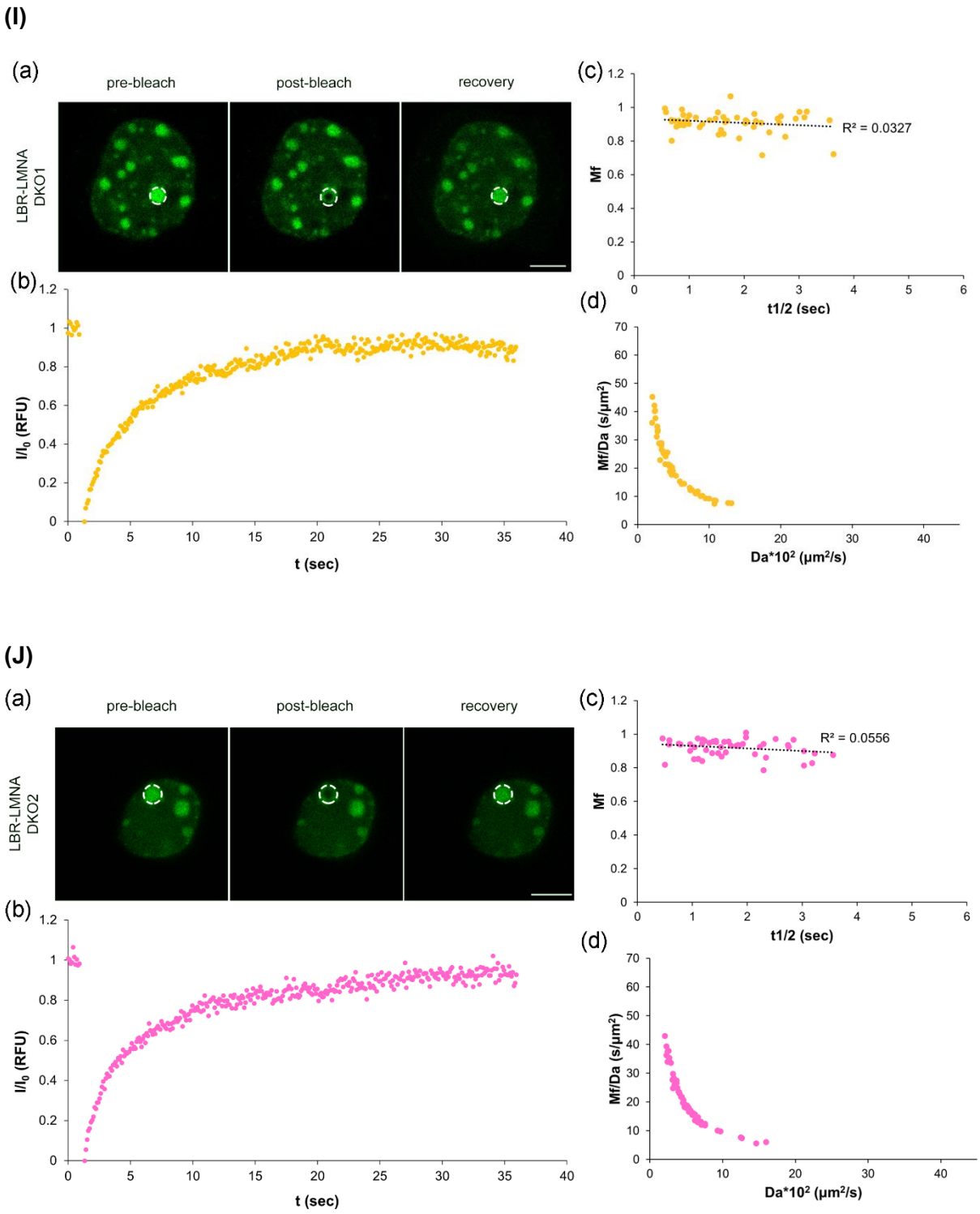

Figure 48. (a) Indicatory images of a FRAP experiment conducted in an (A) NIH WT (10% FBS) cell, (B) NIH WT (15% FBS) cell, (C) LMNA KO1 cell, (D) LMNA KO2 cell, (E) LMNA-LBR DKO1 cell, (F) LMNA-LBR DKO2 cell, (G) LBR KO1 cell, (H) LBR KO2 cell, (I) LBR-LMNA DKO1 cell (by Tsomakian Konstantinos), (J) LBR-LMNA DKO2 cell (by Tsomakian Konstantinos). A single focus (dashed circle) per nucleus was photobleached in each one of a total of 50 independent experiments (scalebar: 5um). (b) Examples of one FRAP readout (grey) of each clone examined plotted as a function of time. (c) *Mf* values were plotted against

t1/2 values in a scatter plot for all clones tested. (d) *Mf/Da* was plotted against *Da* for all clones tested, giving a hyperbole graph.

Table 3. Coefficients of variation of the *Mf*, *t1/2* and *Da* variables for the LMNA KO and LMNA-LBR DKO clones.

Coefficient of Variation (CV)			
	Mf	**$t_{1/2}$**	**Da**
NIH WT (10% FBS)	0.059	0.387	0.999
LMNA KO1	0.077	0.619	0.729
LMNA KO2	0.054	0.493	0.333
LMNA-LBR DKO1	0.071	0.503	0.536
LMNA-LBR DKO2	0.071	0.485	0.442

Table 4. Coefficients of variation of the *Mf*, *t1/2* and *Da* variables for the LBR KO and LBR-LMNA DKO clones.

Coefficient of Variation (CV)			
	Mf	**$t_{1/2}$**	**Da**
NIH WT (15% FBS)	0.077	0.416	0.402
LBR KO1	0.071	0.452	0.347
LBR KO2	0.058	0.467	0.478
LBR-LMNA DKO1	0.068	0.493	0.569
LBR-LMNA DKO2	0.054	0.460	0.542

The coefficient of variation for each parameter (CV_{Mf}, $CV_{t1/2}$ and CV_{Da}) was calculated for all clones tested as the ratio of the standard deviation to the mean of each dataset (Tables 3 and 4). However, no clear evidence was provided from these calculations since the dynamic parameters did not vary systematically in relation to the cell population.

The distribution of the numerical data obtained regarding the *Mf* (Fig. 49 – 52) and *Da* (Fig. 53 – 56) was visualized using violin plots and the data were statistically analysed. Since any differences observed regarding the *Mf* values of each clone

tested were only of no statistical significance (Table A3, Appendix), the attention was focused on the distribution of the *Da* values for each one of the clones.

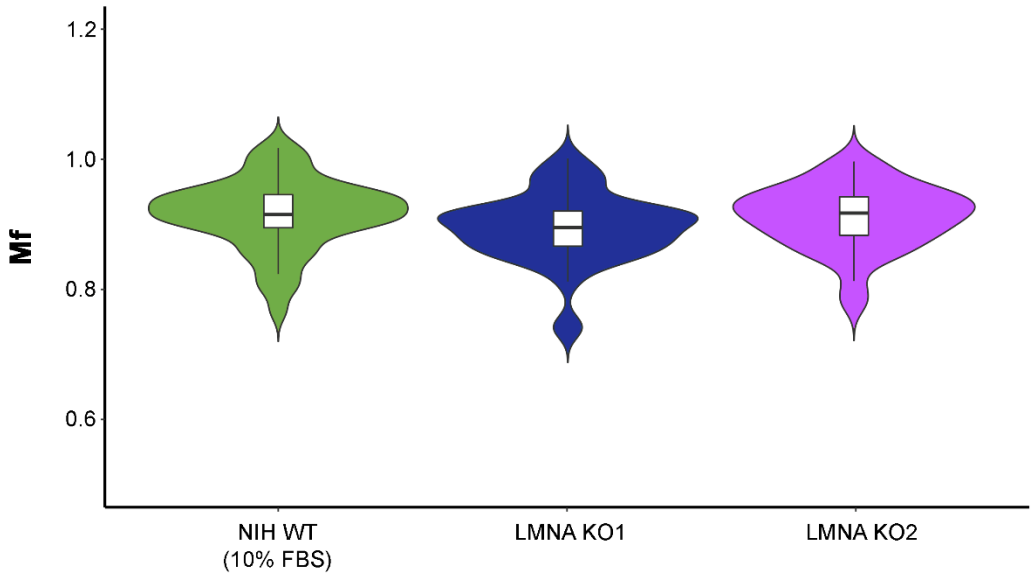

Figure 49. Violin plot depicting the distribution around the mean of the *Mf* values for the following cell populations: NIH WT (10% FBS), LMNA KO1, LMNA KO2.

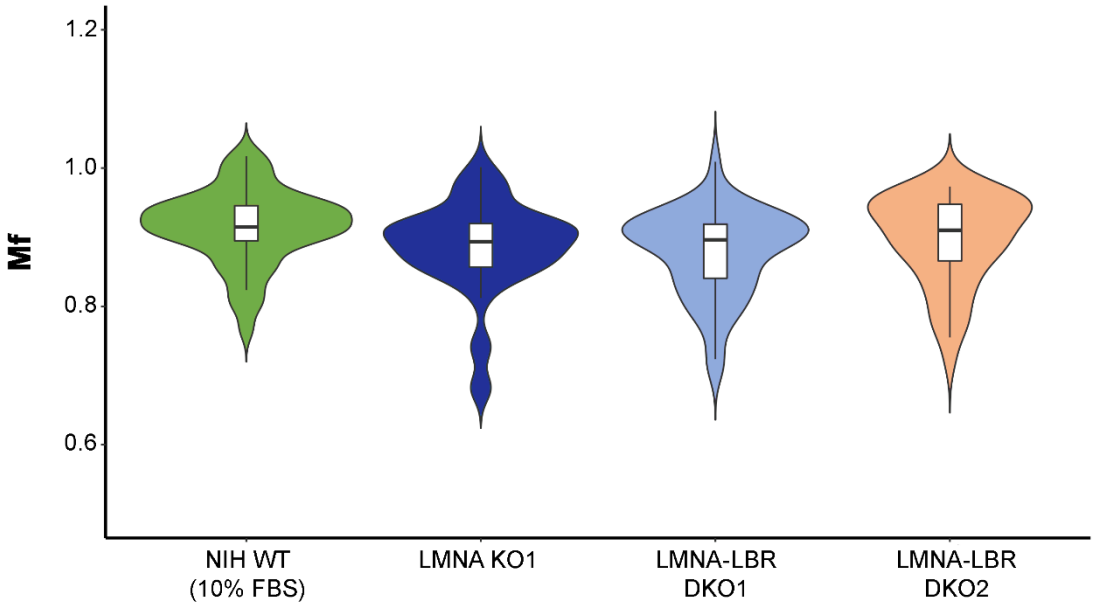

Figure 50. Violin plot depicting the distribution around the mean of the *Mf* values for the following cell populations: NIH WT (10% FBS), LMNA KO1, LMNA-LBR DKO1, LMNA-LBR DKO2.

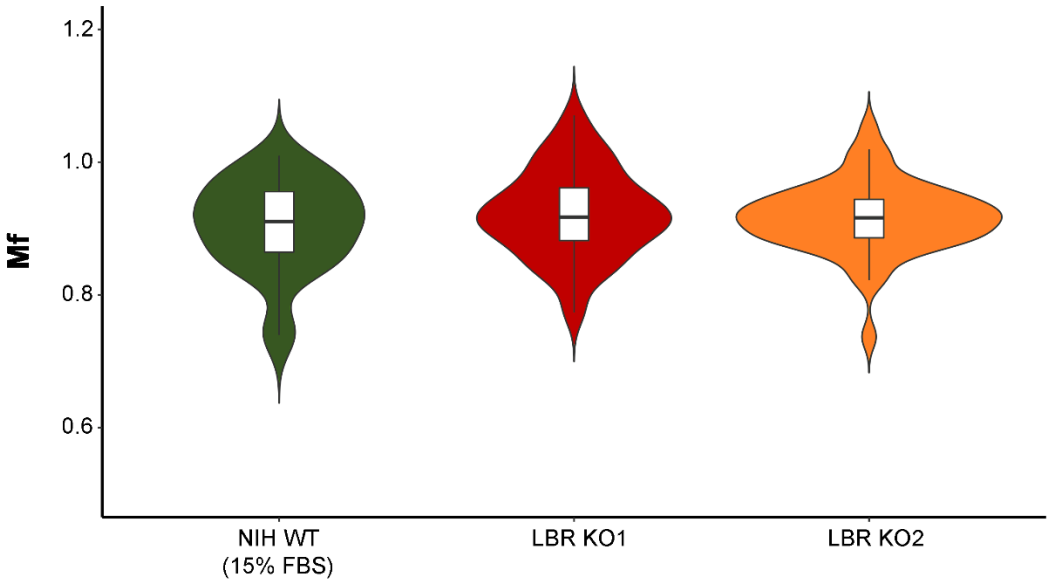

Figure 51. Violin plot depicting the distribution around the mean of the *Mf* values for the following cell populations: NIH WT (15% FBS), LBR KO1, LBR KO2.

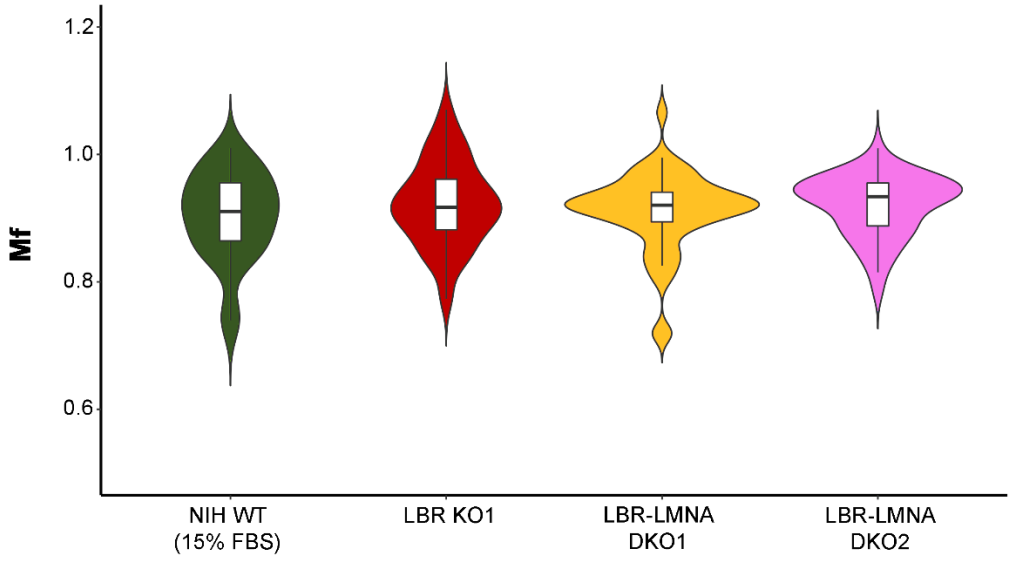

Figure 52. Violin plot depicting the distribution around the mean of the *Mf* values for the following cell populations: NIH WT (15% FBS), LBR KO1, LBR-LMNA DKO1, LBR-LMNA DKO2.

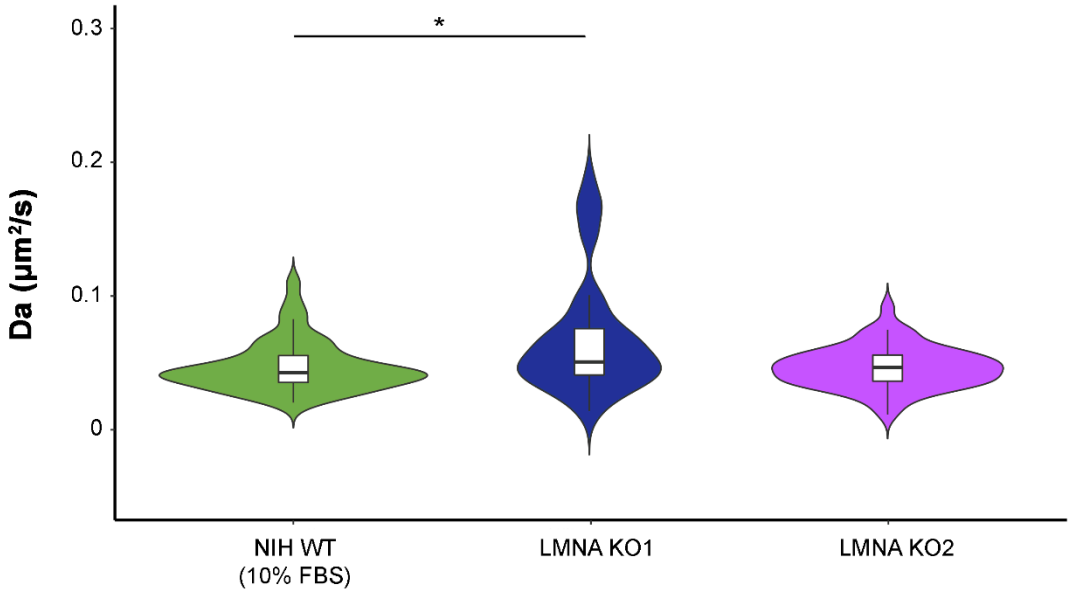

Figure 53. Violin plot depicting the distribution around the mean of the *Da* values for the following cell populations: NIH WT (10% FBS), LMNA KO1, LMNA KO2. Statistical significance is stated with asterisks (*: p<0.05, **: p<0.01, ***: p<0.001).

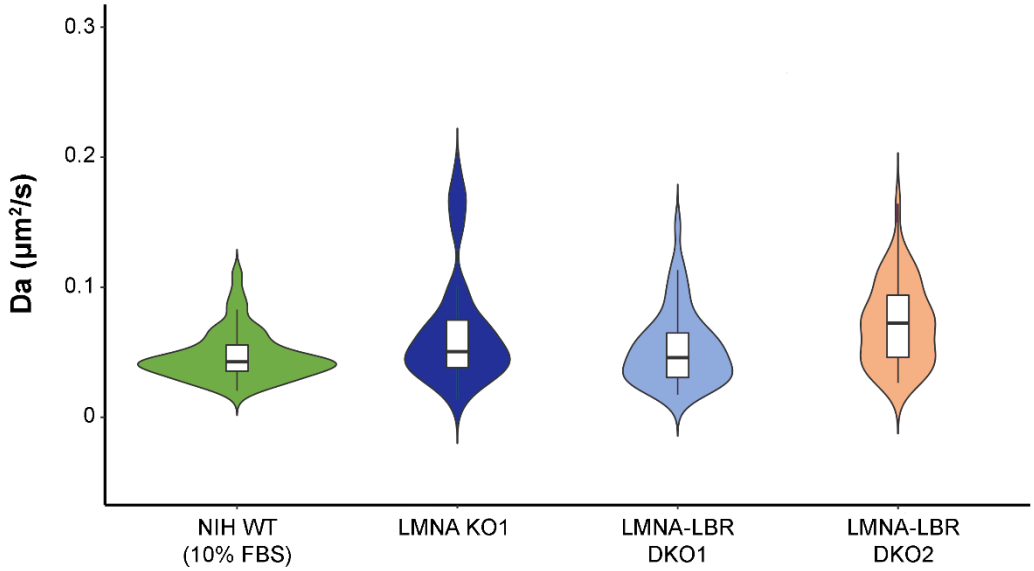

Figure 54. Violin plot depicting the distribution around the mean of the *Da* values for the following cell populations: NIH WT (10% FBS), LMNA KO1, LMNA-LBR DKO1, LMNA-LBR DKO2.

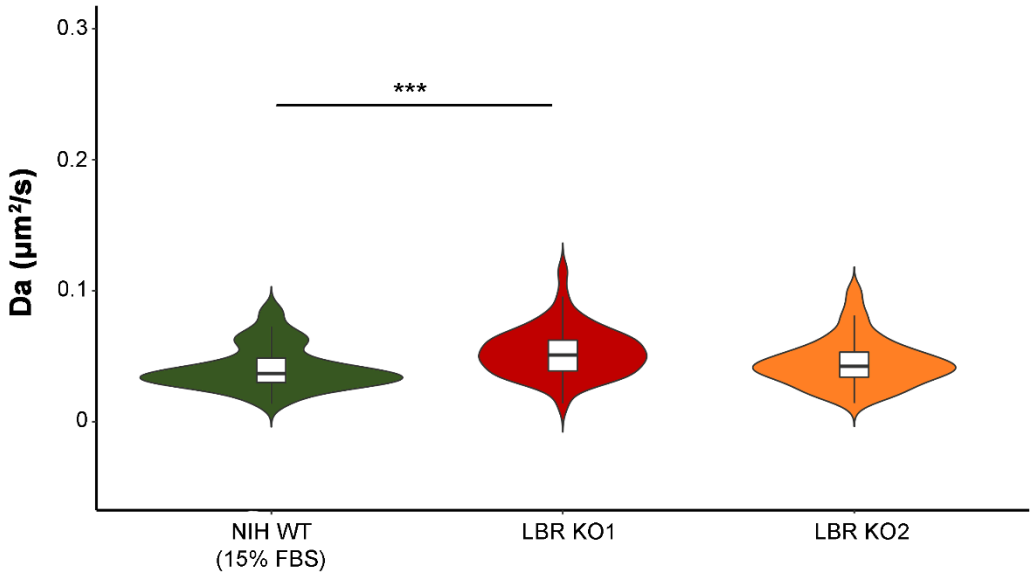

Figure 55. Violin plot depicting the distribution around the mean of the *Da* values for the following cell populations: NIH WT (15% FBS), LBR KO1, LBR KO2. Statistical significance is stated with asterisks (*: p<0.05, **: p<0.01, ***: p<0.001).

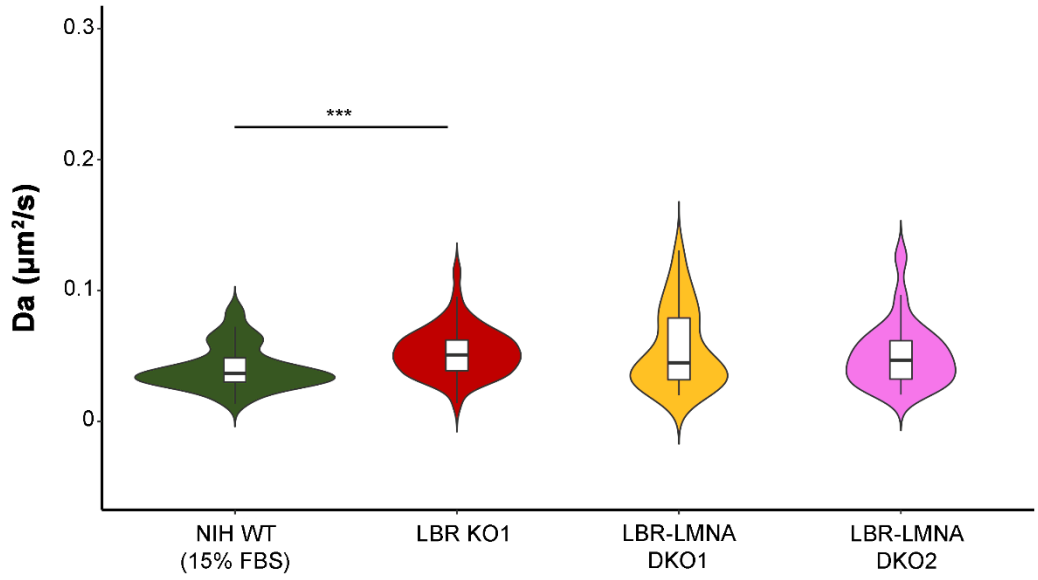

Figure 56. Violin plot depicting the distribution around the mean of the *Da* values for the following cell populations: NIH WT (15% FBS), LBR KO1, LBR-LMNA DKO1, LBR-LMNA DKO2. Statistical significance is stated with asterisks (*: p<0.05, **: p<0.01, ***: p<0.001).

The most prominent, as well as statistically significant, difference was observed between the LBR KO1 clone and its respective control cell population (NIH WT (15% FBS)). The mutant clone exhibited higher *Da* values, implying an increase in the mobility of HP1α, which could mean that there is a shift to more relaxed dynamic chromatin configurations. The LBR KO2 clone was not found to behave in a similar manner. This difference between the two clones that derived from the same stable cell line could be attributed to the different mutations in the LBR gene that each clone carries. In case of the LBR KO1 clone the LBR gene was silenced. On the other hand, in the LBR KO2 cells a short fragment of the LBR protein is expressed, which might allow these cells to maintain a partially functional LBR pool. Interestingly, all other differences observed between the clones that were examined and their respective controls were of only low or no actual statistical significance (Table A4, Appendix).

The SC curves (Fig. 57 – 60) were assessed according to the study of Christogianni et al., who suggested that HP1α dynamics can be affected by alterations in the chromatin condensation state and that such alterations happen in a gradual manner along a continuum of dynamic states. Based on these findings, the SC curves for each one of the mutant clones were compared to those of their respective controls, in order to extract information about potential shuffling from a high to a low dynamics regime and vice versa, upon loss of LBR and/or Lamin A/C. The SC curve that corresponded to the LMNA KO1 clone was slightly shifted in relation to that of the NIH WT 10% FBS cell population, while LMNA KO2 clone agreed with the NIH WT 10% FBS cells (Fig. 57). Regarding the LMNA-LBR DKO1 and LMNA-LBR DKO2 SC curves, the former's behavior was similar to that of the NIH WT 10% FBS cells, while the latter one was shifted in a similar manner as the LMNA KO1 clone (Fig. 58). LBR KO1 and LBR KO2 clones showed no significant difference compared to their NIH WT 15% FBS control cells (Fig. 59), a finding that was contradictory to the difference between the LBR KO1 and the wild-type cells that was observed in the violin plots above. Differences between the LBR KO1 and the two LBR-LMNA clones were observed but they were only moderate (Fig. 60).

(A)

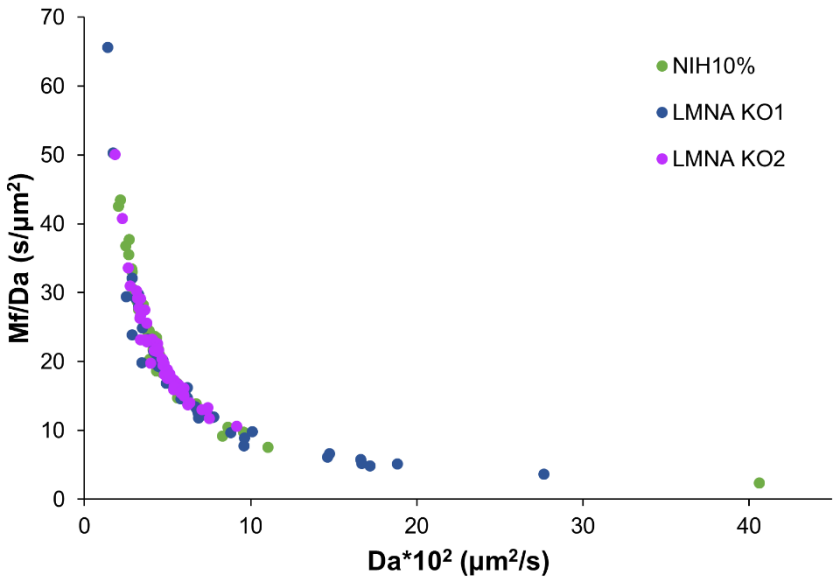
70
60
50
40
30
20
10
0
0
10
20
30
40
Mf/Da (s/µm²)
Da*10² (µm²/s)
NIH10%
LMNA KO1
LMNA KO2

(B)

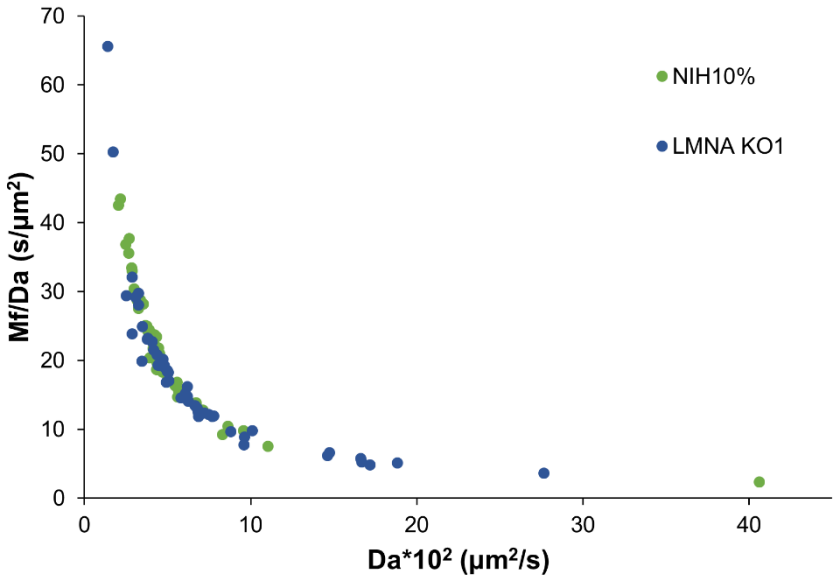
70
60
50
40
30
20
10
0
0
10
20
30
40
Mf/Da (s/µm²)
Da*10² (µm²/s)
NIH10%
LMNA KO1

(C)

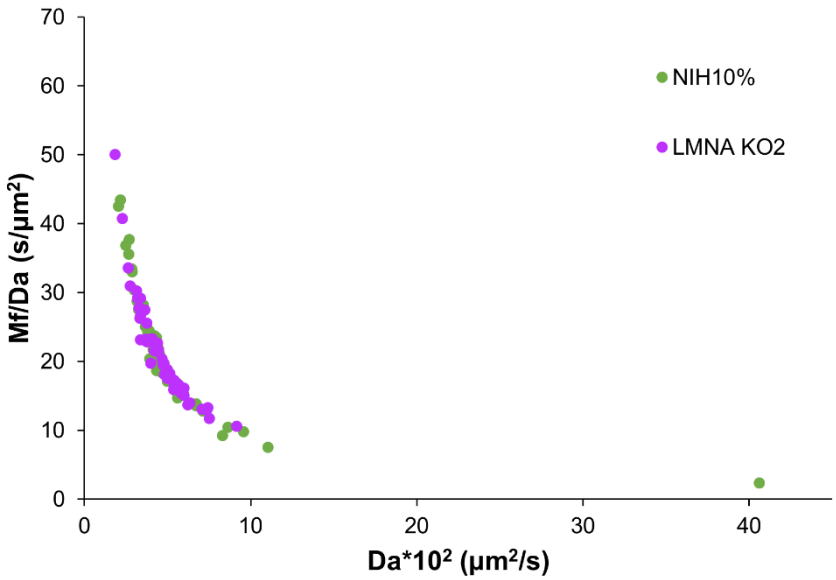

Figure 57. Graphs for the comparison of the *Mf/Da* against *Da* plots between the clones: (A) NIH WT (10% FBS) – LMNA KO1 –LMNA KO2, (B) NIH WT (10% FBS) – LMNA KO1, (C) NIH WT (10% FBS) – LMNA KO2.

(A)

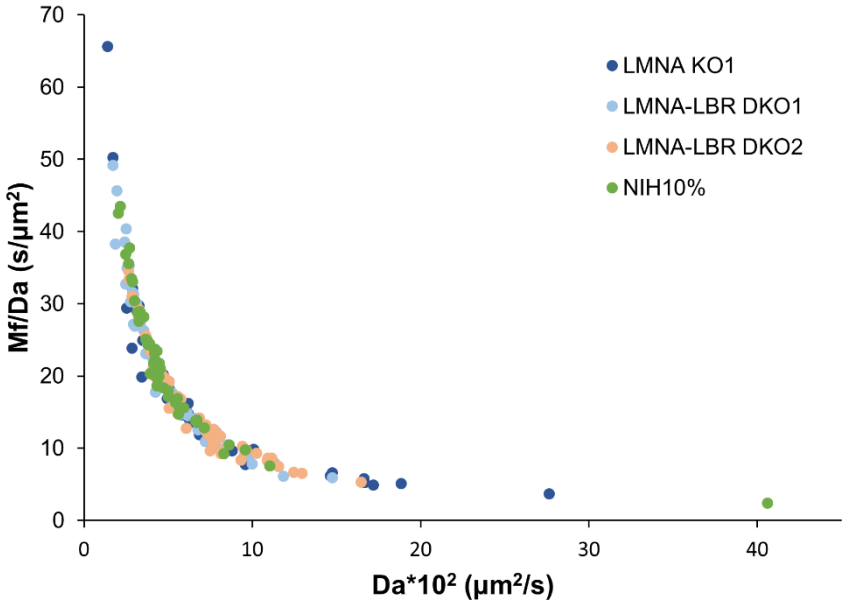

(B)

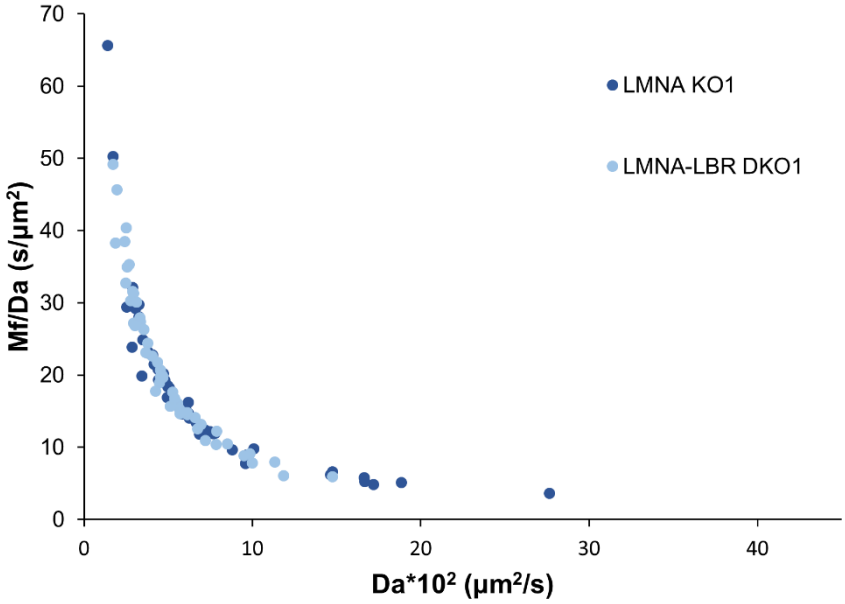

(C)

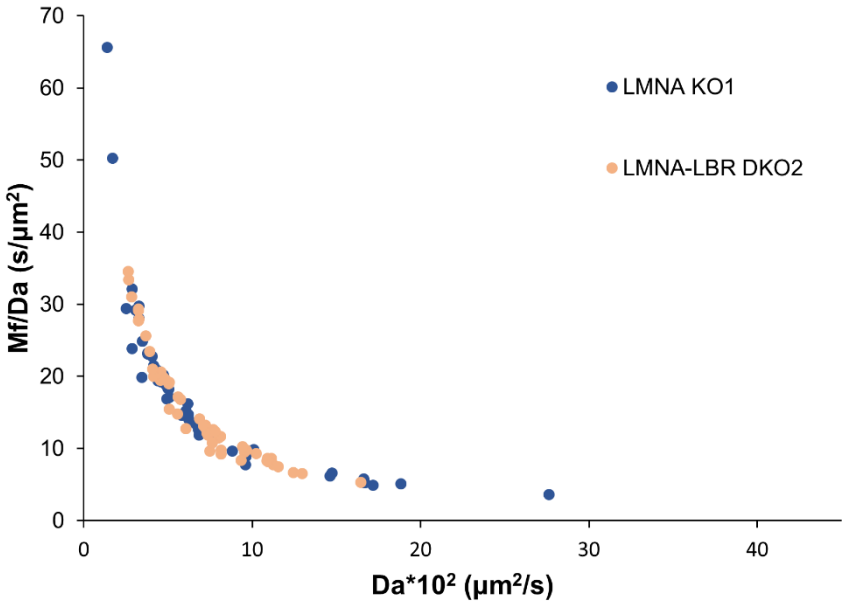

Figure 58. Graphs for the comparison of the *Mf/Da* against *Da* plots between the clones: (A) NIH WT (10% FBS) – LMNA KO1 – LMNA-LBR DKO1 – LMNA-LBR DKO2, (B) LMNA KO1 – LMNA-LBR DKO1, (C) LMNA KO1 – LMNA-LBR DKO2.

(A)

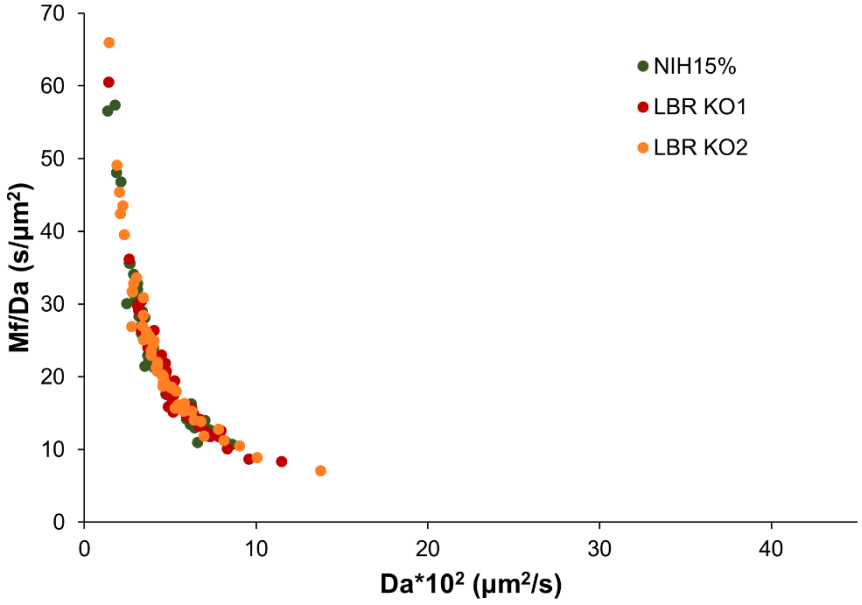
70
60
50
40
30
20
10
0
0
10
20
30
40
Mf/Da (s/µm²)
Da*10² (µm²/s)
NIH15%
LBR KO1
LBR KO2

(B)

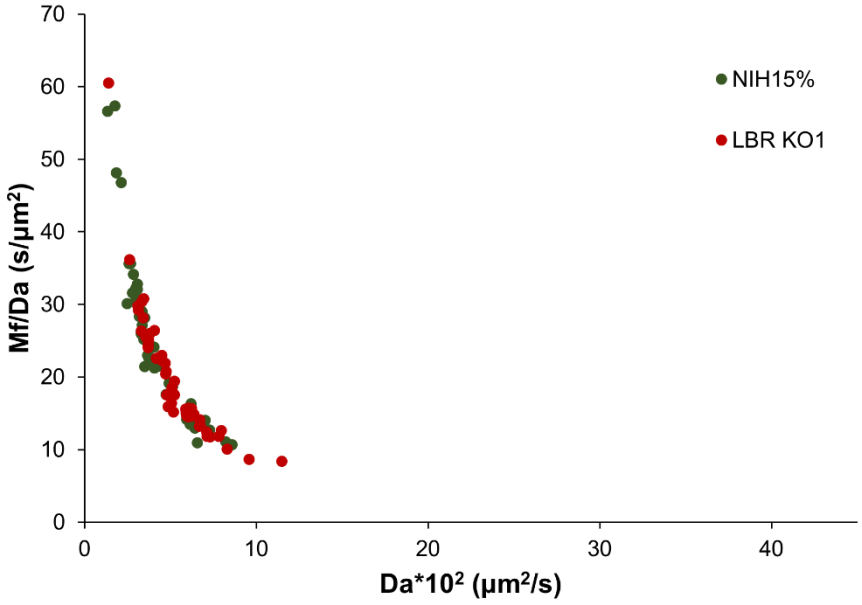
70
60
50
40
30
20
10
0
0
10
20
30
40
Mf/Da (s/µm²)
Da*10² (µm²/s)
NIH15%
LBR KO1

(C)

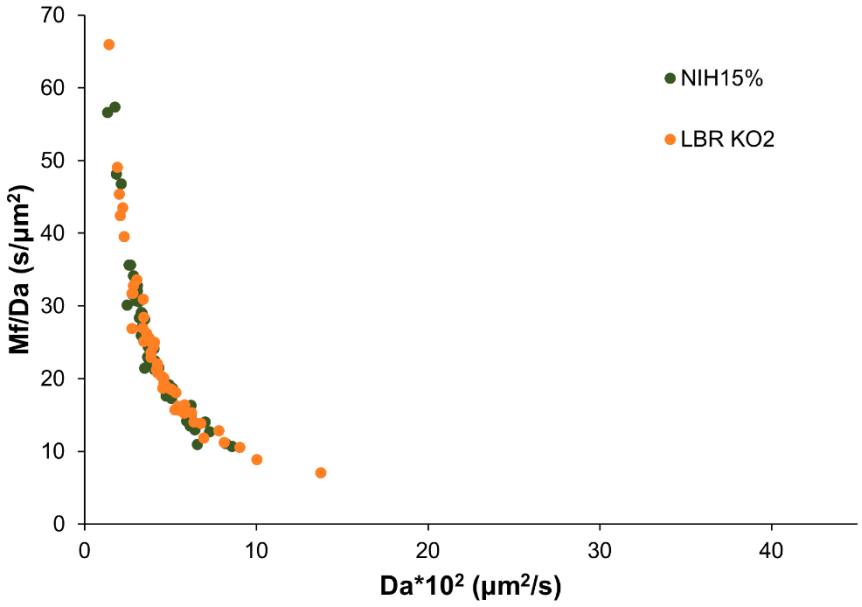

Figure 59. Graphs for the comparison of the Mf/Da against Da plots between the clones: (A) NIH WT (15% FBS) – LBR KO1 – LBR KO2, (B) NIH WT (15% FBS) – LBR KO1, (C) NIH WT (15% FBS) – LBR KO2.

(A)

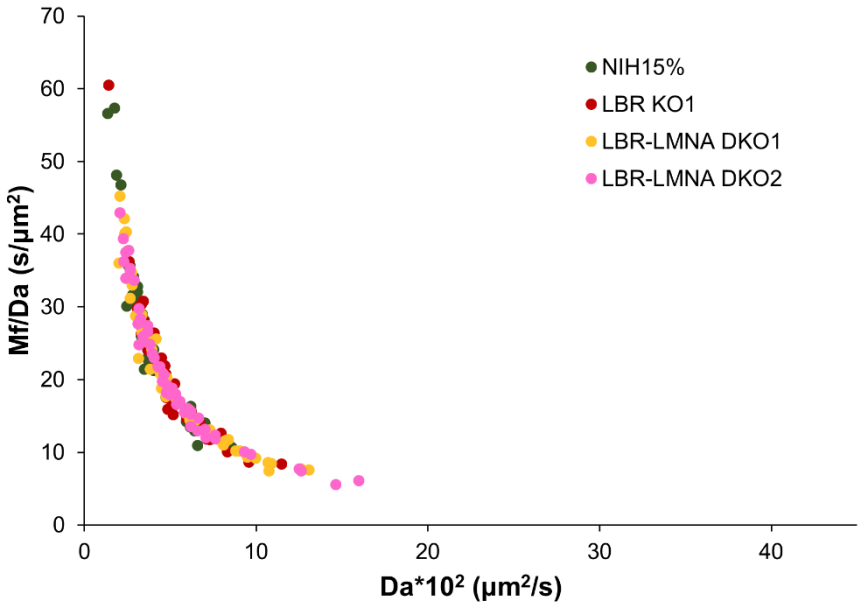

(B)

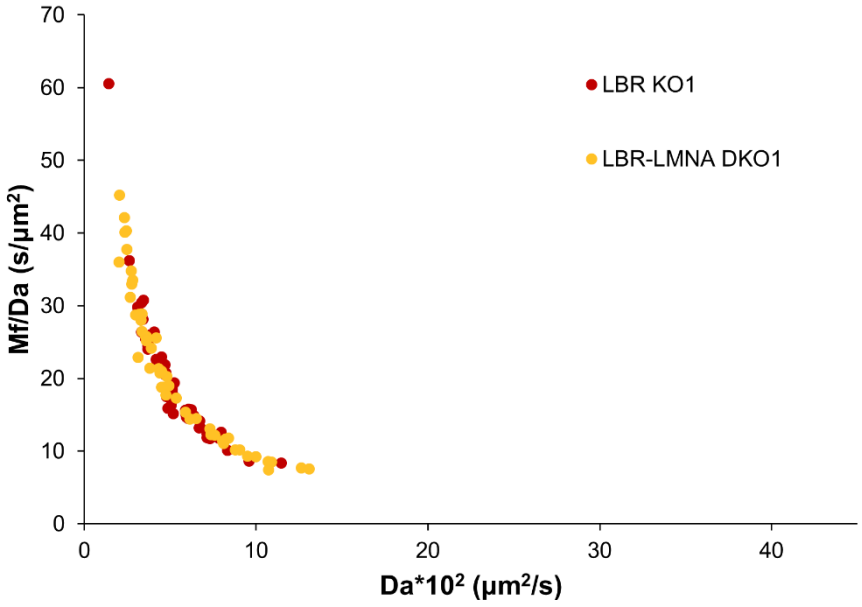

(C)

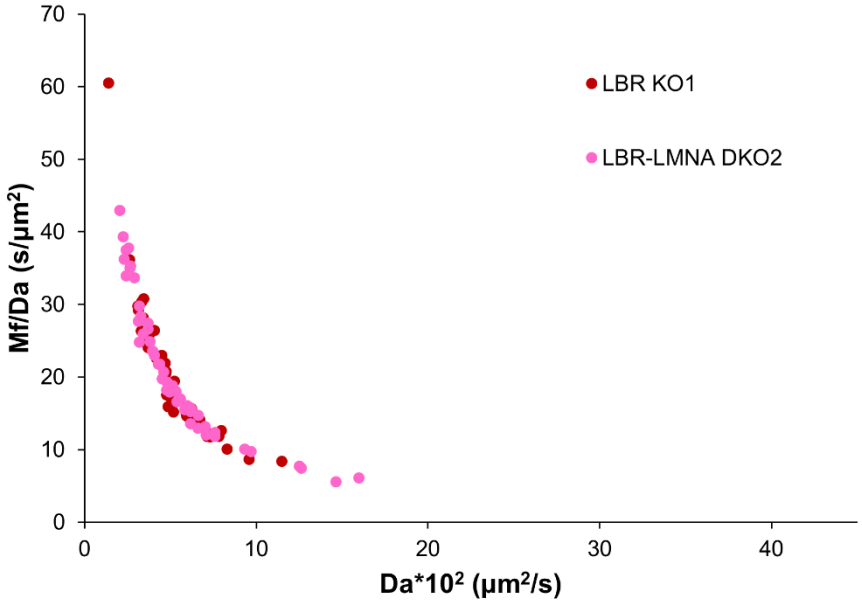

Figure 60. Graphs for the comparison of the Mf/Da against Da plots between the clones: (A) NIH WT (15% FBS) – LBR KO1 – LBR-LMNA DKO1 – LBR-LMNA DKO2, (B) LBR KO1 – LBR-LMNA DKO1, (C) LBR KO1 – LBR-LMNA DKO2.

A rather interesting information that was extracted from these graphs was that even the continua of dynamic chromatin states that correspond to the couples of clones derived from the same cell line do not always agree with each other. A possible explanation for this could be the internal heterogeneity of the distinct cell populations that were examined or heterogeneity at the level of single randomly chosen heterochromatic foci. It should also be taken into consideration that the two sets of clones that were studied (NIH WT 10% FBS – LMNA KO – LMNA-LBR DKO and NIH WT 15% FBS – LBR KO – LBR-LMNA DKO) were cultured under two different conditions (growth medium supplemented with 10% and 15% FBS). The presence of less or more serum in the growth medium could lead to changes regarding the number of cells that enter mitosis or the duration of the different stages of the cell cycle. Thus, the changes in chromatin state could be related to chromatin redistribution events that occur as the cell cycle progresses, and not to the loss of LBR and/or Lamin A/C.

3.5. Lack of Lamin A/C or LBR or both does not affect the ability of cells to adhere and migrate on cell-free surfaces.

Preliminary data from the transcriptomic analysis that was conducted before (by Katerina Soupsana) indicated alterations in the transcriptional profiles of the cells that lack Lamin A/C or LBR or both. Such alterations concerned the expression levels of genes related to the extracellular matrix as well as to the adherence ability of the cells. This evidence along with other findings that associate the position of the nucleus inside the cell (cellular polarization) and cell migration with A-type lamins (Kim *et al.*, 2014) raised the question of whether the loss of one of these NL components or the combinatorial loss of both induces any changes regarding the migrational ability of these cells. In order to investigate this possibility, we employed the wound healing assay. For that purpose, cell-free gaps were created on a confluent monolayer of cells (Fig. 61 and Fig. 62; five independent replicates per clone).

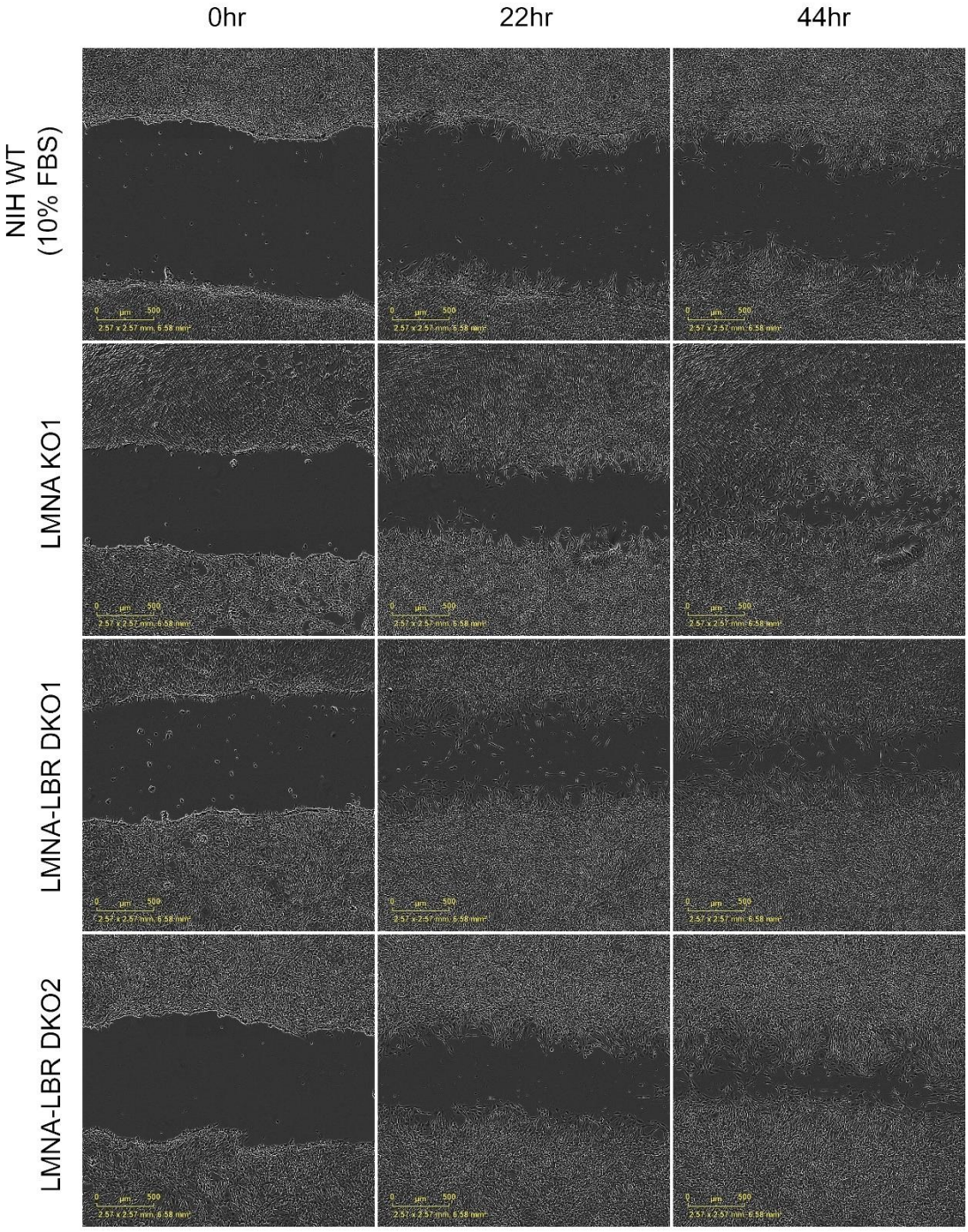

Figure 61. Representative images of the cell-free spaces (wounds) created on confluent monolayers of NIH WT (10% FBS), LMNA KO and LMNA-LBR DKO cells (scalebar: 0.5mm).

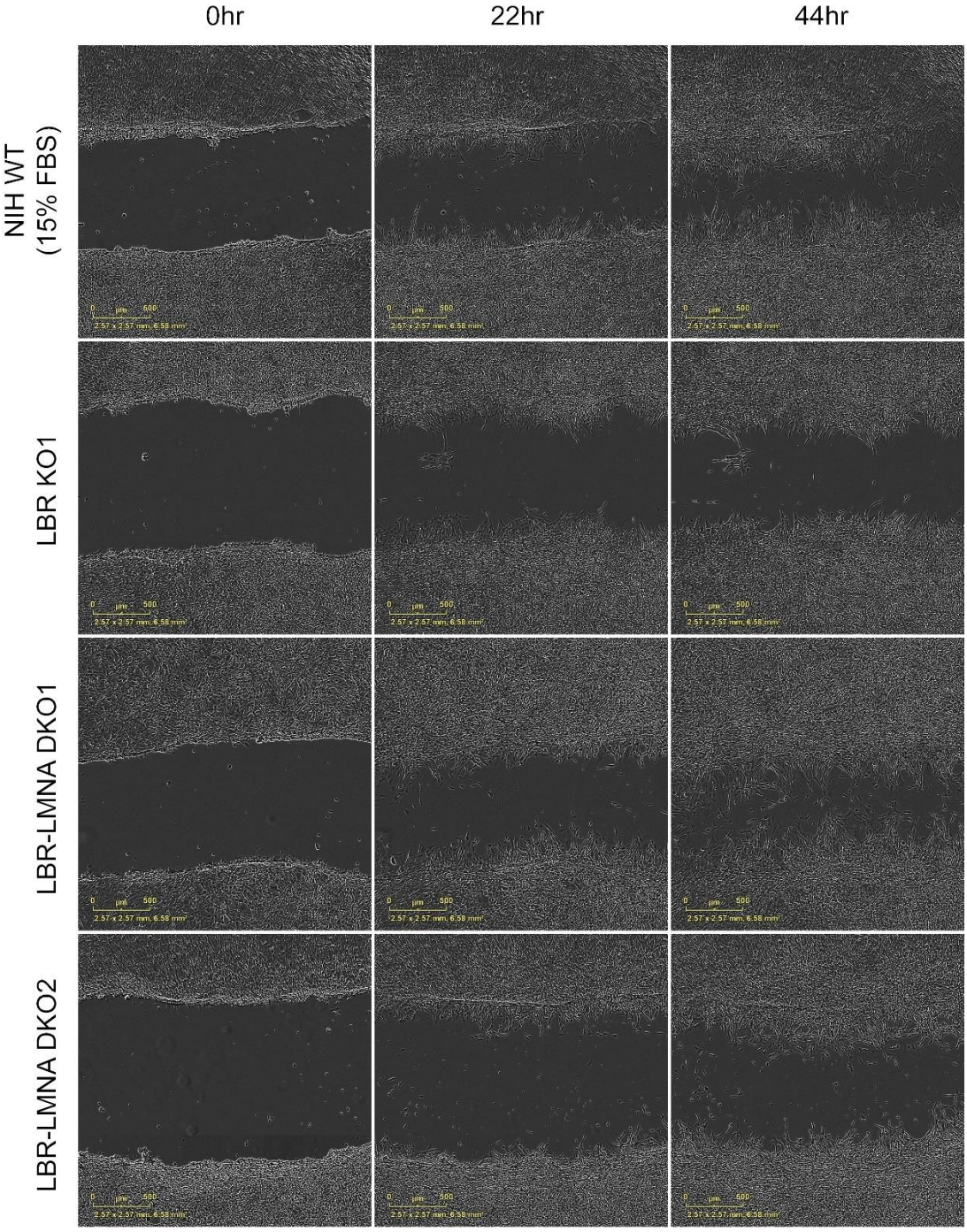

Figure 62. Representative images of the cell-free spaces (wounds) created on confluent monolayers of NIH WT (15% FBS), LBR KO and LBR-LMNA DKO cells (scalebar: 0.5mm).

The wounds were generated manually and the initial gap size was not consistent between the replicates (also apparent in Fig. 61 and Fig. 62). Thus, velocity at which cells migrate towards the cell-free area (Vmigration) (Fig. 63 and Fig. 64) was considered as the most reliable parameter for the comparison of the clones examined, since its calculation was independent from the initial gap area (see paragraph 2.9.2. of Materials & Methods).

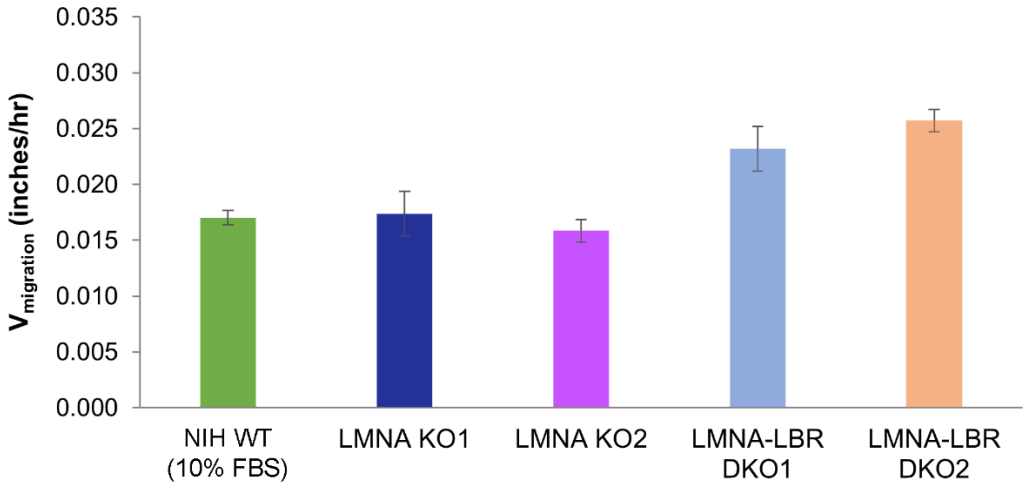

Figure 63. Bar plot depicting the velocity of migration, as it was calculated for each one of the following cell populations: NIH WT (10% FBS), LMNA KO1, LMNA KO2, LMNA-LBR DKO1, LMNA-LBR DKO2.

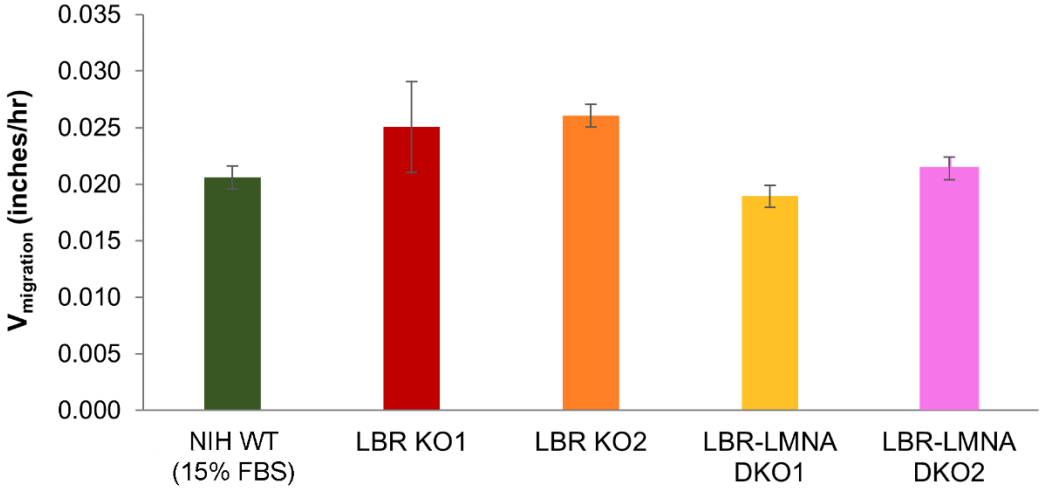

Figure 64. Bar plot depicting the velocity of migration, as it was calculated for each one of the following cell populations: NIH WT (15% FBS), LBR KO1, LBR KO2, LBR-LMNA DKO1, LBR-LMNA DKO2.

The results from the calculation of the velocity of migration for each cell population were not very informative. In the case of LMNA KO and LMNA-LBR DKO clones, the former seem to be unchanged, while the latter present increased migration rates. In the case of LBR KO and LBR-LMNA DKO clones, the double KOs' velocity of migration is almost equal to that of wild type cells, whereas the single KOs' migration rates appear to be higher. Comparing the results between all of the clones reveals that loss of LBR might have an impact on the ability of cells to migrate, as LBR KO and LMNA-LBR DKO clones appear to move faster compared to their controls, even though this does not correlate with the results of the LBR-LMNA DKO clones. On the other hand, loss of Lamin A/C does not seem to affect cell motility. These observations do not support previous observations that associate loss of Lamin A/C with impaired cell migration (Kim *et al.*, 2014). The statistical analysis of these data did not reveal any actual statistical significance regarding the differences observed (Table A5, Appendix) and, thus, the experiment was considered inconclusive.

Discussion 

4. Discussion

Chromatin architecture, a key regulator of many cellular and developmental processes, has been attracting the scientific interest for many years now. During the past two decades, the development of new technologies such as 3C techniques and modern microscopic methods has allowed scientists to gain more insight into the principles of chromatin organization, revealing the existence of chromatin domains considered as the building blocks of the chromatin landscape. Chromatin architecture has been found to be regulated by a multitude of factors and mechanisms. These include the microenvironment of the nuclear periphery, which is comprised of the nuclear envelope membrane system along with its protein cargo, as well as other peripheral nuclear structures, such as the nuclear lamina. The nuclear periphery serves as a binding platform for heterochromatin, and, thus, influences and maintains the spatial organization of the different types of chromatin inside the nucleus. Two types of heterochromatin tethers have been recognized so far: the A-tether, which is comprised of Lamin A/C along with a set of proteins of the nuclear periphery, the composition of which is cell type and developmental stage-specific, and the B-tether which corresponds to LBR. The rod cells of nocturnal mammals have been extensively used as a tool for the investigation of the mechanisms that drive chromatin organization, since they lack both tethers and they exhibit an inverted chromatin distribution pattern. These mechanisms have been found to be controlled by a wide array of factors, that have not yet been fully elucidated, despite the fact that chromatin research spans almost a century.

The present thesis is part of a project aiming to investigate how the loss of two major components of the nuclear periphery, LBR and Lamin A/C, could affect nuclear envelope morphology and chromatin architecture. The experimental design included the use of NIH/3T3 cells knocked out for LBR or Lamin A/C or both and the morphological characterization of the stable cell lines that were generated. The localization of nuclear envelope proteins as well as the possibility of changes in chromatin distribution inside the nucleus upon loss of these two proteins were investigated, mostly using microscopic methods. Finally, the ability of cells to adhere and migrate was also assessed by a wound-healing assay.

One of the most significant findings of this work has been the observation that nuclear envelope properties were affected upon concurrent loss of LBR and Lamin A/C. In the affected cells, major components of the nuclear periphery were found to be excluded from whole parts of the nuclear envelope, including proteins of the inner nuclear membrane, the outer nuclear membrane, the nuclear pore membrane and the nuclear lamina. This phenotype was called “asymmetric” and appeared with a higher frequency in cells lacking the expression of both LBR and Lamin A/C.

The observation of nuclei with altered morphological features and mislocalized nuclear envelope protein components supports previously published work, describing similar abnormalities mostly associated with pathological conditions caused by mutations in the LMNA or the LBR gene or the genes of other related proteins. Examples of such diseases are the Familial Partial Lipodystrophy (FPLD) and the Emery-Dreifuss Muscular Dystrophy (EDMD), both of which are characterized by nuclear defects, such as nuclei with altered shape and structural features (Vigoroux *et al.*, 2001; Sullivan *et al.*, 1999; Raharjo *et al.*, 2001; De Vos *et al.*, 2011).

What was interesting about our findings was that, even though in literature most fibroblastic cells usually exhibit similar nuclear abnormalities upon single loss of Lamin A/C, in our model system of NIH/3T3 mouse fibroblasts, the absence of Lamin A/C was not enough to cause the asymmetric phenotype. Actually, there was only a small percentage of asymmetric cells in the Lamin A/C knock-out clones examined, while the concurrent loss of LBR and Lamin A/C led to an increased number of asymmetric cells within the double null clones. This implies that in this particular cell type LBR might counteract the loss of Lamin A/C, allowing most of the cells to maintain their nuclear properties. However, the additional loss of LBR increases the severity of the phenotype, probably by affecting the B-type lamins’ meshworks.

The attempt to reverse the asymmetric phenotype, by overexpression of at least one of the Lamin A/C, Lamin B1 or LBR in the double knock-out cells, proved to be unsuccessful. As was proposed by Guo et al. in a study of 2014, expression of at least one of the lamins at sufficiently high levels should be enough for the maintenance of the normal distribution of major components of the nuclear periphery in differentiated murine cells (Guo *et al.*, 2014). However, in our case the asymmetric phenotype could not be rescued, implying that the nuclear envelope aberrations caused by the loss of

Lamin A/C and LBR might include irreversible alterations, such as the rupture of nuclear envelope membranes.

Even though our findings were very promising, the phenomenon of the asymmetries has not yet been mechanistically explained in our model system. Firstly, what needs to be investigated is whether the asymmetric localization of major components of the nuclear periphery is associated with potential malformations of the nuclear envelope caused upon loss of LBR and Lamin A/C. In some studies, the asymmetric phenotype has been found to be accompanied by the disconnection of the ONM from the INM, which leads to a dilation of the perinuclear space (Burke *et al.*, 2001). In 2010 Herman and Zwerger described the formation of nuclear envelope herniations in the nuclei of U2OS cells as a result of mutations in the LBR gene (Herman and Zwerger, 2010). The parts of the nuclear envelope membranes that participated in these formations were emptied of NPCs and the LINC complex components (Zwerger *et al.*, 2009). LBR's sterol reductase activity could be key in explaining such nuclear envelope aberrations. Loss of LBR could lead to impaired cholesterol biosynthesis, leading to altered lipid composition of the NE membranes, affecting nuclear envelope integrity. Taking all these into consideration, it is considered important to clarify how the nuclear envelope membranes of the asymmetric nuclei are affected. Staining the lipid membranes of the nuclear envelope with a lipid dye or assessing the nuclear envelope's morphology using electron microscopy could provide important information regarding the effect of LBR and Lamin A/C loss on the nuclear envelope organization of NIH/3T3 cells. One possibility to exclude is the rupture of the nuclear envelope membranes, although inspection of the DNA-stained nuclei does not provide any indication about it. This could be done by causing the overexpression of a fluorescently labelled protein, that is normally exclusively cytosolic and is large enough to not be able to pass through the NPCs, in the double knockout clones. Inspection of fluorescent signal inside the nucleus could mean that the continuum of NE membranes is interrupted, allowing large molecules to freely diffuse from the cytoplasm towards the nucleoplasm and vice versa.

What should also be taken into account when investigating how the loss of LBR and Lamin A/C affect nuclear envelope properties is the role of nuclear lamina in nuclear morphology, structure and mechanics. The use of super-resolution microscopy techniques has revealed the interconnection and interdependency between the

distinct meshworks each type of lamin forms. Loss of Lamin A/C has been found to cause structural changes in the B-type lamins' meshworks (Shimi *et al.*, 2015). Altered nuclear lamina meshworks can affect nuclear properties, such as stiffness and fragility, meaning that the NE integrity might be compromised in the absence of Lamin A/C. In a study of 2016, Xie et al. proposed that, since A-type lamins interact with nucleoporins, the Lamin A/C meshwork may serve as an attachment platform for the NPCs (Xie *et al.*, 2016). Thus, the absence of Lamin A/C could lead to aberrant NPCs' localization and promote their clustering. For this reason, it would be useful to examine the morphology of the remaining nuclear lamina meshworks in the single Lamin A/C or LBR knockout, as well as in the double null cells and assess how this might be related to the asymmetric distribution of the NPCs or other proteins of the nuclear periphery. The use of modern high-resolution microscopic techniques, such as 3D-SIM (3D-Structured Illumination Microscopy), could prove very useful for this attempt.

A closer look at the interconnection between the cytoskeleton and the nucleoskeleton might also provide evidence regarding the mechanisms involved in the nuclear envelope abnormalities that make their appearance in the absence of Lamin A/C and LBR. Kim *et al.* have shown that Lamin A/C mediates the formation of the perinuclear actin cap, an actomyosin filament structure that provides protection of the nucleus against mechanical stress, and thus, facilitates the maintenance of nuclear integrity (Kim *et al.*, 2017). Moreover, the NPCs tend to cluster towards the centrosomes in the absence of Lamin A/C, pulled by a dynein-based mechanism that is associated with centrosome separation in prophase. These pulling forces are counteracted by Lamin A/C, which, when present, prevents NPCs' clustering towards the centrosomes (Guo and Zheng, 2015). Based on these findings, it is considered possible that the asymmetric phenotype observed in cells that do not express Lamin A/C and LBR might be the result of impaired nucleoskeleton-to-cytoskeleton association and forces on the components of the nuclear envelope exerted by structures outside the nucleus. These hypotheses should be further examined, by investigating if there are any cytoskeletal impairments regarding the cells that enter mitosis and regarding the separation of centrosomes in prophase. Findings from previous members of the lab revealed that, in contrast to what Guo et al. proposed, the asymmetric phenotype is not a feature of prophase. Thus, it would be interesting

to examine, by using synchronized cells, at which stage of the cell cycle cells that lack LBR and Lamin A/C undergo this type of alteration.

Regarding the chromatin landscape, previous visual observations of cells with nuclei that carry only few and big in size heterochromatic foci within the double null cell populations implied that simultaneous loss of LBR and Lamin A/C might trigger the reorganization of chromatin inside the nucleus. The quantitative analysis of these observations performed in the context of this thesis further supported this hypothesis. These cells appeared to have less foci compared to the normal average number of foci per nucleus (20-24), while they maintained their peripherally placed heterochromatin. Such nuclei resemble the inverted nuclear architecture of the rod cells of nocturnal mammals (Solovei *et al.*, 2009), but in our experimental model loss of LBR and Lamin A/C seems to only lead to the partial merge of heterochromatic foci, while it is not enough for the detachment of heterochromatin from the nuclear envelope and the complete chromatin inversion. This finding pinpoints the existence of a compensatory mechanism that may act in place and prevent the complete disruption of conventional chromatin architecture and is supported by previous studies. In 2013 Solovei *et al.* showed that loss of LBR or Lamin A/C in multiple cell types led to the partial chromatin inversion (Solovei *et al.*, 2013). In 2019, Falk *et al.* found that nuclei of murine rod cells that ectopically expressed Lamin A/C exhibited a layer of heterochromatin right underneath the nuclear envelope, while, at the same time the single heterochromatic focus in the center of the nucleus persisted (Falk *et al.*, 2019). These could be attributed to the fact that, unlike the B-tether which includes just the LBR itself, the A-tether includes multiple proteins of the nuclear periphery that work along with Lamin A/C to tether peripheral heterochromatin to the nuclear envelope. The specific set of proteins might differ between the different cell types. This could mean that other protein components of the A-tether in NIH/3T3 cells may compensate for the complete inversion of the nuclei, while these proteins might not be present in the rod cells of nocturnal mammals allowing the full inversion of chromatin architecture. The partial chromatin inversion could also be related to the two fractions of Lamin A/C: the peripheral and the nucleoplasmic one. Lamin A/C might form distinct interactomes, depending on whether it is located in the nuclear periphery, forming nuclear lamina meshworks, or in the nuclear interior, where it cross-links chromatin affecting chromatin dynamics (Bronshtein *et al.*, 2015). This could mean that the

protein partners of the peripheral fraction of Lamin A/C might possess the ability to compensate for the loss of Lamin A/C and maintain peripheral heterochromatin, while at the same time loss of nucleoplasmic Lamin A/C can lead to chromatin rearrangements (Ranade *et al.*, 2019). Another possible explanation could be that cells divide very fast, so the time between each mitotic event might not be enough for the complete chromatin inversion (Falk *et al.*, 2019).

The experiments that were aiming to investigate if there are any alterations in chromatin distribution and dynamics upon loss of Lamin A/C and/or LBR did not show any significant difference between the cell populations that were tested. Ectopically expressed HP1a presented the same localization pattern in all clones, with it being present in the nucleoplasm and enriched in the heterochromatic foci, regardless of the presence or absence of the two proteins. The levels and localization of the heterochromatin histone modification H3K9me3 also remained unchanged upon loss of LBR and/or Lamin A/C, in contrast to other studies which suggest that alterations in the epigenetic landscape may occur as a result of the absence of Lamin A/C and LBR (Smith *et al.*, 2021; Vahabikashi *et al.*, 2022).

Regarding the effect of knocking-out Lamin A/C and LBR on chromatin dynamics, the results did not meet our expectations. Our hypothesis, that suggested an overall change in chromatin distribution and dynamics upon loss of LBR and Lamin A/C, was based on what was already known from the literature. Other studies have revealed that the absence of major components of the nuclear lamina can affect chromatin dynamics. More specifically, Bronhshtein *et al.* showed that Lamin A knockout in U2OS cells led to changes in the diffusion of specific genomic loci, including telomeres placed either peripherally or in the nuclear interior (Brohnshtein *et al.*, 2015). Similarly, Chang and his colleagues suggested that Lamin B1 depletion in a breast cancer cell line caused the detachment of LADs from the nuclear envelope, changes in chromosome territories positioning and volume, increased mobility of genomic loci located both in the nuclear periphery and the nucleoplasm, and chromatin decompaction (Chang *et al.*, 2022). Last but not least, as it was revealed in a study by Ranade *et al.*, double knockdown of Lamin A/C and Emerin resulted in altered chromosome territories positioning and an increase in H2A mobility and, as implied, in chromatin dynamics (Ranade *et al.*, 2019).

In our case, the parameters that described the diffusional mobility of HP1α within the heterochromatic foci did not show any significant difference between the clones tested and their respective control cell populations, with a single exception of the diffusion coefficient of one of the LBR null clones. This clone exhibited an increase in the diffusional mobility of HP1α compared to the wild type cells, which implies the loosening of heterochromatin packing in the foci of the LBR depleted nuclei. Interestingly, this effect was not present in the second LBR KO clone, a difference that could be attributed to the different mutations in the LBR gene that each clone carries, which in the case of the second LBR KO clone allow for the expression of a short LBR fragment that might still be functional. Despite the change observed in the LBR KO1 clone, the loss of LBR and Lamin A/C was not found to affect any of the double knockout clones. The comparison of the state of chromatin curves that described the spectrum of dynamic chromatin states in each clone revealed only minor differences between the different cell populations, questioning if there is any actual effect of Lamin A/C and LBR in chromatin dynamics. Considering that NIH/3T3 cells are a hypertriploid cell type characterized by high interpopulation heterogeneity and genomic instability, it is possible that any differences observed between the knockout, the double knockout clones and their control cells result from these cell type specific features rather than the absence of LBR and Lamin A/C. Moreover, changes in chromatin state could also be related to potential chromatin redistribution events that occur during the different stages of the cell cycle, since we are not working with synchronized cell populations. Reassessing chromatin distribution and accessibility using other methods, such as SAMMY-seq, a high-throughput technology based on mapping sequentially extracted differentially compacted chromatin fractions, might prove useful for the better characterization of the chromatin landscape and dynamics in the mutant clones (Sebestyén *et al.*, 2020).

Preliminary data obtained from a set of experiments, in which the DamID-m6A-tracer system was exploited in order to visualize LADs' distribution in the asymmetric nuclei, indicated that peripheral heterochromatin might also be rearranged upon concurrent loss of LBR and Lamin A/C (Pavlina Micha's work; data not shown here). What was found was that LADs gave a thicker fluorescent signal (nuclear rim) in the nuclear periphery of the double null nuclei, compared to the wild type and single knock out cells, implying that their binding to the nuclear envelope might become weaker

upon loss of LBR and Lamin A/C. These findings were quite surprising, since such effect had not been observed in any of the double knockout clones, upon labelling of epigenetic markers of peripheral heterochromatin. Thus, it is important for the alterations observed regarding the positioning of peripheral heterochromatin in the double null cells to be further assessed by quantification and statistical analysis. These experiments could be complemented with the investigation of the identity of LADs in each case, using the DamID technique, as well as with other methods that aim to explore the chromatin landscape in our clones of interest. Exploiting assays, such as CUTnRUN and ChIP-seq, to map specific epigenetic modifications, and employing approaches, such as the Hi-C method, to investigate potential changes in the spatial relationships between known DNA sequences that might result from the loss of LBR and Lamin A/C, could prove very useful for this work. Moreover, it would be helpful to examine if there are any alterations in the positioning of specific chromosome territories or even specific genomic loci inside the nucleus, using FISH (Fluorescence In Situ Hybridization). If present, such alterations might explain the differences between the transcriptional profiles of the clones examined and their respective controls (RNA-seq data not fully analysed yet; data not shown here). Applying all these experimental approaches would give a clearer overview of how LBR and Lamin A/C can affect chromatin organization and examine their potential role in the regulation of gene expression.

The last part of this project concerned the migration potential of cells, since preliminary findings derived from previous transcriptomic analysis (P. Martzios, K. Soupsana) of the LBR or Lamin A/C null cells revealed alterations in the expression levels of genes associated with adherence and the extracellular matrix. A-type lamins have been repeatedly associated with cell motility and have been found to affect the mechanical properties of the nucleus in a way that facilitates migration in the case of cancer or stem cells (Chen *et al.*, 2018; Ovsiannikova *et al.*, 2021). However, when it comes to moving in 2D space, disruption of the Lamin A/C meshwork leads to impaired interactions between the nucleus and actin filament formations that serve cell polarization, thus leading to reduced cell motility (Park *et al.*, 2020; Lee *et al.*, 2021). This along with the fact that all the clones that lacked LBR were growing slower compared to the rest of the clones tested led to the hypothesis that LBR or Lamin A/C knock-out or double-null cells would present impaired cell motility. However, what was

observed during the wound healing assays was that LBR KO and LMNA-LBR DKO clones appeared to move faster compared to their controls, while the LMNA KO and LBR-LMNA DKO clones exhibited similar migration velocities as the wild-type cells. The statistical analysis of these data revealed no actually significant difference between the clones tested. The fact that everything in these experiments, from the creation of cell-free spaces (wounds) to selecting the gap areas that were measured at the different time points, were performed manually could in part explain any small deviations between the calculations for the clones that were examined and their respective controls. However, the overall quantitative data were not in agreement with our initial hypothesis. Most probably, alterations in the transcription levels of genes related to cell adhesion and the ECM, caused by the loss of LBR and Lamin A/C, do not necessarily correlate with altered levels of the proteins produced, leading to no actual effect on the migrational ability of cells. Applying a western blot analysis to examine if there are any differences in the protein levels between the clones tested would confirm this hypothesis.

Conclusions and perspectives

Overall, our findings indicated that loss of Lamin A/C and LBR affects the nuclear envelope properties and chromatin organization, confirming the significant role of the nuclear periphery in the maintenance of nuclear architecture in NIH/3T3 cells. Specifically, concurrent loss of LBR and Lamin A/C leads to impaired localization of major components of the nuclear periphery, as well as alterations regarding the chromatin landscape. Despite the incidence of nuclei that exhibited partially inverted chromatin architecture upon loss of LBR and Lamin A/C, chromatin dynamics were found to be mostly unaffected in the mutant cells. Moreover, cells did not present any impairments regarding their ability to adhere and migrate. The simultaneous absence of the two proteins seems to be a prerequisite for the appearance of the aberrant phenotypes observed, implying that their functions are complementary and that the presence of Lamin A/C can counteract the absence of LBR and vice versa. It is also possible that other proteins of the nuclear periphery can act in place, compensating for the loss of LBR and Lamin A/C. This might explain how, despite the effects caused by the knockouts, these cells retain their ability to proliferate and survive.

Despite the amount of work that has been done so far, there are still many open questions to be answered regarding the mechanistic aspects of the effects of LBR and Lamin A/C loss on NIH/3T3 cells, as well as the causal relationships between the phenotypes generated. Employing modern assays and microscopic methods to further investigate the role of these two major components of the nuclear periphery in nuclear envelope integrity and the establishment of the chromatin landscape could provide new evidence in this direction. Future experiments should be focused on whether there are any changes regarding the continuum of NE membranes that accompany the asymmetric phenotype, using simple assays such as membrane lipid staining or assessing NE's permeability for large molecules, as well as more complex techniques such as electron microscopy. It is also considered important to determine whether the NE and chromatin abnormalities observed are connected to specific stages of the cell cycle and investigate the possibility of these abnormalities being transient and cell cycle stage specific. This could be achieved by inspecting the appearance for such defects in synchronized cell populations. The role of nuclear lamina in the generation of the observed phenotypes should also be clarified, by assessing other types of lamins' meshworks' morphology, exploiting modern high-resolution microscopic methods such as 3D-SIM. Chromatin architecture and dynamics could be reassessed using alternative methods, such as the SAMMY-seq technology, which is used for the genome wide characterization of Lamina associated heterochromatic regions. Last but not least, potential changes regarding other levels of chromatin organization such as chromosome territories, LADs, TADs and epigenetic features could be studied, using techniques such as FISH, DamID, HiC and ChIP-seq or CUTnRUN, respectively. Combined, the results of such experiments would aid the attempt to shed more light onto the principles that govern chromatin organization.

References “”

5. References

- Adam S.A. (2017) The Nucleoskeleton. Cold Spring Harbor Perspectives in Biology, 9:a023556, doi: 10.1101/cshperspect.a023556.
- Amendola M., van Steensel B. (2014) Mechanisms and dynamics of nuclear lamina–genome interactions. Current Opinion in Cell Biology, 28: 61-68, doi: https://doi.org/10.1016/j.ceb.2014.03.003.
- Amendola M., van Steensel B. (2014) Mechanisms and dynamics of nuclear lamina-genome interactions. Current Opinion in Cell Biology, 28: 61-8, doi: 10.1016/j.ceb.2014.03.003.
- Amrichová J., Lukášová E., Kozubek S., Kozubek M. (2003) Nuclear and territorial topography of chromosome telomeres in human lymphocytes. Experimental Cell Research, 289(1): 11-26, doi: https://doi.org/10.1016/S0014-4827(03)00208-8.
- Arai R., En A., Takauji Y., Maki K., Miki M., Fujii M., Ayusawa D. (2019) Lamin B receptor (LBR) is involved in the induction of cellular senescence in human cells. Mechanisms of Ageing and Development, 178:25-32, https://doi.org/10.1016/j.ma.2019.01.001.
- Araki Y., Mimura T. (2017) The Histone Modification Code in the Pathogenesis of Autoimmune Diseases. Mediators of Inflammation, 2017: 2608605, doi: 10.1155/2017/2608605.
- Arents G, Moudrianakis EN. The histone fold: a ubiquitous architectural motif utilized in DNA compaction and protein dimerization. Proc Natl Acad Sci U S A. 1995 Nov 21;92(24):11170-4. doi: 10.1073/pnas.92.24.11170.
- Barton L.J., Soshnev A.A., Geyer P.K. (2015) Networking in the nucleus: a spotlight on LEM-domain proteins. Current Opinion in Cell Biology, 34: 1-8, doi: https://doi.org/10.1016/j.ceb.2015.03.005.
- Bouzid T., Kim E., Riehl B.D., Esfahani A.M., Rosenbohm J., Yang R., Duan B., Lim J.Y. (2019) The LINC complex, mechanotransduction, and mesenchymal stem cell function and fate. Journal of Biological Engineering, **13**: 68, doi: https://doi.org/10.1186/s13036-019-0197-9.

- Briand N., Collas P. (2020) Lamina-associated domains: peripheral matters and internal affairs. Genome Biology, 21(1): 85, doi: 10.1186/s13059-020-02003-5.
- Bronshtein I., Kepten E., Kanter I., Berezin S., Lindner M., Redwood A.B., Mai S., Gonzalo S., Foisner R., Shav-Tal Y., Garini Y. (2015) Loss of lamin A function increases chromatin dynamics in the nuclear interior. Nature Communications, 6: 8044, doi: 10.1038/ncomms9044.
- Burke B., Mounkes L.C., Stewart C.L. (2001) The Nuclear Envelope in Muscular Dystrophy and Cardiovascular Diseases. Traffic, 2(10): 675-683, doi: https://doi.org/10.1034/j.1600-0854.2001.21001.x.
- Chang L., Li M., Shao S., Li C., Ai S., Xue B., Hou Y., Zhang Y., Li R., Fan X., He A., Li C., Sun Y. (2022) Nuclear peripheral chromatin-lamin B1 interaction is required for global integrity of chromatin architecture and dynamics in human cells. Protein & Cell, 13(4): 258-280, doi: 10.1007/s13238-020-00794-8.
- Chen L., Jiang F., Qiao Y., Li H., Wei Z., Huang T., Lan J., Xia Y., Li J. (2018) Nucleoskeletal stiffness regulates stem cell migration and differentiation through lamin A/C. Journal of Cellular Physiology, 233: 5112–5118, doi: https://doi.org/10.1002/jcp.26336.
- Chi Y.H., Chen Z.J., Jeang K.T. (2009) The nuclear envelopathies and human diseases. Journal of Biomedical Science, 16(96), doi: https://doi.org/10.1186/1423-0127-16-96.
- Christogianni A., Chatzantonaki E., Soupsana K., Giannios I., Platania A., Politou A.S., Georgatos S. (2017) Heterochromatin remodelling in embryonic stem cells proceeds through stochastic de-stabilization of regional steady-states. Biochimica et Biophysica Acta (BBA) - Gene Regulatory Mechanisms, 1860(6): 661-673, doi: https://doi.org/10.1016/j.bbagrm.2017.01.009.
- Clowney E.J., LeGros M.A., Mosley C.P., Clowney F.G., Markenskoff-Papadimitriou E.C., Myllys M., Barnea G., Larabell C.A., Lomvardas S. (2012) Nuclear Aggregation of Olfactory Receptor Genes Governs Their Monogenic Expression, Cell, 151(4): 724-737, doi: https://doi.org/10.1016/j.cell.2012.09.043.
- Cremer T., Cremer C. (2001) Chromosome territories, nuclear architecture and gene regulation in mammalian cells. Nature Reviews Genetics, 2: 292–301, doi: https://doi.org/10.1038/35066075.

- Cutter A., Hayes J.J. (2015) A Brief Review of Nucleosome Structure. FEBS Letters, 589(20 0 0): 2914–2922, doi: 10.1016/j.febslet.2015.05.016.
- de Leeuw R., Gruenbaum Y., Medalia O. (2018). Nuclear Lamins: Thin Filaments with Major Functions. Trends in Cell Biology, 28(1): 34–45, doi: https://doi.org/10.1016/j.tcb.2017.08.004.
- De Vos W.H., Houben F., Kamps M., Malhas A., Verheyen F., Cox J., Manders E.M., Verstraeten V.L., van Steensel M.A., Marcelis C.L., van den Wijngaard A., Vaux D.J., Ramaekers F.C., Broers J.L. (2011) Repetitive disruptions of the nuclear envelope invoke temporary loss of cellular compartmentalization in laminopathies. Human Molecular Genetics, 20(21): 4175-86, doi: 10.1093/hmg/ddr344.
- de Wit E., de Laat W. (2012) A decade of 3C technologies: insights into nuclear organization. Genes & Development, 26(1): 11-24, doi: 10.1101/gad.179804.111.
- Dechat T., Adam S.A., Taimen P., Shimi T., Goldman R.D. (2010) Nuclear Lamins. Cold Spring Harbor Perspectives in Biology, 2:a000547, doi: 10.1101/cshperspect.a000547.
- Dechat T., Gesson K., Foisner R. (2011) Lamina-Independent Lamins in the Nuclear Interior Serve Important Functions. Cold Spring Harb Symposia on Quantitative Biology, 75: 533-543, doi: 10.1101/sqb.2010.75.018.
- Dekker J., Marti-Renom M.A., Mirny L.A. (2013) Exploring the three-dimensional organization of genomes: interpreting chromatin interaction data. Nature Reviews Genetics, 14(6): 390-403, doi: 10.1038/nrg3454.
- Demmerle J., Hao S., Cai D. (2023) Transcriptional condensates and phase separation: condensing information across scales and mechanisms. Nucleus, 14(1): 2213551, doi: 10.1080/19491034.2023.2213551.
- Dittmer T., Misteli T. (2011) The lamin protein family. Genome Biology, 12(5): 222, doi: 10.1186/gb-2011-12-5-222.
- Dixon J.R., Selvaraj S., Yue F., Kim A., Li Y., Shen Y., Hu M., Liu J.S., Ren B. (2012) Topological domains in mammalian genomes identified by analysis of chromatin interactions. Nature, 485(7398): 376-80, doi: 10.1038/nature11082.
- Döring V., Stick R. (1990) Gene structure of nuclear lamin LIII of Xenopus laevis; a model for the evolution of IF proteins from a lamin-like ancestor. The

EMBO Journal, 9(12): 4073-4081, doi: https://doi.org/10.1002/j.1460-2075.1990.tb07629.x.

- Dubois M.L., Boisvert F.M. (2016) Th Nucleolus: Structure and Function. The Functional Nucleus, 23: 29–49, doi: 10.1007/978-3-319-38882-3_2.
- Eckersley-Maslin M.A., Bergmann J.H., Lazar Z., Spector D.L. (2013) Lamin A/C is expressed in pluripotent mouse embryonic stem cells. Nucleus, 4(1): 53-60, doi: 10.4161/nucl.23384.
- Ellenberg J., Siggia E.D., Moreira J.E., Smith C.L., Presley J.F., Worman H.J., Lippincott-Schwartz J. (1997) Nuclear membrane dynamics and reassembly in living cells: targeting of an inner nuclear membrane protein in interphase and mitosis. The Journal of Cell Biology, 138(6):1193-206, doi: 10.1083/jcb.138.6.1193.
- En A., Takauji Y., Ayusawa D., Fujii M. (2020) The role of lamin B receptor in the regulation of senescence-associated secretory phenotype (SASP). Experimental Cell Research, 390(1):111927, https://doi.org/10.1016/j.yexcr.2020.111927.
- En A., Takauji Y., Miki K., Ayusawa D., Fujii M. (2020) Lamin B receptor plays a key role in cellular senescence induced by inhibition of the proteasome. FEBS Open Bio, 10:237–250, doi:10.1002/2211-5463.12775.
- Falk M., Feodorova Y., Naumova N., Imakaev M., Lajoie B.R., Leonhardt H., Joffe B., Dekker J., Fudenberg G., Solovei I., Mirny L.A. (2019) Heterochromatin drives compartmentalization of inverted and conventional nuclei. Nature, 570: 395–399, doi: https://doi.org/10.1038/s41586-019-1275-3.
- Feodorova Y., Falk M., Mirny L.A., Solovei I. (2020) Viewing Nuclear Architecture through the Eyes of Nocturnal Mammals. Trends in Cell Biology, 30(4): 276-289, doi: 10.1016/j.tcb.2019.12.008.
- Foisner R. (2003) Cell cycle dynamics of the nuclear envelope. Scientific World Journal, 3: 1-20, doi: 10.1100/tsw.2003.06.
- Fraser J., Williamson I., Bickmore W.A., Dostie J. (2015) An Overview of Genome Organization and How We Got There: from FISH to Hi-C. Microbiology and Molecular Biology Reviews, 79(3): 347–372, doi: 10.1128/mmbr.00006-15.

- Fritz A.J., Sehgal N., Pliss A., Xu J., Berezney R. (2019) Chromosome territories and the global regulation of the genome. Genes Chromosomes Cancer, 58(7): 407-426, doi: 10.1002/gcc.22732.
- Frohns A., Frohns F., Naumann S.C., Layer P.G., Löbrich M. (2014) Inefficient double-strand break repair in murine rod photoreceptors with inverted heterochromatin organization. Current Biology, 24(10): 1080-90, doi: 10.1016/j.cub.2014.03.061.
- Georgatos S. D., Maroulakou I., Blobel G. (1989). Lamin A, lamin B, and lamin B receptor analogues in yeast. The Journal of Cell Biology, 108(6):2069-82, doi: 10.1083/jcb.108.6.2069.
- Georgatos S.D. (2001) The inner nuclear membrane: simple, or very complex? EMBO Journal, 20(12): 2989-2994, doi: 10.1093/emboj/20.12.2989.
- Gesson K., Rescheneder P., Skoruppa M.P., von Haeseler A., Dechat T., Foisner R. (2016) A-type lamins bind both hetero- and euchromatin, the latter being regulated by lamina-associated polypeptide 2 alpha. Genome Research, 26(4): 462-73, doi: 10.1101/gr.196220.115.
- Giannios I., Chatzantonaki E., Georgatos S. (2017) Dynamics and Structure-Function Relationships of the Lamin B Receptor (LBR). PLoS ONE, 12(1): e0169626, doi: https://doi.org/10.1371/journal.pone.0169626.
- Gilbert N., Gilchrist S., Bickmore W.A. (2005) Chromatin organization in the mammalian nucleus. International Review of Cytology, 242: 283-336, doi: 10.1016/S0074-7696(04)42007-5.
- Gruenbaum Y., Foisner R. (2015) Lamins: Nuclear intermediate filament proteins with fundamental functions in nuclear mechanics and genome regulation. Annual Reviews of Biochemistry,84:131–164,doi:https://doi.org/10.1146/annurev-biochem-060614-034115.
- Gruenbaum Y., Medalia O. (2015). Lamins: the structure and protein complexes. Current Opinion in Cell Biology, 32: 7–12, doi: 10.1016/j.ceb.2014.09.009.
- Guarda A., Bolognese F., Bonapace I.M., Badaracco G. (2009) Interaction between the inner nuclear membrane lamin B receptor and the heterochromatic methyl binding protein, MeCP2. Experimental Cell Research, 315(11): 1895-1903, doi: https://doi.org/10.1016/j.yexcr.2009.01.019.

- Guerreiro I., Kind J. (2019) Spatial chromatin organization and gene regulation at the nuclear lamina. Current Opinion in Genetics and Development, 55: 19-25, doi: 10.1016/j.gde.2019.04.008.
- Guillemette B., Drogaris P., Lin H.H., Armstrong H., Hiragami-Hamada K., Imhof A., Bonneil E., Thibault P., Verreault A., Festenstein R.J. (2011) H3 lysine 4 is acetylated at active gene promoters and is regulated by H3 lysine 4 methylation. PLoS Genetics, 7(3): e1001354, doi: 10.1371/journal.pgen.1001354.
- Guo Y., Kim Y., Shimi T., Goldman R.D., Zheng Y. (2014) Concentration-dependent lamin assembly and its roles in the localization of other nuclear proteins. Molecular Biology of the Cell, 25(8): 1287-97, doi: 10.1091/mbc.E13-11-0644.
- Guo Y., Zheng Y. (2015) Lamins position the nuclear pores and centrosomes by modulating dynein. Molecular Biology of the Cell, 26(19): 3379-89, doi: 10.1091/mbc.E15-07-0482.
- Herrmann H., Aebi U. (2016) Intermediate Filaments: Structure and Assembly. Cold Spring Harbor Perspectives in Biology, 8:a018242, doi: 10.1101/cshperspect.a018242.
- Herrmann H., Zwerger M. (2010) The danger of "multi-tasking". Nucleus, 1(4): 319 324, doi: 10.4161/nucl.1.4.11801.
- Hetzer, M.W. (2010) The nuclear envelope. Cold Spring Harbor Perspectives in Biology, 2(3): a000539, doi: 10.1101/cshperspect.a000539.
- Hildebrand E.M., Dekker J. (2020) Mechanisms and Functions of Chromosome Compartmentalization. Trends in Biochemical Sciences, 45(5): 385-396, doi: 10.1016/j.tibs.2020.01.002.
- Hoelz A., Debler E.W., Blobel G. (2011) The structure of the nuclear pore complex. Annual Review of Biochemistry, 80: 613-43, doi: 10.1146/annurev-biochem-060109-151030.
- Holmer L., Pezhman A., Worman H. J. (1998). The Human Lamin B Receptor/Sterol Reductase Multigene Family. Genomics, 54(3):469-76, doi: 10.1006/geno.1998.5615.

- Holmer L., Worman H. (2001) Inner nuclear membrane proteins: functions and targeting. Cellular and Molecular Life Sciences, 58: 1741–1747, doi: 10.1007/PL00000813.
- Hoskins V.E., Smith K., Reddy K.L. (2021) The shifting shape of genomes: dynamics of heterochromatin interactions at the nuclear lamina. Current Opinion in Genetics and Development, 67: 163-173, doi: 10.1016/j.gde.2021.02.003.
- Jahed Z., Domkam N., Ornowski J., Yerima G., Mofrad M.R.K. (2021) Molecular models of LINC complex assembly at the nuclear envelope. Journal of Cell Science, 134 (12): jcs258194, doi: https://doi.org/10.1242/jcs.258194.
- Jahed Z., Soheilypour M., Peyro M., Mofrad M.R.K. (2016) The LINC and NPC relationship – it's complicated! Journal of Cell Science, 129(17): 3219–3229, doi: https://doi.org/10.1242/jcs.184184.
- Janin A., Bauer D., Ratti F., Millat G., Méjat A. (2017) Nuclear envelopathies: a complex LINC between nuclear envelope and pathology. Orphanet Journal of Rare Diseases, 12: 147, doi: 10.1186/s13023-017-0698-x.
- Jonkman J.E.N., Cathcart J., Xu F., Bartolini M.E., Amon J.E., Stevens K.M., Colarusso P. (2014) An introduction to the wound healing assay using live-cell microscopy. Cell Adhesion & Migration, 8(5): 440-451, doi: 10.4161/cam.36224.
- Kang M., Andreani M., Kenworthy A.K. (2015) Validation of Normalizations, Scaling, and Photofading Corrections for FRAP Data Analysis. PLoS ONE, 10(5): e0127966, doi: 10.1371/journal.pone.0127966.
- Kang M., Day C.A., Kenworthy A.K., DiBenedetto E. (2012) Simplified Equation to Extract Diffusion Coefficients from Confocal FRAP Data. Traffic, 13(12): 1589–1600, doi:10.1111/tra.12008.
- Kang S., Yoon M., Park B. (2018) Laminopathies; Mutations on single gene and various human genetic diseases. BMB Reports, 51(7): 327-337, doi: 10.5483/bmbrep.2018.51.7.113.
- Kempfer, R., Pombo, A. (2020) Methods for mapping 3D chromosome architecture. Nature Reviews Genetics, 21: 207–226, doi: https://doi.org/10.1038/s41576-019-0195-2.

- Kim D.H., Cho S., Wirtz D. (2014) Tight coupling between nucleus and cell migration through the perinuclear actin cap. Journal of Cell Science, 127(Pt 11): 2528-41, doi: 10.1242/jcs.144345.
- Kim J.K., Louhghalam A., Lee G., Schafer B.W., Wirtz D., Kim D.H. (2017) Nuclear lamin A/C harnesses the perinuclear apical actin cables to protect nuclear morphology. Nature Communications, 8: 2123, doi: https://doi.org/10.1038/s41467-017-02217-5.
- Kind J., Pagie L., Ortabozkoyun H., Boyle S., de Vries S.S., Janssen H., Amendola M., Nolen L.D., Bickmore W.A., van Steensel B. (2013) Single-cell dynamics of genome-nuclear lamina interactions. Cell, 153(1): 178-92, doi: 10.1016/j.cell.2013.02.028.
- Kreysing M., Boyde L., Guck J., Chalut K.J. (2010) Physical insight into light scattering by photoreceptor cell nuclei. Optics Letters, 35(15): 2639-2641, doi: https://doi.org/10.1364/OL.35.002639.
- Kuhn T.M., Capelson M. (2019) Nuclear Pore Proteins in Regulation of Chromatin State. Cells, 8(11): 1414, doi: 10.3390/cells8111414.
- Kwon S.H., Workman J.L. (2008) The heterochromatin protein 1 (HP1) family: put away a bias toward HP1. Molecules and Cells, 26(3): 217-27.
- Laghmach R., Di Pierro M., Potoyan D. (2022) Frontiers in Molecular Biosciences, 8: 2021, doi: https://doi.org/10.3389/fmolb.2021.781981.
- Larson A.G., Elnatan D., Keenen M.M., Trnka M.J., Johnston J.B., Burlingame A.L., Agard D.A., Redding S., Narlikar G.J. (2017) Liquid droplet formation by HP1α suggests a role for phase separation in heterochromatin. Nature, 547(7662): 236-240, doi: 10.1038/nature22822.
- Lee G., Han S.B., Kim D.H. (2021) Cell-ECM contact-guided intracellular polarization is mediated via lamin A/C dependent nucleus-cytoskeletal connection. Biomaterials, 268: 120548, doi: 10.1016/j.biomaterials.2020.120548.
- Li Y., Danzer J.R., Alvarez P., Belmont A.S., Wallrath L.L. (2003) Effects of tethering HP1 to euchromatic regions of the Drosophila genome. Development, 130(9): 1817-24, doi: 10.1242/dev.00405.
- Lieberman-Aiden E., van Berkum N.L., Williams L., Imakaev M., Ragoczy T., Telling A., Amit I., Lajoie B.R., Sabo P.J., Dorschner M.O., Sandstrom R.,

Bernstein B., Bender M.A., Groudine M., Gnirke A., Stamatoyannopoulos J., Mirny L.A., Lander E.S., Dekker J. (2009) Comprehensive mapping of long-range interactions reveals folding principles of the human genome. Science, 326(5950): 289-93, doi: 10.1126/science.1181369.

- Liokatis S., Edlich C., Soupsana K., Giannios I., Panagiotidou P., Tripsianes K., Sattler M., Georgatos S.D., Politou A.S. (2012) Solution structure and molecular interactions of lamin B receptor Tudor domain. Journal of Biological Chemistry, 287(2):1032-42. doi: 10.1074/jbc.M111.281303.
- Liu J., Ben-Shahar T.R., Riemer D., Treinin M., Spann P., Weber K., Fire A., Gruenbaum Y. (2000) Essential Roles for Caenorhabditis elegans Lamin Gene in Nuclear Organization, Cell Cycle Progression, and Spatial Organization of Nuclear Pore Complexes. Molecular Biology of the Cell, 11(11): 3937–3947, doi: https://doi.org/10.1091/mbc.11.11.3937.
- Liu Q., Pante N., Misteli T., Elsagga M., Crisp M., Hodzic D., Burke B., Roux K.J. (2007) Functional association of Sun1 with nuclear pore complexes. Journal of Cell Biology, 178(5): 785-98, doi: 10.1083/jcb.200704108.
- Lomberk G., Wallrath L., Urrutia R. (2006) The Heterochromatin Protein 1 family. Genome Biology, 7(7): 228, doi: 10.1186/gb-2006-7-7-228.
- Lukášová E., Kovarˇík A., Bacˇíková A., Falk M., Kozubek S. (2017) Loss of lamin B receptor is necessary to induce cellular senescence. Biochemical Journal, 474(2):281–300, doi: https://doi.org/10.1042/BCJ20160459.
- Marcelot A., Worman H.J., Zinn-Justin S. (2020) Protein structural and mechanistic basis of progeroid laminopathies. The FEBS Journal 288: 2757–2772, doi: 10.1111/febs.15526.
- Mariño-Ramírez L., Kann M.G., Shoemaker B.A., Landsman D. (2005) Histone structure and nucleosome stability. Expert Review of Proteomics, 2(5): 719-29, doi: 10.1586/14789450.2.5.719.
- McGinty R.K., Tan S. (2015) Nucleosome Structure and Function. Chemical Reviews, 115(6): 2255−2273, doi: 10.1021/cr500373h.
- Mimura Y., Takagi M., Clever M., Imamoto N. (2016) ELYS regulates the localization of LBR by modulating its phosphorylation state. Journal of Cell Science, 129(22): 4200-4212, doi: 10.1242/jcs.190678.

- Mirza A.N., Gonzalez F., Ha S.K., Oro A.E. (2021) The Sky's the LEMit: New insights into nuclear structure regulation of transcription factor activity. Current Opinion in Cell Biology, 68: 173-180, doi: 10.1016/j.ceb.2020.10.006.
- Naetar N., Ferraioli S., Foisner R. (2017) Lamins in the nuclear interior − life outside the lamina. Journal of Cell Science, 130(13): 2087–2096, doi: https://doi.org/10.1242/jcs.203430.
- Nicholson T.B., Veland N., Chen T. (2015) Chapter 3 - Writers, Readers, and Erasers of Epigenetic Marks. Epigenetic Cancer Therapy, Academic Press, 31-66, doi: https://doi.org/10.1016/B978-0-12-800206-3.00003-3.
- Nielsen P.R., Nietlispach D., Mott H.R., Callaghan J., Bannister A., Kouzarides T., Murzin A.G., Murzina N.V., Laue E.D. (2002) Structure of the HP1 chromodomain bound to histone H3 methylated at lysine 9. Nature, 416(6876): 103-7, doi: 10.1038/nature722.
- Nikolakaki E., Meier J., Simos G., Georgatos S.D., Giannakouros T. (1997) Mitotic phosphorylation of the lamin B receptor by a serine/arginine kinase and p34(cdc2). Journal of Biological Chemistry, 272(10):6208-13, doi: 10.1074/jbc.272.10.6208.
- Nikolakaki E., Mylonis I., Giannakouros T. (2017) Lamin B Receptor: Interplay between Structure, Function and Localization. Cells, 6(3):28, doi: 10.3390/cells6030028.
- Nikolakaki E., Simos G., Georgatos S.D., Giannakouros T. (1996) A nuclear envelope-associated kinase phosphorylates arginine-serine motifs and modulates interactions between the lamin B receptor and other nuclear proteins. Journal of Biological Chemistry, 271(14):8365-72, doi: 10.1074/jbc.271.14.8365.
- Nmezi B., Xu J., Fu R., Armiger T.J., Rodriguez-Bey G., Powell J.S., Ma H., Sullivan M., Tu Y., Chen N.Y., Young S.G., Stolz D.B., Dahl K.N., Liu Y., Padiath Q.S. (2019) Concentric organization of A- and B-type lamins predicts their distinct roles in the spatial organization and stability of the nuclear lamina. PNAS, 116(10): 4307-4315, doi: https://doi.org/10.1073/pnas.1810070116.
- Ovsiannikova N.L., Lavrushkina S.V., Ivanova A.V., Mazina L.M., Zhironkina O.A., Kireev I.I. (2021) Lamin A as a Determinant of Mechanical Properties of

the Cell Nucleus in Health and Disease. Biochemistry (Moscow), 86: 1288–1300, doi: https://doi.org/10.1134/S0006297921100102.

- Papoutsopoulou S., Nikolakaki E., Giannakouros T. (1999) SRPK1 and LBR Protein Kinases Show Identical Substrate Specificities. Biochemical and Biophysical Research Communications, 255(3):602– 607, doi: 10.1006/bbrc.1999.0249.
- Park J.W., Han S.B., Hah J., Lee G., Kim J.K., Kim S.H., Kim D.H. (2020) Biological Aging Modulates Cell Migration via Lamin A/C-Dependent Nuclear Motion. Micromachines (Basel), 11(9): 801, doi: 10.3390/mi11090801.
- Polioudaki H., Kourmouli N., Drosou V., Bakou A., Theodoropoulos P.A., Singh P.B., Giannakouros T., Georgatos S.D. (2001) Histones H3/H4 form a tight complex with the inner nuclear membrane protein LBR and heterochromatin protein 1. EMBO Reports, 2(10): 920-5, doi: 10.1093/embo-reports/kve199.
- Rada-Iglesias A., Grosveld F.G., Papantonis A. (2018) Forces driving the three-dimensional folding of eukaryotic genomes. Molecular Systems Biology, 14: e8214, doi: https://doi.org/10.15252/msb.20188214.
- Raharjo W.H., Enarson P., Sullivan T., Stewart C.L., Burke B. (2001) Nuclear envelope defects associated with LMNA mutations cause dilated cardiomyopathy and Emery-Dreifuss muscular dystrophy. Journal of Cell Science, 114(24): 4447–4457, doi: https://doi.org/10.1242/jcs.114.24.4447.
- Ranade D., Pradhan R., Jayakrishnan M., Hegde S., Sengupta K. (2019) Lamin A/C and Emerin depletion impacts chromatin organization and dynamics in the interphase nucleus. BMC Molecular and Cell Biology, 20: 11, doi: https://doi.org/10.1186/s12860-019-0192-5.
- Rullens P.M.J., Kind J. (2021) Attach and stretch: Emerging roles for genome-lamina contacts in shaping the 3D genome. Current Opinion in Cell Biology, 70: 51-57, doi: 10.1016/j.ceb.2020.11.006.
- Saksouk N., Simboeck E., Déjardin J. (2015) Constitutive heterochromatin formation and transcription in mammals. Epigenetics & Chromatin, 8: 3, doi: 10.1186/1756-8935-8-3.
- Saksouk N., Simboeck E., Déjardin, J. (2015) Constitutive heterochromatin formation and transcription in mammals. Epigenetics & Chromatin, 8(3), doi: https://doi.org/10.1186/1756-8935-8-3.

- Sazer S., Schiessel H. (2017) The biology and polymer physics underlying large-scale chromosome organization. Traffic, 19(2): 87-104, doi: https://doi.org/10.1111/tra.12539.
- Schirmer E.C., Foisner R. (2007) Proteins that associate with lamins: many faces, many functions. Experimental Cell Research, 313(10): 2167-79, doi: 10.1016/j.yexcr.2007.03.012.
- Schoelz J.M., Riddle N.C. (2022) Functions of HP1 proteins in transcriptional regulation. Epigenetics & Chromatin, 15(14), doi: https://doi.org/10.1186/s13072-022-00453-8.
- Schuler E., Lin F., Worman H.J. (1994) Characterization of the human gene encoding LBR, an integral protein of the nuclear envelope inner membrane. Journal of Biological Chemistry, 269(15):11312-7.
- Schütz W., Benavente R., Alsheimer M. (2005) Dynamic properties of germ line-specific lamin B3: the role of the shortened rod domain. European Journal of Cell Biology, 84(7):649-62, doi: 10.1016/j.ejcb.2005.03.001.
- Sebestyén E., Marullo F., Lucini F, Petrini C., Bianchi A., Valsoni S., Olivieri I., Antonelli L., Gregoretti F., Oliva G., Ferrari F., Lanzuolo C. (2020) SAMMY-seq reveals early alteration of heterochromatin and deregulation of bivalent genes in Hutchinson-Gilford Progeria Syndrome. Nature Communications, 11(6274, doi: https://doi.org/10.1038/s41467-020-20048-9.
- Sellis D., Drosou V., Vlachakis D., Voukkalis N., Giannakouros T., Vlassi M. (2012) Phosphorylation of the arginine/serine repeats of lamin B receptor by SRPK1—Insights from molecular dynamics simulations. Biochimica et Biophysica Acta, 1820(1):44-55, doi: 10.1016/j.bbagen.2011.10.010.
- Shimi T., Kittisopikul M., Tran J., Goldman A.E., Adam S.A., Zheng Y., Jaqaman K., Goldman R.D. (2015) Structural organization of nuclear lamins A, C, B1, and B2 revealed by super resolution microscopy. Molecular Biology of the Cell, 26(22): 3893-4181, doi: https://doi.org/10.1091/mbc.E15-07-0461.
- Shimi T., Kittisopikul M., Tran J., Goldman A.E., Adam S.A., Zheng Y., Jaqaman K., Goldman R.D. (2015) Structural organization of nuclear lamins A, C, B1, and B2 revealed by superresolution microscopy. Molecular Biology of the Cell, 26(22): 4075-86, doi: 10.1091/mbc.E15-07-0461.

- Shin J., Worman H.J. (2022) Molecular Pathology of Laminopathies. Annual Review of Pathology, 17: 159-180, doi:10.1146/annurev-pathol-042220-034240.
- Silve S., Dupuy P. H., Ferrara P., Loison G. (1998). Human lamin B receptor exhibits sterol C14-reductase activity in Saccharomyces cerevisiae. Biochimica et Biophysica Acta, 1392(2-3):233-44, doi: 10.1016/s0005-2760(98)00041-1.
- Smet-Nocca C., Page A., Cantrelle F., Nikolakaki E., Landrieu I., Giannakouros T. (2018) The O-β-linked N-acetylglucosaminylation of the Lamin B receptor and its impact on DNA binding and phosphorylation. Biochimica et Biophysica Acta - General Subjects, 1862(4):825-835, https://doi.org/10.1016/j.bbagen.2018.01.007.
- Smith C.L., Poleshko A., Epstein J.A. (2021) The nuclear periphery is a scaffold for tissue-specific enhancers. Nucleic Acids Research, 49(11): 6181-6195, doi: https://doi.org/10.1093/nar/gkab392.
- Smothers J.F., Henikoff S. (2000) The HP1 chromo shadow domain binds a consensus peptide pentamer. Current Biology, 10(1): 27-30, doi: 10.1016/s0960-9822(99)00260-2.
- Solovei I., Kreysing M., Lanctot C., Kösem S., Peichl L., Cremer T., Guck J.,2, Joffe B. (2009) Nuclear Architecture of Rod Photoreceptor Cells Adapts to Vision in Mammalian Evolution. Cell, 137(2): 356-368, doi: https://doi.org/10.1016/j.cell.2009.01.052.
- Solovei I., Kreysing M., Lanctôt C., Kösem S., Peichl L., Cremer T., Guck J., Joffe B. (2009) Nuclear architecture of rod photoreceptor cells adapts to vision in mammalian evolution. Cell, 137(2): 356-68, doi: 10.1016/j.cell.2009.01.052.
- Solovei I., Thanisch K., Feodorova Y. (2016) How to rule the nucleus: divide et impera. Current Opinion in Cell Biology, 40: 47-59, doi: https://doi.org/10.1016/j.ceb.2016.02.014.
- Solovei I., Wang A.S., Thanisch K., Schmidt C.S., Krebs S., Zwerger M., Cohen T.V., Devys D., Foisner R., Peichl L., Herrmann H., Blum H., Engelkamp D., Stewart C.L., Leonhardt H., Joffe B. (2013) LBR and Lamin A/C Sequentially Tether Peripheral Heterochromatin and Inversely Regulate Differentiation. Cell, 152(3): 584-598, doi: https://doi.org/10.1016/j.cell.2013.01.009.

- Solovei I., Wang A.S., Thanisch K., Schmidt C.S., Krebs S., Zwerger M., Cohen T.V., Devys D., Foisner R., Peichl L., Herrmann H., Blum H., Engelkamp D., Stewart C.L., Leonhardt H., Joffe B. (2013) LBR and lamin A/C sequentially tether peripheral heterochromatin and inversely regulate differentiation. Cell, 152(3): 584-98, doi: 10.1016/j.cell.2013.01.009.
- Strahl B., Allis C. (2000) The language of covalent histone modifications. Nature, 403: 41–45, doi: https://doi.org/10.1038/47412.
- Strambio-De-Castillia C., Niepel M., Rout M.P. (2010) The nuclear pore complex: bridging nuclear transport and gene regulation. Nature Reviews Molecular Cell Biology, 11(7): 490-501, doi: 10.1038/nrm2928.
- Strom A., Emelyanov A., Mir M., Fyodorov D.V., Darzacq X., Karpen G.H. (2017) Phase separation drives heterochromatin domain formation. Nature 547: 241–245, doi: https://doi.org/10.1038/nature22989.
- Sullivan T., Escalante-Alcalde D., Bhatt H., Anver M., Bhat N., Nagashima K., Stewart C.L., Burke B. (1999) Loss of A-type lamin expression compromises nuclear envelope integrity leading to muscular dystrophy. Journal of Cell Biology, 147(5): 913-20, doi: 10.1083/jcb.147.5.913.
- Sullivan T., Escalante-Alcalde D., Bhatt H., Anver M., Bhat N., Nagashima K., Stewart C.L., Burke B. (1999) Loss of A-type lamin expression compromises nuclear envelope integrity leading to muscular dystrophy. The Journal of Cell Biology, 147(5): 913-20, doi: 10.1083/jcb.147.5.913.
- Szabo Q., Bantignies F., Cavalli G. (2019) Principles of genome folding into topologically associating domains. Science Advances, 5(4): eaaw1668, doi: 10.1126/sciadv.aaw1668.
- Szczepińska T., Rusek A.M., Plewczynski D. (2019) Intermingling of chromosome territories. Genes Chromosomes Cancer, 58(7): 500-506, doi: 10.1002/gcc.22736.
- Talbert P.B., Henikoff S. (2021) Histone variants at a glance. Journal of Cell Science, 134(6): jcs244749, doi: 10.1242/jcs.244749.
- Thanisch K., Song C., Engelkamp D., Koch J., Wang A., Hallberg E., Foisner R., Leonhardt H., Stewart C.L., Joffe B., Solovei I. (2017) Nuclear envelope localization of LEMD2 is developmentally dynamic and lamin A/C dependent

yet insufficient for heterochromatin tethering. Differentiation, 94: 58-70, doi: 10.1016/j.diff.2016.12.002.

- Torvaldson E., Kochin V., Eriksson J.E. (2015) Phosphorylation of lamins determine their structural properties and signaling functions. Nucleus, 6(3): 166-171, doi: 10.1080/19491034.2015.101716.
- Tsai P. L., Zhao C., Turner E., Schlieker C. (2016). The Lamin B receptor is essential for cholesterol synthesis and perturbed by disease-causing mutations. Elife, 5: e16011, doi: 10.7554/eLife.16011.
- Turner B.M. (2002) Cellular memory and the histone code. Cell, 111(3): 285-91, doi: 10.1016/s0092-8674(02)01080-2.
- Ungricht R., Klann M., Horvath P., Kutay U. (2015) Diffusion and retention are major determinants of protein targeting to the inner nuclear membrane. The Journal of Cell Biology, 209(5): 687-703, doi: 10.1083/jcb.201409127.
- Vahabikashi A., Adam S.A., Medalia O., Goldman R.D. (2022) Nuclear lamins: Structure and function in mechanobiology. APL Bioengineering. 6: 011503, doi: 10.1063/5.0082656.
- Vahabikashi A., Sivagurunathan S., Nicdao F.A.S., Han Y.L., Park C.Y., Kittisopikul M., Wong X., Tran J.R., Gundersen G.G., Reddy K.L., Gant Luxton G.W., Guo M., Fredberg J.J., Zheng Y., Adam S.A., Goldman R.D. (2022) Nuclear lamin isoforms differentially contribute to LINC complex-dependent nucleocytoskeletal coupling and whole-cell mechanics. PNAS, 119(17): e2121816119, doi: https://doi.org/10.1073/pnas.2121816119.
- Vahabikashi A., Sivagurunathan S., Nicdao F.A.S., Han Y.L., Park C.Y., Kittisopikul M., Wong X., Tran J.R., Gundersen G.G., Reddy K.L., Luxton G.W.G., Guo M., Fredberg J.J., Zheng Y., Adam S.A., Goldman R.D. (2022) Nuclear lamin isoforms differentially contribute to LINC complex-dependent nucleocytoskeletal coupling and whole-cell mechanics. Proceedings of the National Academy of Sciences of the United States of America, 119(17): e2121816119, doi: 10.1073/pnas.2121816119.
- Vigouroux C., Auclair M., Dubosclard E., Pouchelet M., Capeau J., Courvalin J., Buendia B. (2001) Nuclear envelope disorganization in fibroblasts from lipodystrophic patients with heterozygous R482Q/W mutations in the lamin A/C

gene. Journal of Cell Science, 114(24): 4459–4468, doi: https://doi.org/10.1242/jcs.114.24.4459.

- Wang W., Shi Z., Jiao S., Chen C., Wang H., Liu G., Wang Q., Zhao Y., Greene M.I., Zhou Z. (2012) Structural insights into SUN-KASH complexes across the nuclear envelope. Cell Research, 22: 1440-1452, doi: https://doi.org/10.1038/cr.2012.126.
- Wong X., Cutler J.A., Hoskins V.E., Gordon M., Madugundu A.K., Pandey A., Reddy K.L. (2021) Mapping the micro-proteome of the nuclear lamina and lamina-associated domains. Life Science Alliance, 4(5): e202000774, doi: 10.26508/lsa.202000774.
- Wong X., Stewart C.L. (2020) The Laminopathies and the Insights They Provide into the Structural and Functional Organization of the Nucleus. Annual Review of Genomics and Human Genetics, 21(1): 263–288, doi: https://doi.org/10.1146/annurev-genom-121219-083616.
- Worman H. J., Evans C. D., Blobel G. (1990). The lamin B receptor of the nuclear envelope inner membrane: a polytopic protein with eight potential transmembrane domains. The Journal of Cell Biology, 111(4):1535-42. doi: 10.1083/jcb.111.4.1535.
- Worman H. J., Yuan J., Blobel G., Georgatos S. D. (1988). A lamin B receptor in the nuclear envelope. Proceedings of the National Academy of Sciences USA, 85(22):8531-4, doi: 10.1073/pnas.85.22.8531.
- Worman H.J. (2012) Nuclear lamins and laminipathies. Journal of Pathology, 226: 316–325, doi: 10.1002/path.2999.
- Xie W., Chojnowski A., Boudier T., Lim J.S., Ahmed S., Ser Z., Stewart C., Burke B. (2016) A-type Lamins Form Distinct Filamentous Networks with Differential Nuclear Pore Complex Associations. Current Biology, 26(19): 2651-2658, doi: 10.1016/j.cub.2016.07.049.
- Xie W., Chojnowski A., Boudier T., Lim J.S.Y., Ahmed S., Ser Z., Stewart c., Burke B. (2016) Current Biology 26(19), 2651–2658, doi: https://doi.org/10.1016/j.cub.2016.07.049.
- Yáñez-Cuna J.O., van Steensel B. 2017) Genome–nuclear lamina interactions: from cell populations to single cells. Current Opinion in Genetics & Development, 43: 67-72, doi: https://doi.org/10.1016/j.gde.2016.12.005.

- Ye Q., Callebaut I., Pezhman A., Courvalin J.C., Worman H.J. (1997) Domain-specific interactions of human HP1-type chromodomain proteins and inner nuclear membrane protein LBR. The Journal of Biological Chemistry, 272(23): 14983-9, doi: 10.1074/jbc.272.23.14983.
- Zhang H., Ji X., Li P., Liu C., Lou J., Wang Z., Wen W., Xiao Y., Zhang M., Zhu X. (2020) Liquid-liquid phase separation in biology: mechanisms, physiological functions and human diseases. Science China Life Sciences, 63(7): 953-985, doi: 10.1007/s11427-020-1702-x.
- Zhang Y., Sun Z., Jia J., Du T., Zhang N., Tang Y., Fang Y., Fang D. (2020) Overview of Histone Modification. Histone Mutations and Cancer, Advances in Experimental Medicine and Biology, 1283: 1-16, doi: https://doi.org/10.1007/978-981-15-8104-5_1.
- Zheng H., Xie W. (2019) The role of 3D genome organization in development and cell differentiation. Nature Reviews Molecular Cell Biology, 20: 535–550, doi: https://doi.org/10.1038/s41580-019-0132-4.
- Zwerger M., Kolb T., Richter K., Karakesisoglou I., Herrmann H. (2010) Induction of a Massive Endoplasmic Reticulum and Perinuclear Space Expansion by Expression of Lamin B Receptor Mutants and the Related Sterol Reductases TM7SF2 and DHCR7. Molecular Biology of the Cell, 21(2): 354-368, doi: https://doi.org/10.1091/mbc.e09-08-0739.

Appendix

Appendix

Table A1. Results of the statistical analysis of the data obtained by the calculation of the number of cells that presented asymmetric Lamin B2 distribution for all the examined clones (p-values<0.05 are marked with red).

Cell Line	Clone Comparison	p-value	Statistical Test
LMNA KO	LMNA KO1 vs. NIH 10%	< 0.00001	Chi-square test
	LMNA KO2 vs. NIH 10%	< 0.00001	
	LMNA KO1 vs. LMNA KO2	2.28E-02	
LBR KO	LBR KO1 vs. NIH 15%	5.63E-01	Chi-square test
	LBR KO2 vs. NIH 15%	5.63E-01	
	LBR KO1 vs. LBR KO2	1.00E+00	
LMNA-LBR DKO	LMNA KO1 vs. NIH 10%	< 0.00001	Chi-square test
	LMNA-LBR DKO1 vs. NIH 10%	< 0.00001	
	LMNA-LBR DKO2 vs. NIH 10%	< 0.00001	
	LMNA KO1 vs. LMNA-LBR DKO1	< 0.00001	
	LMNA KO1 vs. LMNA-LBR DKO2	< 0.00001	
	LMNA-LBR DKO1 vs. LMNA-LBR DKO2	< 0.00001	
LBR-LMNA DKO	LBR KO1 vs. NIH 15%	5.63E-01	Chi-square test
	LBR-LMNA DKO1 vs. NIH 15%	< 0.00001	
	LBR-LMNA DKO2 vs. NIH 15%	< 0.00001	
	LBR KO1 vs. LBR-LMNA DKO1	< 0.00001	
	LBR KO1 vs. LBR-LMNA DKO2	< 0.00001	
	LBR-LMNA DKO1 vs. LBR-LMNA DKO2	2.26E-04	

Table A2. Results of the statistical analysis of the data obtained by the calculation of the number of heterochromatic foci per nucleus for all the examined clones (p-values<0.05 are marked with red).

Cell Line	Clone Comparison	p-value	Statistical Test
LMNA KO	LMNA KO1 vs. NIH 10%	>0.05	One way Anova (0.09)
	LMNA KO2 vs. NIH 10%	>0.05	
	LMNA KO1 vs. LMNA KO2	>0.05	
LBR KO	LBR KO1 vs. NIH 15%	>0.05	One way Anova (0.07
	LBR KO2 vs. NIH 15%	>0.05	
	LBR KO1 vs. LBR KO2	>0.05	
LMNA-LBR DKO	LMNA KO1 vs. NIH 10%	3.22E-01	One way Anova (4.02E-9) with Levene test >0.05 and Brown-Forsythe test <0.05, Bonferroni post-hoc test
	LMNA-LBR DKO1 vs. NIH 10%	1.92E-03	
	LMNA-LBR DKO2 vs. NIH 10%	2.47E-03	
	LMNA KO1 vs. LMNA-LBR DKO1	3.71E-07	
	LMNA KO1 vs. LMNA-LBR DKO2	5.27E-07	
	LMNA-LBR DKO1 vs. LMNA-LBR DKO2	1.00E+00	
LBR-LMNA DKO	LBR KO1 vs. NIH 15%	9.13E-02	One way Anova (5.3E-31) with Levene test <0.05 and Welch test <0.05, Tukey post-hoc test
	LBR-LMNA DKO1 vs. NIH 15%	9.38E-14	
	LBR-LMNA DKO2 vs. NIH 15%	8.05E-16	
	LBR KO1 vs. LBR-LMNA DKO1	2.26E-23	
	LBR KO1 vs. LBR-LMNA DKO2	4.40E-21	
	LBR-LMNA DKO1 vs. LBR-LMNA DKO2	1.00E+00	

Table A3. Results of the statistical analysis of the data obtained by the calculation of the mobile fraction (*Mf*) of HP1α (FRAP experiments) for all the examined clones (p-values<0.05 are marked with red).

Cell Line	Clone Comparison	p-value	Statistical Test
LMNA KO	LMNA KO1 vs. NIH 10%	7.40E-02	K-sample test
	LMNA KO2 vs. NIH 10%	1.00E+00	
	LMNA KO1 vs. LMNA KO2	2.64E-01	
LBR KO	LBR KO1 vs. NIH 15%	1.00E+00	K-sample test
	LBR KO2 vs. NIH 15%	8.10E-01	
	LBR KO1 vs. LBR KO2	1.00E+00	
LMNA-LBR DKO	LMNA KO1 vs. NIH 10%	7.10E-02	K-sample test
	LMNA-LBR DKO1 vs. NIH 10%	1.10E-02	
	LMNA-LBR DKO2 vs. NIH 10%	1.00E+00	
	LMNA KO1 vs. LMNA-LBR DKO1	1.00E+00	
	LMNA KO1 vs. LMNA-LBR DKO2	8.66E-01	
	LMNA-LBR DKO1 vs. LMNA-LBR DKO2	1.87E-01	
LBR-LMNA DKO	LBR KO1 vs. NIH 15%	1.00E+00	K-sample test
	LBR-LMNA DKO1 vs. NIH 15%	1.00E+00	
	LBR-LMNA DKO2 vs. NIH 15%	8.10E-01	
	LBR KO1 vs. LBR-LMNA DKO1	1.00E+00	
	LBR KO1 vs. LBR-LMNA DKO2	1.00E+00	
	LBR-LMNA DKO1 vs. LBR-LMNA DKO2	1.00E+00	

Table A4. Results of the statistical analysis of the data obtained by the calculation of the diffusion coefficient (*Da*) of HP1α (FRAP experiments) for all the examined clones (p-values<0.05 are marked with red).

Cell Line	Clone Comparison	p-value	Statistical Test
LMNA KO	LMNA KO1 vs. NIH 10%	1.60E-02	K-sample test
	LMNA KO2 vs. NIH 10%	1.00E+00	
	LMNA KO1 vs. LMNA KO2	2.40E-02	
LBR KO	LBR KO1 vs. NIH 15%	6.00E-04	K-sample test
	LBR KO2 vs. NIH 15%	5.18E-01	
	LBR KO1 vs. LBR KO2	5.70E-02	
LMNA-LBR DKO	LMNA KO1 vs. NIH 10%	7.20E-02	K-sample test
	LMNA-LBR DKO1 vs. NIH 10%	1.00E+00	
	LMNA-LBR DKO2 vs. NIH 10%	1.00E-04	
	LMNA KO1 vs. LMNA-LBR DKO1	8.09E-01	
	LMNA KO1 vs. LMNA-LBR DKO2	5.25E-01	
	LMNA-LBR DKO1 vs. LMNA-LBR DKO2	1.3E-02	
LBR-LMNA DKO	LBR KO1 vs. NIH 15%	1.00E-03	K-sample test
	LBR-LMNA DKO1 vs. NIH 15%	9.20E-02	
	LBR-LMNA DKO2 vs. NIH 15%	2.75E-01	
	LBR KO1 vs. LBR-LMNA DKO1	1.75E-01	
	LBR KO1 vs. LBR-LMNA DKO2	1.00E+00	
	LBR-LMNA DKO1 vs. LBR-LMNA DKO2	1.00E+00	

Table A5. Results of the statistical analysis of the data obtained by the Wound Healing assay for all the examined clones (p-values<0.05 are marked with red).

Cell Line	Comparisons	p-value	Statistical Test
LMNA KO	LMNA KO1 vs. NIH 10%	>0.05	One way Anova (0.72)
	LMNA KO2 vs. NIH 10%	>0.05	
	LMNA KO1 vs. LMNA KO2	>0.05	
LBR KO	LBR KO1 vs. NIH 15%	>0.05	One way Anova (0.27)
	LBR KO2 vs. NIH 15%	>0.05	
	LBR KO1 vs. LBR KO2	>0.05	
LMNA-LBR DKO	LMNA KO1 vs. NIH 10%	1.00E+00	One way Anova (4.16E-3) with Levene test >0.05 and Brown-Forsythe test <0.05, Bonferroni post-hoc test
	LMNA-LBR DKO1 vs. NIH 10%	1.29E-01	
	LMNA-LBR DKO2 vs. NIH 10%	1.54E-02	
	LMNA KO1 vs. LMNA-LBR DKO1	1.29E-01	
	LMNA KO1 vs. LMNA-LBR DKO2	1.54E-02	
	LMNA-LBR DKO1 vs. LMNA-LBR DKO2	1.00E+00	
LBR-LMNA DKO	LBR KO1 vs. NIH 15%	>0.05	One way Anova (0.28)
	LBR-LMNA DKO1 vs. NIH 15%	>0.05	
	LBR-LMNA DKO2 vs. NIH 15%	>0.05	
	LBR KO1 vs. LBR-LMNA DKO1	>0.05	
	LBR KO1 vs. LBR-LMNA DKO2	>0.05	
	LBR-LMNA DKO1 vs. LBR-LMNA DKO2	>0.05	

Table A6. List of the markers of the nuclear periphery that had been tested by indirect immunofluorescence, along with the observations regarding their distribution pattern (S: Symmetric, A: Asymmetric, M: Mislocalized).

	Distribution			
Protein	**LMNA KOs**	**LBR KOs**	**LMNA-LBR DKOs**	**LBR-LMNA DKOs**
LBR	S	-	-	-
Lamin A/C	-	S	-	-
Lamin B1	S	S	A	A
Lamin B2	S	S	A	A
Nups	S	S	A	A
Emerin	M	S	M	M
TMPO	S	S	A	A
Nesprin3	S	S	A	A